NAVAL POSTGRADUATE SCHOOL
Monterey, California

DTIC
S ELECTE D
JUL 1 8 1980
A

Master's THESIS

THE TRANSPARENCY OF SOUTHEAST ASIAN
AND INDONESIAN WATERS.

by

John H. Murdock

March 1980

Thesis Advisor: S. P. Tucker

Approved for public release; distribution unlimited

80 7 14 081

REPORT DOCUMENTATION PAGE		READ INSTRUCTIONS BEFORE COMPLETING FORM
1. REPORT NUMBER	2. GOVT ACCESSION NO. AD-A086 824	3. RECIPIENT'S CATALOG NUMBER
4. TITLE (and Subtitle) The Transparency of Southeast Asian and Indonesian Waters		5. TYPE OF REPORT & PERIOD COVERED Master's Thesis March 1980
		6. PERFORMING ORG. REPORT NUMBER
7. AUTHOR(s) John H. Murdock		8. CONTRACT OR GRANT NUMBER(s)
9. PERFORMING ORGANIZATION NAME AND ADDRESS Naval Postgraduate School Monterey, California 93940		10. PROGRAM ELEMENT, PROJECT, TASK AREA & WORK UNIT NUMBERS
11. CONTROLLING OFFICE NAME AND ADDRESS Naval Postgraduate School Monterey, California 93940		12. REPORT DATE March 1980
		13. NUMBER OF PAGES 160
14. MONITORING AGENCY NAME & ADDRESS(if different from Controlling Office) Naval Postgraduate School Monterey, California 93940		15. SECURITY CLASS. (of this report) Unclassified
		15a. DECLASSIFICATION/DOWNGRADING SCHEDULE

16. DISTRIBUTION STATEMENT (of this Report)

Approved for public release; distribution unlimited.

17. DISTRIBUTION STATEMENT (of the abstract entered in Block 20, if different from Report)

18. SUPPLEMENTARY NOTES

19. KEY WORDS (Continue on reverse side if necessary and identify by block number)

Transparency - Turbidity - Bathymetry - Ocean Transparency - Water Clarity - Laser Bathymetry - Secchi Depth - Ocean Optics - Lidar Bathymetry - Secchi Disc - Optical Oceanography - Attenuation Coefficient - Beam Attenuation Coefficient - Diffuse Attenuation Coefficient - Hydrographic Surveys -

20. ABSTRACT (Continue on reverse side if necessary and identify by block number)

Secchi data (transparency) were obtained for Southeast Asian and Indonesian waters from 20°S to 30°N and from 90°E to 140°E. Some 10,269 points were used to determine the seasonal variation of transparency from specific subregions and depths. Seasonal and annual charts of Secchi depth (Z_s) were made for 16 subregions. The irradiance attenuation coefficient (K) was computed from Z_s. Charts of Kd, the

→ over

DD FORM 1473 EDITION OF 1 NOV 68 IS OBSOLETE
1 JAN 73
(Page 1)   S/N 0102-014-6601

1

19. (continued) Light Attenuation - Andaman Sea - Banda Sea-
Ceram Sea - East China Sea - Flores Sea - Gulf of Thailand -
Gulf of Tonkin - Halmahera Sea - Java Sea - Makassar Strait -
Malacca Strait - Molukka Sea - Philippine Sea - South China Sea-
Sulawesi Sea - Indian Ocean - Pacific Ocean - Indonesian Waters -
Southeast Asian Waters.

20. (continued) product of K and water depth, showed that
some nearshore areas can be surveyed by laser bathymetry.
For inshore areas $Z_s \lesssim 10$ m. Shelf regions with depths
less than 200 m have $10 \lesssim Z_s \lesssim 20$ m. For the deep enclosed
seas of eastern Indonesia, the Andaman Sea, the South China Sea
and the East China Sea, $20 \lesssim Z_s \lesssim 30$ m. For the Philippine
Sea, Pacific Ocean and Indian Ocean, $30 \lesssim Z_s \lesssim 55$ m. Trans-
parency shows a seasonal change in many areas.

Accession For

NTIS G.....

DDC Tab

Unannounced

Justification

By

Distribution

Availability Codes

Dist | Avail and/or Special

A

The Transparency of Southeast Asian and Indonesian Waters

by

John H. Murdock
U. S. Naval Oceanographic Office
Sc. B. in Engineering, Brown University, 1971

Submitted in partial fulfillment of the
requirements for the degree of

MASTER OF SCIENCE IN OCEANOGRAPHY-HYDROGRAPHY

from the

NAVAL POSTGRADUATE SCHOOL
· March 1980

Author _____

Approved by: _____

                                        Thesis Advisor

_____

                                            Reader

_____

Chairman, Department of Oceanography

_____

                                Dean of Science and Engineering

ABSTRACT

Secchi data (transparency) were obtained for Southeast
Asian and Indonesian waters from 20°S to 30°N and from 90°E
to 140°E. Some 10,269 points were used to determine the
seasonal variation of transparency for specific subregions
and depths. Seasonal and annual charts of Secchi depth (Z_s)
were made for 16 subregions. The irradiance attenuation
coefficeint (K) was computed from Z_s. Charts of Kd, the
product of K and water depth, showed that some nearshore areas
can be surveyed by laser bathymetry. For inshore areas
$Z_s \lesssim 10$ m. Shelf regions with depths less than 200 m have
$10 \lesssim Z_s \lesssim 20$ m. For the deep enclosed seas of eastern Indonesia,
the Andaman Sea, the South China Sea and the East China Sea,
$20 \lesssim Z_s \lesssim 30$ m. For the Philippine Sea, Pacific Ocean and
Indian Ocean, $30 \lesssim Z_s \lesssim 55$ m. Transparency shows a seasonal
change in many areas.

4

TABLE OF CONTENTS

LIST OF FIGURES

56	Secchi Depths, Philippine Sea and Pacific Ocean 20°N – 30°N, Jul-Sep
57	Secchi Depths, Philippine Sea and Pacific Ocean 20°N – 30°N, Oct-Dec
58	Secchi Depths, Philippine Sea and Pacific Ocean 20°N – 30°N, entire year
59	Secchi Depths, Philippine Sea and Pacific Ocean 2°S – 10°N, entire year
60	Secchi Depths, Southeast Asian and Indonesian Waters
61	KD Values, Jakarta Approaches, Apr-Jun
62	KD Values, Jakarta Approaches, Jul-Sep
63	KD Values, Jakarta Approaches, Oct-Dec
64	KD Values, Java Sea, Jan-Mar
65	KD Values, Java Sea, Apr-Jun
66	KD Values, Java Sea, Jul-Sep
67	KD Values, Java Sea, Oct-Dec
68	KD Values, Java Sea, entire year
69	KD Values, Makassar Strait, Flores Sea and Bali Sea, entire year
70	KD Values, Malacca Strait, Dec-Apr
71	KD Values, Bangkok Approaches, Apr-Oct
72	KD Values, Bangkok Approaches, Nov-Dec
73	KD Values, Gulf of Thailand, entire year
74	KD Values, South China Sea (Southern Section), entire year
75	KD Values, South China Sea (Central Section), entire year
76	KD Values, South China Sea (Northern Section), Apr-Nov
77	KD Values, South China Sea (Northern Section), Dec-Mar
78	KD Values, East China Sea, entire year

ACKNOWLEDGEMENTS

I.   INTRODUCTION

A.   USES AND APPLICATIONS OF SEAWATER TRANSPARENCY DATA

Seawater transparency data have widespread applications in many fields, including marine biology, phyical oceanography, military operations and laser bathymetry. Marine biologists use transparency measurements to determine the biological productivity of a region. The presence of phytoplankton may be indicated by transparency measurements. An abundance of phytoplankton leads to an abundance of higher organisms in the food chain, such as zooplankton and fish, and can indicate the likely presence of commercially valuable fish. Much of the impetus for measuring Secchi depths in Southeast Asian waters comes from the desire of Japan and other nations to locate valuable fisheries in the area.

One goal of marine biologists is to define the depth of the euphotic zone, which extends downward to the level where the irradiance is reduced to 1% to its surface value. For example, Jerlov and Nygard (1961) determined the topography of the 1% level for an area of the North Atlantic Ocean off the Strait of Gibraltar. It is common practice for marine biologists interested in primary production at a location to estimate the depth of the euphotic zone by multiplying the Secchi depth by three (Holmes, 1970).

Uda (1963) found that dissolved oxygen content and transparency as indicated by Secchi depth were useful in investigating productivity levels. An inverse relationship between the amount of phytoplankton and the Secchi depth has been noted by Voytov and Dement'yeva (1970).

There is evidence that oceanic productivity affects both scattering and absorption, the two independent processes that cause light attenuation and determine the water transparency. Scattering measurements taken in the equatorial Pacific Ocean show a congruence between particle distribution and the topography of the depth of the thermocline (Jerlov, 1964). Areas with high particle content occur at the equatorial Ekman divergence region, which is an upwelling area with high productivity.

Absorption at the shorter wavelengths of visible light is caused by "yellow substance" or Gelbstoff, a complex mixture of organic compounds. Jerlov (1953a) used a beam transmission meter with filters to study the distribution of yellow substance in the transition area between the Baltic and the Skagerrak. He noted that the amount of yellow substance present in a water mass may often be considered a characteristic property of that water mass. Steeman Nielsen (1963) found that the regional distribution to color in the South Atlantic conforms closely to the regional distribution of primary production.

Physical oceanographers use transparency data as a means of delineating and tracing water masses. The beam

14

transmittance meter is a powerful tool for measuring attenuation to great depths in the ocean. Joseph (1955) used measurements made with the beam transmittance meter in an area between the Dutch and Norwegian coasts, revealing a layer rich in particles at the thermocline. Ball and LaFond (1962) used a beam transmittance meter to study the nearshore waters off Mission Beach, California. They observed an increase in turbidity at the thermocline, a cycle in the distribution of water turbidity corresponding to the tidal cycle and a sound scattering layer corresponding to the depth of maximum turbidity.

Another optical instrument, the scattering meter or nephelometer, provides a sensitive indication of particle distribution. Particle content may be considered an inherent property of the water mass; observations of particle content can be used to distinguish between adjacent water masses. Jerlov (1953b) developed scatterance profiles for various offshore locations including the Mediterranean offshore from the Nile Delta; the Indian, Pacific and Atlantic Oceans; and the Caribbean Sea. For example, one profile clearly shows the flow of water of relatively high turbidity from the Mediterranean westward over the ridges at the Strait of Gibraltar and its sinking on the Atlantic side, forming Mediterranean Intermediate Water. Since rivers are an important source of particles, the flow of river water in the oceans can be traced with the use of scattering measurements. H. Pak, G. F. Beardsley and P. K. Park (1970) plotted the

distribution of the scattering function off the mouth of the Columbia River. The plot showed the plume of highly turbid water flowing southwestward.

Transparency data are important to military operations. A submarine commander must consider the transparency of the water in which he is operating, since the submarine is always susceptible to visual detection by aircraft and surface ships. Water transparency is also an important factor in mine detection, diver operations, and underwater photography.

In the field of anti-submarine warfare (ASW), the Naval Air Development Center, Warminster, Pennsylvania, has been developing its Optical Ranging and Detection/Optical Ranging IFF Communication (ORAD/ORIC) System, which uses an airborne laser system. The usefulness of lasers in water is critically dependent upon the transparency of water in the specific locality.

Transparency data are also important in airborne laser bathymetry, as the transparency determines the practical limits of the laser bathymetry system. Currently, a number of agencies are developing laser bathymetry systems. The Naval Ocean Research and Development Activity (NORDA), Bay St. Louis, Mississippi, is developing the Hydrographic Airborne Laser Sounder (HALS) system. The HALS system will be used by the Naval Oceanographic Office (NAVOCEANO), Bay St. Louis, Mississippi. This system will probably be available for field operation in 1981 and ready for full deployment in the field in late 1981 or 1982. It is planned for the HALS

system to be mounted on the helicopter of the USNS CHAUVENET
and to be used in shallow water hydrographic surveys comple-
menting the deep water hydrographic surveys to be done by
the ship and its soundboats. The expected area of opera-
tion is Indonesia. It is possible that at some future date
the HALS system will be mounted on a fixed-wing aircraft and
that its operations may become independent of ship operations.
The Global Positioning System (GPS) may become available
around 1986 or 1987. This will provide continuous satellite
positioning of the aircraft, obviating the need for shore-
based electronic positioning systems and providing greater
flexibility for laser bathymetry operations.

The National Ocean Survey (NOS) of the National Oceanic
and Atmospheric Administration (NOAA) is developing an
airborne laser bathymetry system for use in the coastal
waters of the United States.

B. PURPOSE OF INVESTIGATION

The purpose of this investigation is to study the trans-
parency patterns of the waters in the Indonesian-Southeast
Asian region, from 20°S to 30°N and from 90°E to 140°E. As
far as is known, no comprehensive transparency study has been
conducted of the vast complex of seas located within the
Indonesian-Philippine archipelago. This region, lying between
the Pacific and Indian Oceans, has acquired greater military
and economic importance in recent years.

The main type of transparency data available in the area is the Secchi depth. Due to the large geographical area involved, each body of water was considered separately. Seasonal trends in Secchi depths were determined for each water depth range.

Contour charts of Secchi depths were plotted for each body of water. A chart was produced for each season if seasonal variability was indicated and enough Secchi depths were available. Otherwise a chart was produced for the entire year.

Finally, in order to reach conclusions leading to the applicability of laser bathymetry to this region, a series of charts showing the product Kd was produced for selected areas containing significant amounts of shallow water. Here K is the irradiance attenuation coefficient and d is the bottom depth. The significance of this product is discussed in Section IIB3.

II. SOME PRINCIPLES OF MARINE OPTICS

A. METHODS OF MEASURING AND DESCRIBING TRANSPARENCY

Three quantities used to express the transparency of
water are the beam attenuation coefficient (c), the irra-
diance attenuation coefficient (K), and the Secchi depth (Z_s).

1. Beam Attenuation Coefficient

The beam (volume) attenuation coefficient (c or α)
characterizes the amount of attenuation experienced by a
collimated beam of monochromatic light traversing a fixed
path-length of homogenous water is such a way that the
residual beam does not contain any scattered light. The
power content of radiant flux traveling along a fixed path
decreases exponentially with distance as expressed by the
formula:

$$P_r = P_o e^{-cr}$$

where:

P_o = initial radiant power of collimated beam

P_r = radiant power of residual beam after traveling a
distance r through the water

r = water path length

c = beam attenuation coefficient

Figure 1 shows schematically the method of measuring the beam attenuation coefficient using a beam transmittance meter (also known as a beam transmissometer or alpha meter). A projector with a light source sends out a collimated beam across a water path with a fixed distance (such as one meter). Here the light is subject to the two attenuation mechanisms of absorption and scattering. It is assumed that no photons having undergone a scattering event will remain within or be returned to the beam. It is also assumed that no photons originating outside the beam (such as from the sun) will be scattered into the beam. After having traversed the water path (r), the residual power of the light beam is measured by a photocell within the receiver. From this measurement the value of the beam attenuation coefficient is computed with the use of the equation:

$$c = \frac{1}{r} \ln \left(\frac{P_o}{P_r} \right)$$

The beam transmittance meter can be lowered to any desired oceanic depth. Since the value of the beam attenuation coefficient is independent of light beam orientation (assuming homogenous water along the path length) and is independent of the ambient light conditions, the beam attenuation coefficient may be considered an inherent optical property of the water.

The beam attenuation coefficient (c) is related to the absorption coefficient (a) and the scattering coefficient (b) by the expression:

$$c = a + b$$

The magnitudes of all three quantities are functions of wavelength. They all have units of reciprocal length (usually m^{-1}). The formula expresses the fact that light attenuation in water is caused by the two separate mechanisms of absorption and scattering.

Absorption results when a photon strikes a water molecule or other particle and is stopped and transformed into heat energy. Absorption is caused by water molecules, by yellow substance and other dissolved matter, and by particulates. Yellow substance is probably formed from carbohydrates; the formation is favored by heat and the presence of amino acids (Jerlov, 1976). The particulates may be either living or decayed plankton, or they may be inorganic particles transported to the sea by rivers or lifted from the sea bottom by turbulence.

Scattering results from the deflection of photons by particles in the water through reflection, refraction or diffraction of the particles. Scattering is caused by water molecules and dissolved inorganic sea salts and – more appreciably – by organic and inorganic particulate matter.

2. Irradiance Attenuation Coefficient

The irradiance attenuation coefficient from down-welling light (also known as the diffuse attenuation coefficient or the extinction coefficient), K, is the vertical gradient of the logarithm of the irradiance:

$$K = - \frac{d(\ln H)}{dz} = - \frac{1}{H} \frac{dH}{dz}$$

where:

H = irradiance of light

z = depth

The coefficient K characterizes the amount of attenuation experienced by a diffuse field of monochromatic light traversing a fixed vertical distance of water. In the ocean, the diffuse downwelling daylight decreases exponentially with depth as expressed by the following formula:

$$H_z = H_o e^{-Kz}$$

where:

H_o = solar irradiance at the sea surface

H_z = downwelling irradiance on a horizontal plane at depth z

z = depth measurement

K = diffuse attenuation coefficient

Figure 2 shows schematically the method of measuring the irradiance attenuation coefficient using a relative

irradiance meter (also known as a K-meter). The method uses
two upward-facing photosensors, one at the surface and one
submerged to depth z. Diffuse light is collected by a
cosine collector made of opal glass on each photosensor.
The intensity of the collected light is measured by a photo-
cell. This provides an approximate measure of the downward
irradiance at each point. Usually a continuous record is
taken as the irradiance meter is lowered to a depth of 100 m
or so. When relative irradiance is plotted versus depth on
semilogarithmic paper, the magnitude of K can then be deter-
mined by measuring the slope of the plotted line.

It should be noted that K, unlike c, is an <u>apparent</u>
optical property of the water, since its value at any location
can change depending upon the ambient light fields. If the
sky were overcast rather than sunny, the value of K in a
particular water would change, while c would remain the same.

The magnitude of K is wavelength-dependent, and K has
units of reciprocal length (usually m^{-1}).

These two systems of measurement have the advantage
of providing a relatively precise quantitative measurement
of light attenuation. The meters can be lowered to various
depths, and values of c and K can be determined over the
entire water column. Disadvantages include the expense of
the meters and the need for qualified operators to make the
measurements and maintain the equipment.

3. Secchi Depth

The Secchi depth (Z_s) is determined by lowering
a Secchi disc, a white disc 30 cm in diameter, into the
water until it is no longer visible. The depth at which
visibility is lost is the Secchi depth. Though not the
best, this is, nevertheless, the oldest, simplest and most
widely used method of determining water transparency.

The Secchi disc was first used by Commander Cialdi
of the Papal Navy in 1866. He conducted a study with P. A.
Secchi of the factors affecting the visibility of a disc
lowered vertically in the sea. Cialdi's report on their
investigations was recently translated into English by Collier
(1968). Factors which affected the Secchi depth were found
to include - to varying degrees - disc color, solar alti-
tude, sea surface reflections and refractions, ship's
shadow, sky clearness, water color, disc diameter, and the
height of the viewer above the water surface.

Following the pioneering work of Cialdi and Secchi,
the Secchi disc has been widely used by oceanographers and
marine biologists to measure water transparency. The limita-
tions of the Secchi disc as an oceanographic tool have also
been noted. Postma (1961) noted that the Secchi disc can
give information on transparency only in surface waters and
only in daylight of sufficient brightness. No continuous
registration at various depths is possible. The result of
a measurement with a Secchi disc depends to a certain degree

on the visual acuity of the observer. None of these
limitations apply to beam transmittance meters or irra-
diance meters. Postma noted, however, that Secchi measure-
ments made by observers with good eyesight, carried out in
sufficient daylight and in the shadow of the ship, are
quite reproducible, especially for typical coastal Secchi
depths of 5 m or less. Duplicate readings by two observers
hardly differed by more than 5 cm under these conditions.

Tyler (1968) noted that although the Secchi disc
has become a widely used piece of equipment, it has never
really been standardized. A consistent method for its use
has not been established. The physical properties of the
disc, such as the reflectance of its white paint, have
never been fully specified. Tyler also noted that the
Secchi disc was usually lowered on the shadow side of the
vessel to avoid surface reflection. Although the objective
of this procedure was commendable, lowering the disc through
the ship's underwater shadow could result in large errors
in the Secchi disc reading.

Although the irradiance attenuation coefficient (K)
is wavelength-dependent, a Secchi measurement does not
establish values of K at the various wavelengths but pro-
vides only a single weighted value of transparency. The
Secchi reading is affected by these wavelength-dependent
factors: the downward irradiance of the sky, the irradiance
attenuation coefficient (K) of the water column, and the
sensitivity of the eye. Sky irradiance usually peaks at a

wavelength of 480-500 nm, as shown in the 0 m curves of
Figure 3. In certain locations and under certain cloud con-
ditions the skylight is approximately flat spectrally. The
values of K for seawater vary greatly with wavelength and
with location, Figure 4. And the spectral response of the
eye peaks at 555 nm.

The Secchi disc measurement provides no information
about the variation of water clarity with depth, but provides
only one number which expresses integrated water clarit· in
the water column from the surface to the Secchi depth itself.
The water transparency below the Secchi depth remains unknown.
It has been shown by many investigators that the light attenua-
tion coefficient may increase markedly at the thermocline,
the region of greatest negative temperature gradient (Ball
and LaFond, 1962, and others). Neuymin and Sorokiva (1976)
have shown a strong correlation between the vertical distri-
butions of attenuation coefficient and density gradient for
regions with high plankton concentration. Particulate matter
tends to find neutral buoyancy near the bottom of the mixed
layer or within the thermocline. This accumulation of par-
ticulate matter may be too deep to be detected within the
Secchi disc.

Also, the Secchi disc may not reveal the presence
of a bottom scattering layer or bottom nepheloid layer (BNL).
Turbulence caused by bottom currents may lead to an increase
of particle content and scattering near the sea bottom
(Jerlov, 1953b). Also, advection may cause the movement

of turbid water along the bottom from coastal areas to areas further removed from the coast, causing a wide distribution of the BNL (Pak and Zaneveld, 1977).

Although these limitations and difficulties are present, Secchi measurements can still give valuable results. The Secchi disc has found widespread use because of its convenience and low cost, and to date, Secchi depths provide the most complete picture of transparency patterns over most of the world's ocean areas. Much research has been conducted to establish its utility as a practical instrument for measuring water transparency. Particularly, many investigators have sought to establish mathematical relations between the Secchi depth (Z_S), the beam attenuation coefficient (c), and the irradiance attenuation coefficient (K).

4. Relationships Between Secchi Depth, Beam Attenuation Coefficient and Irradiance Attenuation Coefficient

Poole and Atkins (1929) developed an empirical formula for approximating the irradiance attenuation coefficient:

$$K = \frac{1.7}{Z_s}$$

where K is the irradiance attenuation coefficient in reciprocal meters and Z_s is the Secchi depth in meters. This formula, derived from data collected in the English Channel, has been used widely since the report was published.

27

Graham (1966) determined empirical relationships
between K, the reciprocal of Z_s, and the Forel-Ule color
scale measurements (FC), for different parts of the eastern
North Pacific Ocean.

Tyler (1968) derived a theoretical relationship
linking the Secchi depth with the sum of (c + K):

$$(c + K) = \frac{8.69}{Z_s}$$

where c is the beam attenuation coefficient in reciprocal
meters. The relation shows that c and K are individual
variables whose _sum_ is inversely proportional to Z_s. In
theory, K by itself cannot be determined from Z_s.

However, Holmes (1970) has noted that an estimate of
K useful to biologists might be obtained from Z_s, theory
notwithstanding. Such an estimate would have a relatively
large standard error but might be acceptable in certain
types of study. Holmes developed such an empirical relation-
ship from data collected in the relatively turbid waters of
Goleta Bay, near Santa Barbara, California. His formula is:

$$K = \frac{1.44}{Z_s}$$

Shannon (1979) derived an empirical relationship
based on simultaneous K and Z_s values taken in different ocean
waters of various turbidities by the Naval Air Development
Center and the Naval Oceanographic Office. The majority of
the Naval Air Development Center measurements were made in

coastal waters of relatively high turbidity. The Naval Oceano-
graphic Office measurements obtained by R. Wargelin (1976)
were made in straits in the Philippine region (Bashi Channel,
San Bernardino Strait, and Surigao Strait). They represent
relatively clear tropical waters. Using a least squares linear
fit between K and $^1/_{Z_s}$, Shannon obtained the following rela-
tion:

$$K = \frac{1.15}{Z_s} + 0.03 \text{ for } 4 \leq Z_s \leq 43 \text{ m}$$

where K is the irradiance attenuation coefficient in reciprocal
waters, depth-averaged over the entire water column, and Z_s
is the Secchi depth in meters.

Shannon's formula was used in this study for the pur-
pose of relating Z_s and K. His inclusion of data from the
Philippine region makes the formula appropriate for the high-
transparency waters to be found in the offshore regions in
the general vicinity of Indonesia and Southeast Asia. His
inclusion of data from more turbid waters makes the formula
also appropriate for the high-turbidity waters near the coasts
and near the river outflows.

B. EFFECTS OF WATER TRANSPARENCY ON LASER OPERATIONS

1. Hydrographic Airborne Laser Sounder

Reference has been made to the development of the
HALS system by NORDA and of the future use of HALS by

NAVOCEANO in its hydrographic operations. A brief description of the HALS system will be made and the effects of water turbidity will be discussed.

The HALS system consists of a laser transmitter, optical scanner, laser receiver, clock, precision time counter, electronic positioning equipment, inertial orientation equipment, computer and the recorder display units (NORDA, 1978).

A frequency-doubled Nd:YAG laser is being proposed for the Hydrographic Airborne Laser Sounder because of its high peak pulse power (355 KW), high pulse rates (400 Hz), and small size and weight. The scanner consists of a nutating mirror rotating at a constant speed, resulting in an elliptical scan pattern (Figure 5). Each dot represents one light pulse produced by the laser, directed obliquely downward by the scanner, reflected by the sea surface and the sea bottom, and detected by the receiver. This elliptical scan pattern, although dense and redundant at the edges, satisfies the requirements for data distribution. The swath width can be altered by changing the angle off nadir toward which the beam is directed.

The receiver consists of a telescope which accepts reflected laser energy from the water surface, the subsurface scatter and the bottom reflection. The field of view (FOV) of the receiver is variable from 0 to 30 milliradians, and is controllable from the computer. The return pulse is digitized and is handled by the computer, which performs a large set of arithmetic and data acquisition system functions.

Starting with the digitized laser return time series, the computer eventually determines the depth and position of each data point in real time. The data are stored on magnetic tape.

2. System Attenuation Coefficient

The laser beam is subject to attenuation while passing through water. The attenuation in the atmosphere is considered negligible. The performance of the laser bathymetry system in water can be expressed by the following relation (Shannon, 1978a):

$$P_r \cong P_x \cdot C \cdot e^{-2kd}$$

where:

P_r = peak power received (watts)

P_x = peak power transmitted (watts)

C = constant which combines factors representing the effects of bottom reflectivity, water and air transmission, aircraft altitude and other variables

k = "system" attenuation coefficient due to water (m^{-1}); i.e., the effective water attenuation coefficient which the bathymetry system "sees"

d = bottom depth (meters)

The major environmental factors which determine the strength of the return signal and which determine the efficacy of the laser system are measured by k and d. The figure of merit (FOM) of the laser bathymetry system can be described by the product kd. It should be emphasized that the laser

31

system attenuation coefficient (k) is a different quantity from the irradiance attenuation coefficient (K). However, as will be shown, K provides a good approximation for k.

Krumboltz (1979) conducted an experimental investigation of the system attenuation coefficient (k) for HALS, while simultaneously measuring c and K. The results show (Table I) that as the field of view of the laser receiver is increased toward 80°, the system attenuation coefficient (k) decreases and approaches the depth-averaged irradiance coefficient (K) measured with an underwater irradiance meter. This is to be expected, since a wider field of view allows the acceptance of a greater amount of scattered light, thus decreasing k. In all cases, the values of k remain well below the values of the depth-averaged beam attenuation coefficient (c). These results agree with previous observations.

Since the maximum field of view of the HALS system in an operational status will be 30 mrad, the value of k will be somewhat larger than K. Based on the data presented in Table I, for a field of view of 30 mrad:

$$k \simeq 1.4 \ K$$

The above relationship shows that, under the proposed operating conditions of HALS, k is comparable but not precisely equal to K.

3. <u>Figure of Merit (Kd)</u>

Values of the system attenuation coefficient (k) are scarce while values of the irradiance attenuation coefficient (K)

32

are relatively common. Since the two values are comparable, it has become customary to describe the capability of a laser bathymetry system by the product Kd. For the HALS system, the figure of merit Kd has been specified to be 3.2 (Hauck, 1979). This means that the system is capable of depth measurement at any location where the product of the irradiance attenuation coefficient (K) and depth (d) is less than or equal to 3.2. As the turbidity as expressed by K increases, the maximum measurable depth (d) decreases, Figure 6.

III. INVESTIGATION OF SOUTHEAST ASIAN AND INDONESIAN WATERS

A. REASONS FOR INVESTIGATING SOUTHEAST ASIAN AND INDONESIAN WATERS

The vast collection of seas, gulfs and bays located
between the Pacific and Indian Oceans and stretching between
Asia and Australia can be considered to be a single geo-
graphical entity. In one sense, most of these seas might be
considered part of the Pacific Ocean, since they derive their
waters from the Pacific (Wyrtki, 1961). However, the island
chain of New Guinea, Halmahera, the Philippines, and Taiwan
provides a distinct boundary between these seas and the Pacific
Ocean proper (Figure 7). Likewise, the island arc extending
from the Andaman Islands through Sumatra, Java and the Lesser
Sundas to Timor serves as an even stronger boundary between
the seas and the Indian Ocean. Wyrtki (1961) refers to the
collection of seas enclosed by these island arcs and stretching
from the Asian mainland to Australia and New Guinea as South-
east Asian waters.

These waters have achieved greater importance in recent
years. With the production of petroleum in Indonesia and the
expansion of trade within the region, there has been increased
commercial use of the waters. As the Indonesian Archipelago
separates the Indian and Pacific Oceans, the straits which
pass through the island chain have achieved great commercial,
political and military significance. Many trade goods pass

34

through these stratis. Much of the petroleum shipped from the Mideast to Japan passes through the Malacca Strait. With the expansion of American and Russian naval activity in the Indian Ocean, the various straits and passages in Indonesia achieve greater strategic importance.

There has been a vast increase in the amount of oceanographic research including optical oceanographic work in this region during recent years. However, as far as is known, no water clarity analysis has been done that deals with the Southeast Asian and Indonesian waters as a single unit.

Morita (1973) investigated the transparency of the Western Pacific Ocean. The limits of his investigation are shown in Figure 8. Using Secchi depths averaged over each one-degree square, he made contour plots of the Secchi depths for all four seasons.

Voytov and Dement'yeva (1970) contoured Secchi depths of the Indian Ocean for the winter months only.

Frederick (1970) produced an atlas of Secchi depths and Forel-Ule color codes for most of the world's ocean areas. She produced annual Secchi-depth contour plots and Forel-Ule color code contour plots for the South China Sea, Gulf of Tonkin and Gulf of Thailand. She also produced annual small-scale contour plots for the Western Pacific Ocean which included Indonesian waters.

Brown (1973) examined the Secchi depths of various Marsden squares in the Western Pacific Ocean and Southeast Asian

35

waters including the northern South China Sea and other bodies of water. He examined possible correlations between Secchi depths and other simultaneously measured oceanographic parameters, such as color, bottom depth, temperature, salinity, sigma-t, oxygen and silicate.

York (1974) examined the Secchi depths of various Marsden squares in the Western Pacific Ocean and various one-degree squares off the coasts of Japan and Korea. Like Brown, he examined possible correlations between Secchi depths and other simultaneously measured oceanographic parameters.

The outline of the area to be examined in this study is shown in Figure 7. The limits of the area were chosen to include all of the Southeast Asian and Indonesian waters, plus some of the adjoining Pacific and Indian Ocean waters. The area was also intended to adjoin the areas of investigation of Morita, Voytov, Brown and York.

B. SOURCES OF DATA

All of the transparency data used in this study were Secchi depths. The number of existing data points in this area with beam or irradiance attenuation coefficients was quite small.

The major source of Secchi depths was a magnetic tape of Secchi depts and Forel-Ule colors obtained from the World Data Center A, National Oceanographic Data Center (NODC). This tape, generated from their files in January 1979, provided a total of 9,986 Secchi depths within the area of

interest. Of these, a total of 7,129 Secchi depths was collected by Japanese institutions. Other major contributors include Thailand (1,539 Secchi depths), Indonesia (668), the Soviet Union (352) and the United States (113).

Data obtained from Wargelin of NAVOCEANO provided 42 additional data points in San Bernardino Strait and Surigao Strait in the Philippines.

In addition, an intensive literature search was conducted to locate other Secchi depths which may not have found their way onto the NODC tape. This endeavor produced 241 additional data points. Apparently NODC has been quite successful in acquiring Secchi data which had been collected by foreign institutions and published in foreign oceanographic journals. The sources of the non-NODC Secchi depths include recent Data Reports of the Cooperative Study of the Kuroshio (Data Report of CSK, Nos. 337, 357, 368, 372 and 414); recent cruise reports of the Institute of Marine Research of Indonesia, Oceanographical Cruise Reports, Nos. 13, 14 and 16; a South Korean oceanographic cruise (Korea, 1968); and an early U. S. report which consolidated prewar Japanese Secchi data (Russell and Clarke, 1944).

The Cooperative Study of the Kuroshio (CSK) program, in which Japan cooperates with the Southeast Asian nations, the Soviet Union, and the United States in collecting oceanographic data has been a notable source of transparency data. Another noteworthy source is the Institute of Marine Research of Indonesia.

C. OVERALL CLIMATIC AND OCEANOGRAPHIC CONDITIONS IN THE
   AREA

1. Monsoon Regime

The climate of Southeast Asia and Indonesia is domi-
nated by the monsoon regime. Between March and September the
Asian continent is heated and a low-pressure zone develops
over the land mass. The south monsoon is in effect at this
time. In Figure 9 the chartlet at the upper right-hand
corner shows the wind pattern during August: southeast winds
in the Southern Hemisphere, south winds crossing the equator,
and southwest winds in the Northern Hemisphere.

October is a transition month when the winds switch
from south to north. Between November and February the Asian
continent is cooled and a high-pressure zone develops over
the land mass. The north monsoon is in effect at this time.
Figure 10 shows the wind pattern during December: northeast
winds in the Northern Hemishpere and north winds crossing the
equator. South of the equator, the north winds from the
Northern Hemisphere turn eastward and merge with the south
winds from the Southern Hemisphere. The result is a strong
west wind north of Java and the Lesser Sunda Islands. March
and April constitute a transition period between the north
and south monsoon periods.

Therefore, this region has two long monsoon seasons
with short transition periods. During each monsoon season

the winds are constant; during the transition period the winds are extremely variable. The precise time of the transition period cannot be specified and may vary according to location.

The variation of atmospheric circulation is paralleled by the variation of the ocean currents. The direction of the currents reverses with each monsoon season.

During the south monsoon (Figure 9), surface currents flow westward through the Banda Sea, the Flores Sea and the Java Sea, and then flow northward into the South China Sea. They flow northeastward between the Philippines and Taiwan, where they join currents flowing northward along the eastern coast of Luzon to form the Kuroshio. There is much circulation between the Pacific Ocean and Southeast Asian waters, contrasted by little circulation between Southeast Asian waters and the Indian Ocean.

During the north monsoon (Figure 10), current flow within the Southeast Asian area is reversed. Currents flow northwestward between the Philippines and Taiwan into the South China Sea. They circulate westward along the China coast, and then flow at great speeds southward along the Vietnam coast. The currents flow southeastward as they leave the South China Sea, and then flow eastward through the Java Sea, the Flores Sea and the Banda Sea.

During the transition months the currents tend to be much weaker.

Precipitation varies according to the monsoon cycle. Between March and September precipitation is concentrated in the Northern Hemisphere (Figure 11). Rainfall is particularly heavy along the Burma coast, in parts of Indochina, and in the western Philippines. There is moderate rainfall in most of Indonesia.

Between November and February precipitation is concentrated in the Southern Hemisphere (Figure 12). Rainfall is particularly heavy in Java. There are some isolated spots in the Northern Hemisphere with heavy precipitation (Malaysia and the eastern Philippines), but most of the Northern Hemisphere has very little rainfall during these months.

2. Factors Affecting Transparency

The atmospheric and ocean factors described above - winds, currents and precipitation - all affect the transparency of the Southeast Asian waters. But while the winds, currents and precipitation generally adhere to a two-season monsoon pattern, the water transparency at any one place does not necessarily exhibit a two-season pattern. The variation of transparency with season tends to be more complex.

Precipitation has a strong effect on water clarity, particularly in coastal waters. The Southeast Asian area is subject to heavy rainfall which follows a seasonal pattern in most localities. This precipitation leads to a large amount of river runoff which carries particulate matter in

suspension into the nearshore waters. This effect is most pronounced near the mouth of a large river such as the Mekong, but it also occurs along the coast of any large land mass with significant rainfall like Borneo and Sumatra. The turbid waters, upon entering the sea, tend to move along the coastline in the same direction as the currents. There may be a time lag between the time of maximum precipitation on land and the time of maximum turbidity offshore, since a certain amount of time is required for the particulate matter to be transported down the river and be carried out into the open sea. Thus the season of highest precipitation may not coincide precisely with the season of highest turbidity.

In addition to carrying inorganic particulate matter, the rivers also carry nutrients into the sea. Since the coastal waters then contain more nutrient phosphates, silicates, nitrates and dissolved organic substance, they can support a higher concentration of plankton. This leads to a higher turbidity at these times.

In shallower areas, wind and wave mixing bring nutrients and particulate matter from the bottom to the surface layers and increases the turbidity. This phenomenon is most pronounced during storms or during the strong winds of the monsoon season. The Sunda Shelf is susceptible to this phenomenon. This shelf is an extensive region, shallower than 100 meters, which includes the western part of the Makassar Strait, the Java Sea, most of the Malacca Strait, the southern third of the South China Sea and the Gulf of

41

Thailand. In general, the turbidity of the Sunda Shelf
region increases during the two monsoon periods and decreases
during the two transition periods.

In deeper waters wind and wave mixing brings nutrients
from the thermocline up to the euphotic zone, which helps
the growth of plankton and decreases the transparency.

Tidal currents bring particulate matter from the
bottom to the surface layers and increase the turbidity in
shallower areas. The strength of tidal currents varies from
one area to another, as some areas have much higher tide
ranges than others. Tidal currents tend to be stronger
in straits. The strength of tidal currents also varies
with time, with maximum current velocity during spring
tides and minimum velocity during neap tides.

Islands and shoals in the paths of currents cause
localized upwelling, turbulence, and horizontal eddies
which bring nutrients to the surface (LaFond, 1963). These
localized areas tend to be rich in plankton and thus, have
lower transparencies.

Upwelling is a mechanism which brings nutrient-rich
matter up toward the surface layer, greatly increasing the
growth of plankton and thereby decreasing the transparency.
Coastal upwelling is generally associated with offshore
Ekman transport. In the Northern Hemisphere, when the wind
blows parallel to the coast with the water on the right-hand
side, if one faces downwind, the surface water will be dis-
placed offshore. Subsurface water then upwells toward the

42

surface. Such coastal upwelling occurs off Vietnam during the southwest monsoon in the summer months.

Another large area of upwelling occurs in the Banda and Arafura Seas. The southeast monsoon pushes the surface water to the west, and subsurface water upwells to replace it. This upwelling takes place between May and August (Wyrtki, 1961).

Other coastal areas with upwelling include the Andaman Sea between December and March (Wyrtki, 1961) and the Makassar Strait at the southern end of Sulawesi (Ilahude) between June and September.

Upwelling also takes place at the divergence of the main current systems. This occurs in the open ocean areas of the Pacific and Indian Oceans.

The open oceans and the deep-water portion of the enclosed Southeast Asian waters tend to have high surface transparencies. Because these waters are located in a tropical region with much rainfall, they have high surface temperatures and low surface salinities. Under the mixed layer there is a strong thermocline which exists throughout the year. This thermocline lends stability to the water column and inhibits mixing. Thus the recirculation of nutrients from subsurface waters is slight and the growth of plankton is inhibited. There is some vertical mixing close to the surface caused by winds and currents resulting in a shallow mixed layer. The depth of the mixed layer varies from zero to about 100 meters, depending upon the time of year and specific location.

IV. ANALYSIS OF DATA

The data base for this study consisted of 10,269 Secchi
data points. The 9,986 Secchi data points from NODC were
recorded on magnetic tape, while the remaining 283 Secchi
data points were punched on computer cards. Associated with
each Secchi data point were latitude, longitude, Secchi depth,
year, month, date, Greenwich mean time, and a code number
representing the nationality of the vessel. The bottom depth
was often included.

The greatest concentration of Secchi points is in the
northern latitudes close to Japan. This reflects Japanese
interest in using Secchi depths for fisheries research and
other purposes. There is a moderately high concentration
of data points in the South China Sea and the Pacific Ocean.
Data points become sparser in eastern Indonesian waters and
are very sparse in the Indian Ocean. There are particularly
dense concentrations in the Gulf of Thailand near Bangkok,
in the Java Sea near Jakarta, and in the Malacca Strait.

A. VARIATION OF SECCHI DEPTH BY MONTH AND WATER DEPTH FOR EACH BODY OF WATER

An analysis was done to determine the seasonal variation
of water transparency throughout the Southeast Asian region.

Because of the large area being investigated and because of the wide variations in bottom topography, winds, currents, and precipitation throughout the Southeast Asian area, it was necessary to subdivide the area into a number of smaller regions for data analysis, as shown in Figure 13. In general, each individual sea was studied separately. The boundaries between regions were made to conform approximately to the International Hydrographic Bureau specifications of limits between seas (International Hydrographic Bureau, 1953). The South China Sea and the Northwest Pacific Ocean were each subdivided into three sections because of their large size.

The Secchi data points were further subdivided according to bottom depth. Waters which are closer to land and have shallower sea bottoms are subject to oceanographic phenomena which tend to increase turbidity. Thus the data points were placed into five separate categories depending upon their bottom depth: 0-50 m, 50-100 m, 100-200 m, 200-1000 m, and greater than 1000 m. The bottom depths of some Secchi data points were unknown; these data points were not used in this portion of the analysis.

For each body of water and for each bottom depth range, the following information was computed for each month of the year: average Secchi depth, standard deviation, and number of data points used. This information is plotted in Figures 14 through 19. In each figure, the abscissa represents the months of the year from January through the entire year and the ordinate represents the Secchi depth in meters. For each

45

month with two or more Secchi depths, a vertical bar is plotted; the midpoint of the bar represents the average Secchi depth, while the upper and lower ends of the bar represent the average Secchi depth plus and minus one standard deviation. The number of data points used in the computation for each particular month is written along the abscissa above the symbol for the month.

This method of analysis is most valid for a small geographical area with a high concentration of data points. In such a case, any change in Secchi depth observed from season to season is known to be due to temporal change of transparency and not to change in location of the Secchi data points.

There are certain dangers when this type of analysis is extended to entire seas and other large bodies of water. First, Secchi depths might have been taken in different parts of the sea in each season. Thus what may appear to be seasonal changes in the transparency of the sea are actually spatial changes in the transparency from one part of the sea to another. A second problem is that many of the seasonal changes are quite localized. When Secchi depths are averaged over the entire seas, the local variations cancel each other out, resulting in an apparent uniformity over the year which may hide local seasonal variations.

For these reasons special attention was paid to three areas with a high concentration of data points: (1) the Jakarta approaches in the Java Sea with 224 points; (2) the

46

Bangkok approaches in the Gulf of Thailand, with 661 points; and (3) a two-degree square centered about 29°N 135°E in the North Pacific Ocean, with 940 points.

1. Jakarta Approaches

The yearly variation in Secchi depth for the Jakarta approaches in the Java Sea has two transparency maxima and two minima, Figure 14. The maxima occur in May and December and the minima in September and January.

The reason for this variation in transparency cannot be attributed to turbidity from land runoff, for the area around the Java Sea has one rainy season and one dry season. Jakarta and the other cities located near the Java Sea report a precipitation maximum around January and a minimum around August (Environmental Data Service, 1968). A more likely explanation for the variation in transparency may be wind and wave mixing. The east monsoon lasts from May through October, with the steadiest winds in August. This corresponds roughly with a period of decreasing transparency. The west monsoon lasts from December until February, with the steadiest winds in January. This corresponds with another period of decreasing transparency. It may be that the steadier wind and wave action during this period bring silt and nutrients to the surface, thus decreasing the transparency during these periods (Verwey, 1929).

2. Java Sea

The yearly variation in Secchi depth for the Java
Sea (excluding the data points in the Jakarta appraches
already examined) has the same four-season pattern, Figure 15.
There are transparency minima during the May-October and
December-February monsoon periods and transparency maxima
during the transition months. The Java Sea is shallow,
being part of the Sunda Shelf, and thus wind and wave mixing
have great importance with respect to transparency. The
data suggest the following seasonal scheme: January through
March - low transparency; April through June - high transparency;
July through September - low transparency; October through
December - high transparency.

3. Makassar Strait, Sulawesi Sea, Bali Sea, Flores Sea, Banda Sea, Molukka Sea, Halmahera Sea and Ceram Sea

The sparsity of Secchi depths in these eastern Indo-
nesian waters made it impossible to reach any conclusions
concerning the seasonal variation of transparency. The shallow
western part of the Makassar Strait can be assumed to have
the same general seasonal trends as the Java Sea. But the
rest of the region consists of a series of basins with exten-
sive areas deeper than 3000 meters in which the effects of
wind and wave mixing are less pronounced. Upwelling, which
occurs in the Banda Sea from May through August, may be a
factor.

4. Malacca Strait

All of the Secchi depths in the Malacca Strait were taken during the north monsoon period from December through April, and no conclusions about the seasonal variation can be made.

5. Bangkok Approaches

The yearly variation in Secchi depth for the Bangkok approaches (the Bight of Bangkok) in the Gulf of Thailand suggests high transparency from April through October, Figure 16. However, the large standard deviation bars suggest that this plot be viewed cautiously. The large standard deviations in this case are to be expected considering that Secchi depths were taken from points close inshore at the head of the Bight to points 60 miles south at the mouth of the Bight.

There is a strong riverine influence on the water clarity here. The Chao Phyra River, which drains a large area of Thailand, flows into the head of the Bight. Rainfall throughout the Chao Phrya watershed is close to zero in February, increases as the year progresses, and reaches a peak in September and October. The flow rate of the Chao Phrya River near its mouth is subsequently near zero from January through May, increases slowly through July, and increases rapidly to a peak in October, after which the flow drops off abruptly (Robinson, 1974). This corresponds with the Secchi disc plot (Figure 16), which shows minimum transparency during the months of maximum river flow.

49

6. Gulf of Thailand

The yearly variation in Secchi depth for the Gulf of Thailand (excluding the data points in the Bangkok appraches already examined) suggests no seasonal trend, Figure 17. However it is still quite possible that there are local seasonal variations. One example is the change of turbidity near the Mekong Delta. The outflow of the Mekong River reaches a peak around October and November, is carried into the Gulf of Thailand by the northeast monsoon, and adds to the turbidity in the waters off the Mekong Delta.

7. South China Sea

The yearly variation in Secchi depth was plotted for the northern, central and southern sections of the South China Sea, but the plots have not been included in this report. In shallow waters the plots indicate a possible decrease in transparency from December through February. However, in different seasons the Secchi depths were collected in different localities within the South China Sea and this may account for the apparent change in average transparency indicated by the plots. With this type of analysis, the exact nature of the seasonal variation in transparency within the South China Sea cannot be established, since an apparent change in average transparency may be due to a change in location of the Secchi measurements.

8. Pacific Ocean (29°N 135°E)

A study of the yearly variation in Secchi depths was made for the two-degree square centered on 29°N x 135°E because of the tremendous number of data points around this position. The seasonal variation is shown in Figure 18. The Secchi depths form a sine-like pattern with the highest transparency in August and the lowest in February.

Uda (1955) showed the same type of annual transparency variation for Secchi depths taken along 30°N between 130°E and 160°E. The reasons for this annual variation, with a maximum transparency in August and a minimum in February, are not clear. The position 29°N x 135°E is located in the westward Kuroshio Countercurrent, the present knowledge of which is still rather limited. The Kuroshio Countercurrent forms the southern part of an eddy located south of Japan.

The Kuroshio flows eastward along the southern coast of Japan. Some parts of the Kuroshio seem to turn southward between 138° and 140° E and then turn westward, forming the Kuroshio Countercurrent (Rikiishi and Yoshida, 1974). The exact nature of the annual variation of this eddy system is not known. In particular, the seasonal variation of the direction and speed of the Kuroshio Countercurrent is not known precisely. Uda and Hasunama (1969) published charts showing a general westward trend of the countercurrent at 29°N x 135°W during the entire year. But Uda (1955) stated that the Kuroshio Countercurrent appears to flow southerly more strongly as the winter monsoon becomes stronger.

Since the precise configuration of the current
system over the entire year is not known, it is not possible
to give a definite reason for the observed variation in
transparency. If the currents vary so that turbid water from
the north, richer in nutrients, flows into the area during
the winter months, this might account for the decrease in
transparency during that period.

9. Pacific Ocean ($20^\circ N$ - $30^\circ N$)

The yearly variation in Secchi depths for the deep-
water portion of the Pacific Ocean from $20^\circ N$ to $30^\circ N$ and
west of $140^\circ E$ is shown in Figure 19. This whole region
exhibits the same general pattern shown in Figure 18. There
is a definite seasonal fluctuation, with higher-than-average
transparencies from June through October, and lower-than-
average transparencies from November through May.

10. Pacific Ocean ($10^\circ N$ - $20^\circ N$ and $2^\circ S$ - $10^\circ N$)

The deep-water portions of the Pacific Ocean from
$10^\circ N$ to $20^\circ N$ and from $2^\circ S$ to $10^\circ N$ have fairly similar annual
variations. Each region has two transparency minima, one
at June and July and the other at December, with Secchi
depths of about 30 m. The transparency maxima have Secchi
depths of about 38 m.

B. SEASONAL AND ANNUAL PLOTS OF SECCHI DEPTH FOR EACH BODY
    OF WATER

Contour charts of Secchi depths were produced for each

body of water within the Southeast Asian area. The limits

of each chart are shown in Figure 20, with the figure number

of each chart indicated. The contour charts themselves are

shown in Figures 21 through 59. Each Secchi depth was

rounded to the nearest meter and plotted by a Versatec

electrostatic plotter on a Mercator projection at the pre-

cise position of the Secchi depth. When two or more Secchi

depths were close enough to result in overprints, the computer

program averaged the adjacent Secchi depths and plotted the

average Secchi depth at a mean location to prevent overlaps.

Latitude and longitude scales, shorelines, and 100-fm

depth curves were added manually. Secchi-depth contour lines

were drawn at 10-m intervals. In general, the contour lines

were drawn to follow closely the Secchi depths as shown on

the charts. This has led to irregular contour patterns in

many instances. However, it was felt that this manner of

presentation would emphasize the patchiness of transparency

which normally exists in the waters. Transparency at any

location changes with time; therefore, the contour lines

on these charts provide only a general guide to the actual

transparency at any particular time.

When the Secchi data points in a particular body of

water were numerous enough to allow it, transparency plots

for each season were included. If the method of analysis
described in Section IV.A revealed a definite seasonal trend,
the year was generally divided into seasons in accordance
with the indicated trend. If no trend was revealed, the
year was divided into the following four periods: January-
March, April-June, July-September, October-December. In any
case, an annual plot was usually included along with the
series of seasonal plots. If there was a sparse concentra-
tion of data points for a body of water, only an annual plot
was included.

1. Jakarta Approaches

Large-scale plots of the transparency contours for
the approaches to Jakarta, within the Java Sea, are shown
in Figures 21 through 24. From January through March
(Figure 21) and July through September (Figure 23) there
is decreased transparency over the entire area. During
these months the east and west monsoon winds blow with the
greatest consistency, causing wind and wave mixing and
increased turbidity. From April through June (Figure 22)
and October through December (Figure 24), the transparency
is greater; these months include the two transition periods
between monsoons.

In all four charts the lowest transparencies exist
along the shoreline near Jakarta and also at the northern
edge of the chart area with areas of higher transparency

in between. This corresponds with the bottom topography; a slight trough runs through the middle of the area, with shallower waters to the north and south.

2. Java Sea

Seasonal and annual transparency contours for the Java Sea are shown in Figures 25 through 29. Figure 25 shows a relatively low transparency from January through March; Secchi depths in the central part of the sea reach 15 m. This time period includes the latter part of the west monsoon and the low transparency is a probable result of wind and wave mixing. Figure 26 shows a relatively high transparency from April through June with Secchi depths reacing 28 m. This time period includes the transition period between monsoons. Figure 27 shows another low-transparency period from July through September with Secchi depths reaching 18 m. This time period includes the east monsoon period. Figure 28 shows another high-transparency period from October through December with Secchi depths reaching 28 m. This time period includes the other transition period between monsoons.

Unfortunately, few data points close to the shores of Java and Borneo have been taken, except for the points near Jakarta discussed in Section IV.B.1. The area experiences heavy rainfall from December through March and there is un-doubtedly increased turbidity from river runoff in nearshore waters. This increased nearshore turbidity, however, cannot be documented with existing Secchi data.

55

Secchi data from the entire year is shown in
Figure 29. The extreme patchiness evident in this chart
is caused by the inclusion of data points from all seasons
in the year.

3. Makassar Strait, Flores Sea and Bali Sea

Figure 30 gives the annual contours of transparency
for the Makassar Strait, Flores Sea and Bali Sea. The
western part of the region, being part of the Sunda Shelf,
has the lowest transparency, generally less than 20 m. The
northern Makassar Strait, which is deeper than 2000 m, and
the Flores Sea, which reaches a depth of 5000 m, both have
a higher transparency, generally greater than 20 m.

4. Sulawesi Sea

Figure 31 gived the annual contours of transparency
for the Sulawesi (Celebes) Sea. The deep Sulawesi Sea averages
about 4500 m; its basin has a flat bottom and steep sides.
The waters are oceanic with high transparency. The northern
half of the Sea has Secchi depths in the 30-40 m range, and
the southern half has Secchi depths in the 20-30 m range.

5. Banda Sea

Figure 32 gives the annual contours of transparency
for the Banda Sea. The Sea consists of several deep basins
each having an average depth greater than 4000 m. The Sea

also has a large number of volcanic islands. Most Secchi depths are in the 20-30 m range. There is a large degree of patchiness evident. Some of it may be due to the inclusion of all the seasons on one chart, and some of it may be caused by islands which can produce local areas of high productivity. Although upwelling occurs over large areas of the eastern Banda Sea from May through August under the influence of the southeast monsoon (Wyrtki, 1961), this plot gives no indication of decreased transparency in the eastern Banda Sea.

6. Molukka, Halmahera and Ceram Seas

Figure 33 gives the annual contours of transparency for the Molukka, Halmahera and Ceram Seas. There are two narrow basins within this region: the Molukka Basin within the Molukka Sea, with depths to 4800 m; and the Ceram Basin, north of Ceram Island (Fairbridge, 1966). The Secchi depths in the Molukka Basin are relatively large, being greater than 30 m.

A shelf region west of New Guinea has Secchi depths less than 20 m. Generally, however, the Secchi depths within these three seas are between 20 and 30 m.

There is considerable water flow between the Pacific Ocean and the Banda and Flores Sea to the south, passing through the Molukka, Halmahera and Ceram Seas. This flow reverses itself in each monsoon period (Wyrtki, 1961).

7. Malacca Strait

Figure 34 gives the contours of transparency for the Malacca Strait between December and April. During this period the northeast monsoon is fully developed. North-westward current flow through the strait is at a maximum for the year. The shallowness of the water, the high winds, and the runoff from precipitation cause the transparency to be low. The Secchi depths slowly increase from 1 m near Singapore to 20 m at the 100-fm line at the northwest opening of the Strait. Secchi depths in the open Andaman Sea, to the northwest, are greater than 20 m.

8. Bangkok Approaches

Figure 35 and 36 give two seasonal contours of trans-parency for the Bangkok approaches (the Bight of Bangkok). Figure 35, for the months April through October, shows Secchi depths varying from 1 m at the head of the Bight to 13 m at the mouth. The 10-m contour line extends just within the mouth of the Bight. Figure 36, for the months November through March, shows Secchi depths varying from 3 m near the head of the Bight to 17 m at the mouth. The 10-m contour line now extends well into the Bight. There is a definite increase in transparency throughout the lower two-thirds of the Bight during this time period.

The low transparency from April through October may be due to increased flow of the Chao Phrya River into the Bight, caused by the intense summer monsoon rains.

58

9. Gulf of Thailand

Figure 37 gives the annual contours of transparency
for the Gulf of Thailand. Most of the coastal areas
surrounding the Gulf exhibit Secchi depths of less than 10 m.
Further offshore the Secchi depths are larger, ranging from
10 to 20 m. The central portion of the Gulf has Secchi
depths greater than 20 m, with a maximum of 37 m.

At the southeast entrance to the Gulf is the large
plume of turbid water that flows out from the Mekong Delta
during the latter part of the year.

10. South China Sea (Southern Section)

Because of its large size the South China Sea was
divided into three sections. Figures 38 through 42 give
the seasonal and annual transparency contours for the
southern third of the South China Sea.

This section of the South China Sea, being part of
the Sunda Shelf, is generally shallower than 100 m. The
depth gradually increases from south to north. An examina-
tion of the four seasonal charts (Figures 38 through 41)
shows that Secchi depths were taken in completely different
areas in different parts of the year, occasionally making
it impossible to note the seasonal changes in specific loca-
tions. From examination of the available data, it appears
that there is little seasonal variation in Secchi depth. Both
the 10-m contour line and the 20-m contour line retain their

general positions throughout the year. There is no evidence of the sort of seasonal variation of transparency which occurs in the Java Sea.

The west coast of Borneo has fairly high precipitation throughout the year, so there is probably high turbidity along the coast. There are not enough data points to accurately delineate this high-turbidity zone, however.

The transparency in the open sea increases in a northerly direction, corresponding to the increase in bottom depth in a northerly direction.

11. South China Sea (Central Section)

Figures 43 through 47 give the seasonal and annual transparency contours for the central section of the South China Sea. The bottom topography of this section is diverse. It includes the northern reaches of the Sunda Shelf, the southern half of a deep sea basin which attains a depth of 5016 m, and a large number of coral reefs, atolls and banks. In particular, there is one extensive region of islands and reefs west of Palawan and northern Borneo.

Each of the four seasonal charts (Figure 43 through 46) has large gaps devoid of Secchi depths. For this reason it is difficult to discern seasonal trends. The chart for October through December (Figure 46) shows the plume of highly turbid water to the southwest of the Mekong Delta. The outflow of the Mekong River reaches a maximum around October and November, and the turbid water is carried to the southwest

by the wind-induced currents of the northeast monsoon.
This plume is much smaller in the July-September chart
(Figure 45).

There is upwelling off the coast of Vietnam during
the southwest monsoon in the summer months, but there is
insufficient data in this region to indicate any changes
in transparency.

The annual contour chart (Figure 47) gives the most
complete picture of the transparency pattern, although much
patchiness is evident. The waters of the deep sea basin
generally have transparencies in the 20-40 m range.

12. South China Sea (Northern Section)

Figures 48 and 49 give the seasonal transparency
contours for the northern section of the South China Sea.
The northern coast of the Sea has a wide continental shelf
off China and Vietnam. South of the shelf there is the
deep sea basin with its oceanic waters. As Figure 48
shows, many Secchi depths less than 10 m appear along the
China coast and in the Gulf of Tonkin. The Secchi depths
increase with increasing depth, and most Secchi depths
taken in the deep waters are in the 20-40 m range.

There is a lack of data on the wide continental shelf
region along the coast of China, especially for the winter
months. However, the oceanographic factors described by
Chan (1970) suggest that coastal turbidity would increase
in the summer and decrease in the winter. First, the Pearl

River, which empties into the South China Sea near Hong Kong, has its flood cycle from May to October, resulting in decreased transparency during these months. Secondly, the southwest monsoon occuring during the summer inhibits the flow of clear oceanic waters into the South China Sea. The northeast monsoon winds, lasting from November to March, cause an increase of water flow from the Pacific Ocean into the South China Sea. These oceanic waters dominate the whole continental shelf area and can be expected to increase the transparency on the continental shelf during the winter months.

13. <u>East China Sea (South of 30°N)</u>

Figures 50 through 53 give the seasonal contours of transparency for the East China Sea. This sea has two distinct areas, the wide continental shelf and the broad trough extending from Taiwan to Kyushu along the inner side of the Ryukyu island arc (Fairbridge, 1966). The Kuroshio current flows northeastward through the Sea; it enters the Sea east of Taiwan and flows roughly along the 100-fm depth curve. North of 30°N, the main axis of the Kuroshio turns eastward and flows along the south coast of Japan. The Kuroshio is greatly strengthened by the southwest monsoon wind in summer, but is still important in winter.

The Secchi depths increase eastward, being less than 10 m along the China coast and greater than 30 m to the east of the Ryukyu Islands. Outflow from the Yangtze and other

rivers increases the turbidity along the coast. Transparency in the East China Sea is much greater during summer than winter. The 10-m, 20-m, and 30-m contours all shift inland in summer. This may partly be caused by the greater strength of the Kuroshio in the summer, which brings a large infusion of relatively clear tropical water into the East China Sea.

14. Philippine Sea and Pacific Ocean (20°N - 30°N)

Figures 54 through 57 give the seasonal contours of transparency for the Philippine Sea between 20°N and 30°N and east to 140°E. The main oceanographic features in this area, from north to south, are the westward-flowing Kuroshio Countercurrent, the eastward-flowing Subtropical Counter-current, the Subtropical Convergence, and the North Pacific Central Water Mass. The existence of the Subtropical Counter-current was recently established (Uda and Hasunuma, 1969). This feature is believed to occur from 20°N to 25°N.

The Subtropical Convergence marks a break between the relatively transparent Central Pacific water to the south and the more turbid Kuroshio Countercurrent water to the north. This change in transparency is evident in the winter (Figure 54) when the Secchi depths south of 24°N are greater than 30 m and the Secchi depths north of 24°N are less than 30 m. In the summer (Figure 56) Secchi depths tend to be greater than 30 m over the entire area. There is much patchiness but no appreciable north-south variation in transparency in the summer.

15. Philippine Sea and Pacific Ocean ($10°N - 20°N$)

Figure 58 gives the annual contours of transparency for the Philippine Sea between $10°N$ and $20°N$ and east to $140°E$. This area consists of the southern part of the North Pacific Central Water Mass which rotates clockwise in a great gyre. The North Equatorial Current, which flows westward from about $20°N$ to $25°N$, is part of this gyre. Upon reaching the Philippines, the greater part of the North Current turns northward to form the root of the Kuroshio. Some of the current turns southward, either entering the Celebes Sea or becoming part of the eastward Equatorial Countercurrent.

The transparency of this entire region is high, with Secchi depths generally greater than 30 m. In these low latitudes the waters have large negative temperature gradients. With the resulting stratification, depletion of nutrients in the photic zone occurs and little organic production takes place.

16. Philippine Sea and Pacific Ocean ($2°S - 10°N$)

Figure 59 gives the annual contours of transparency for the Philippine Sea and the Pacific Ocean between $2°S$ and $10°N$ and east to $140°E$. The two principal currents in this area are the eastward Equatorial Countercurrent and the westward South Equatorial Current, the latter running just north of the New Guinea coast. The shifting monsoon winds markedly alter the strengths of these currents throughout the year.

The transparency of the northeasternpart of the area
is generally high, with Secchi depths greater than 30 m. In
the southern and western parts of the area the Secchi depths
tend to be less than 20 m. This decrease in transparency
may be due to eddies and divergences caused by the confluence
of the various currents that tend to recirculate nutrients
and increase biological production. The decrease in trans-
parency might also be caused by the movement of less trans-
parent waters with a higher nutrient content from the Indonesian
seas northeastward into the Pacific Ocean.

17. Entire Southeast Asian Waters

Figure 60 gives the annual contours of transparency
for the entire Southeast Asian region. The average Secchi
depth for each one-degree square was calculated with a com-
puter program. Each average Secchi depth was plotted in the
center of the one-degree square and contours were drawn at
10-m intervals. This figure shows the overall transparency
pattern. Secchi depths less than 10 m appear only at some
coastal locations. Secchi depths in the 10-20 m range tend
to cover the shelf regions: the Java Sea, the Gulf of
Thailand, certain parts of the Malacca Strait and the South
China Sea, and the continental shelves of Vietnam and China.
Secchi depths in the 20-30 m range occur in the deeper
enclosed seas: the eastern Indonesian seas, the Andaman
Sea, the South China Sea, and the East China Sea. Secchi
depths in the 30-40 m range occur in the open Pacific and

Indian Oceans. Secchi depths greater than 40 m (to a maximum of 55 m) occur in isolated locations in the open Pacific and Indian Oceans.

C. SEASONAL AND ANNUAL PLOTS OF Kd FOR EACH BODY OF WATER

As mentioned in Section II.B, a Hydrographic Airborne Laser Sounder (HALS) is being developed by the Naval Ocean Research and Development Activity (NORDA) and will be ready for deployment by the Naval Oceanographic Office (NAVOCEANO) in 1981 or 1982. Indonesian waters are a prime candidate for its use. Consequently, the transparency data of the shallower waters near Indonesia and the mainland of Southeast Asia were examined in an attempt to determine the applicability of laser bathymetry to the region.

The capability of a laser bathymetry system is described by the figure of merit Kd, where K is the irradiance attenuation coefficient and d is the bottom depth, as discussed in Section II.B.3. Since the figure of merit for the HALS system specified to be 3.2, it is capable of depth measurement at any location where the product of K and d is less than or equal to 3.2.

A computer program was used to convert each Secchi depth (Z_s) to a depth-averaged irradiance attenuation coefficient (K), using Shannon's formula described in Section II.A.4 (Shannon, 1979). Whenever the depth of water (d) was known, the product Kd was made. This dimensionless figure was then plotted on a Mercator projection at the same position where the Secchi

depth was taken. The value of Kd was rounded to the nearest tenth when Kd was less than ten, and was rounded to the nearest integer when Kd was greater than or equal to ten. When two or more Kd figures were close enough to result in overprints, the computer program averaged the adjacent figures and plotted the average figure at a mean location to prevent overlaps. Latitude and longitude scales, shore-lines, and 100-fm depth curves were added manually.

A series of charts for each body of water resulted with each chart showing the values of Kd at the various locations in the body of water. Since the limit of usability for the HALS system has been specified to be Kd = 3.2, a contour line at 3.2 was drawn on the charts. The charts of Kd are shown in Figures 61 through 78.

A serious limitation of this method of analysis is the paucity of nearshore optical data. There is not enough data to delineate the areas which can be surveyed with laser bathymetry. An example is Figure 68, which shows Kd values in the Java Sea for the entire year. Along the entire north coast of Java, an island more than 600 miles long, there is only a handful of data points. One data point near the east end of the island has a value less than 3.2; a number of data points near the west end have values less than 3.2. In between, there are no data points to indicate that laser bathymetry can be used at all.

However, this by no means implies that laser bathymetry cannot be used in this area. There is strong reason to believe

that laser bathymetry can be a useful surveying method along the entire coast of northern Java. There may well be a band of shallow water extending the entire length of Java which would be surveyable using a laser system. The important point here is that there are not sufficient data presently available to delineate this band. A lack of Kd values less than 3.2 does not necessarily mean that laser bathymetry cannot be done here. This point should be borne in mind when the other charts are examined, many of which have few data points less than 3.2.

Since there is a scarcity of nearshore data, the detailed spatial and temporal variabilities cannot be indicated. Some parts of the nearshore zone may be unsurveyable during the rainy season, for example, when river runoff produces localized areas of high turbidity downstream from the river mouths. These same areas may become surveyable during the dry season.

Another limitation is the small scale of the charts, which makes it more difficult to accurately depict the distance from shore where Kd becomes equal to 3.2.

These limitations should be kept in mind when the Kd charts are examined. The charts show the limits of use of the laser bathymetry system in a very general way, and the locations of the line where Kd is equal to 3.2 is only approximate.

Charts of Kd were produced for all bodies of water containing shallow shelf areas. In some cases a chart was produced for each season of the year; in other cases only an

annual chart was produced. Charts were produced for the Jakarta approaches (Figure 61 through 63), Java Sea (Figures 64 through 68), Makassar Strait (Figure 69), Malacca Strait (Figure 70), the Bangkok approaches (Figures 71 and 72), Gulf of Thailand (Figure 73), South China Sea in three sections (Figures 74 through 77), and East China Sea (Figure 78).

Charts of Kd were not made for the open Pacific Ocean, the Philippine Sea, or the eastern Indonesian seas. Since these bodies of water are quite deep, with the sea bottom dropping off rapidly from the adjacent coastlines, the potential of laser bathymetry in these areas is limited.

An examination of Figures 61 through 78 shows that every body of water with a gently sloping bottom has some localized areas which are surveyable with a laser system. These surveyable areas, in general, do not extend more than 40 to 60 miles offshore, and constitute only a small percentage of the total continental shelf area. Still, a laser bathymetry system may offer advantages of speed, economy and accessibility in surveying these coastal areas. The laser system offers the special advantage of being able to survey the water depth all the way to the shoreline, while sounding vessels cannot safely come close to shore.

As mentioned earlier, the nearshore transparency varies with time, and it would be advisable to consider the seasonal environmental factors which affect the transparency when planning laser bathymetry operations. The rainy season is

least acceptable since heavy precipitation leads to increased river runoff and decreased transparency. The transition periods between monsoons may be preferable to the monsoon seasons themselves since the monsoon seasons bring steady winds which induce wind and wave mixing and decrease transparency. Since a storm may increase turbidity, it may be advisable to wait for several days after a storm before starting survey operations.

The use of satellite data such as that from the Nimbus 7 Coastal Zone Color Scanner (CZCS) may be of value in estimating the average irradiance attenuation coefficient (K) to depths $Z \simeq \frac{1}{K}$. Techniques for such estimates have been suggested by Gordon (1977).

V. CONCLUSIONS

Transparency varies markedly among the various bodies of water in the Southeast Asian region. Inshore areas have Secchi depths less than 10 m. The shallow waters of the Sunda Shelf of western Indonesia and the Continental Shelf of mainland Asia with depths less than 200 m generally have Secchi depths from 10 to 20 m. The deep enclosed seas of eastern Indonesia, the Andaman Sea, the South China Sea, and the East China Sea, have Secchi depths from 20 to 30 m. The open Philippine Sea, Pacific Ocean and Indian Ocean generally have Secchi depths from 30 to 40 m. The open oceans have Secchi depths greater than 40 m to a maximum of 55 m in isolated locations.

Within each body of water transparency is lowest in nearshore regions and increases seaward.

Transparency is subject to seasonal variations. Wind and wave mixing decrease transparency in the shelf regions. In the Sunda Shelf region of western Indonesia, transparency decreases during the two monsoon seasons and increases during the two transition periods.

River runoff decreases transparency in nearshore areas, especially near the mouths of large rivers. This effect occurs during or shortly after the time of heaviest precipitation.

A change in the direction or strength of currents can alter the type of water mass present in the body of water, thus affecting transparency. This occurs in the South China Sea and the East China Sea.

Charts with the product of irradiance attenuation coefficient and water depth (Kd) were made for the bodies of water containing large shelf regions. These charts show that areas with values of Kd which are less than 3.2, and are thus surveyable by the Hydrographic Airborne Laser Sounder, form narrow strips along parts of the coastline. Due to the scarcity of data and the small scale of the charts, the exact dimensions of these strips cannot be ascertained. Also, the limits of the surveyable areas vary over time. The surveyable areas constitute only a small percentage of the total continental shelf regions, but the laser bathymetry systems may still offer advantages of speed, economy and accessibility in surveying these areas.

TABLE I

COMPUTED VALUES OF SYSTEM ATTENUATION COEFFICIENT FOR ALL TEST CONDITIONS (FROM KRUMBOLTZ 1979)

Buoy No.	D	H	K	20	30	40	FOV/SAC 50	60	70	80	C
4 May 1	32.8	500	0.123	0.204	0.176	0.161	0.149	0.142	-	0.134	.452
2	75.5	500	0.140	-	-	-	0.173	0.160	0.149	0.143	.527
3	78.7	500	0.118	0.203	0.191	0.179	0.168	0.177	0.159	0.149	.432
4	88.6	500	0.098	0.191	0.178	-	0.169	-	0.162	0.157	.361
1	32.8	1500	0.123	0.186	0.171	-	-	-	-	-	.452
2	75.5	1500	0.140	0.175	-	-	-	-	0.129	0.129	.527
3	78.7	1500	0.118	0.172	0.161	-	-	-	-	-	.432
5 May 1	19.7	500	0.108	0.198	0.148	0.137	0.138	0.132	0.139	0.132	.335
2	34.4	500	0.190	0.289	0.266	0.244	0.228	0.215	0.217	0.194	.762
1	19.7	1500	0.108	0.162	0.139	0.135	-	-	-	-	.335
2	34.4	1500	0.190	0.229	0.203	-	-	-	-	-	.762

Note: FOV = field of view $[mrad]$; D = water depth $[M]$; H = aircraft altitude $[ft]$; K = diffuse attenuation coefficient $[m^{-1}]$; SAC = system attenuation coefficient $[m^{-1}]$; C = beam attenuation coefficient $[m^{-1}]$

73

$$P_r = P_o e^{-cr}$$
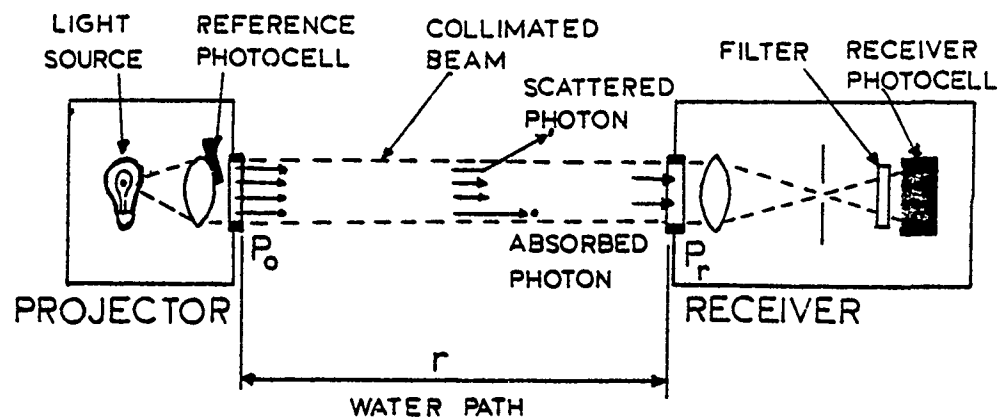
where P_o = initial radiant power

P_r = residual power of unscattered radiation

r = water path length

c = beam attenuation coefficient

FIGURE 1: CONCEPT OF BEAM ATTENUATION
COEFFICIENT (c) MEASUREMENT (from Shannon, 1975)

74

SURFACE
PHOTOSENSOR

H_0

SEA
SURFACE

Z

UNDERWATER
PHOTOSENSOR

H_z
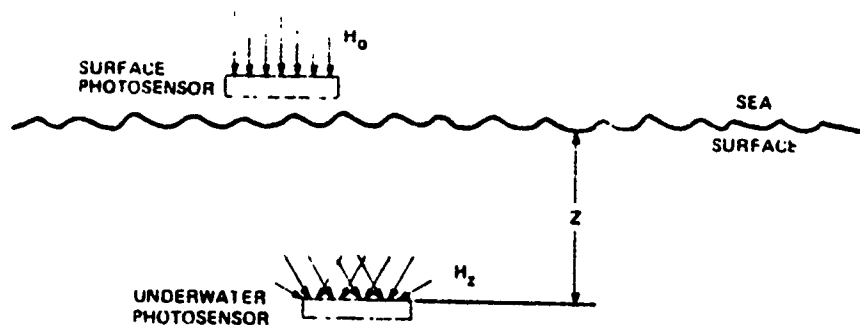
$$H_z = H_0 \, e^{-KZ}$$

WHERE
H_0 = SOLAR IRRADIANCE AT SEA SURFACE

H_z = DOWNWELLING IRRADIANCE AT DEPTH Z

Z = PATH LENGTH (DEPTH) OF MEASUREMENT

K = DIFFUSE ATTENUATION COEFFICIENT OF DAYLIGHT IN SEA WATER

FIGURE 2: CONCEPT OF IRRADIANCE ATTENUATION COEFFICIENT (K) MEASUREMENT (from Shannon, 1975)

75
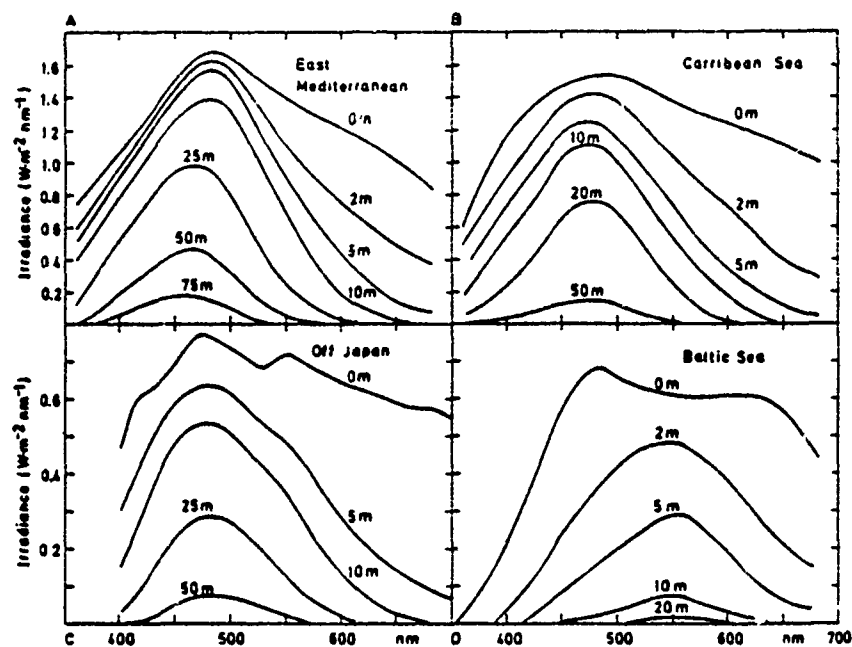
FIGURE 3: SPECTRAL DISTRIBUTION OF DOWNWARD IRRADIANCE
FOR HIGH SOLAR ELEVATIONS (from Jerlov, 1976)

76
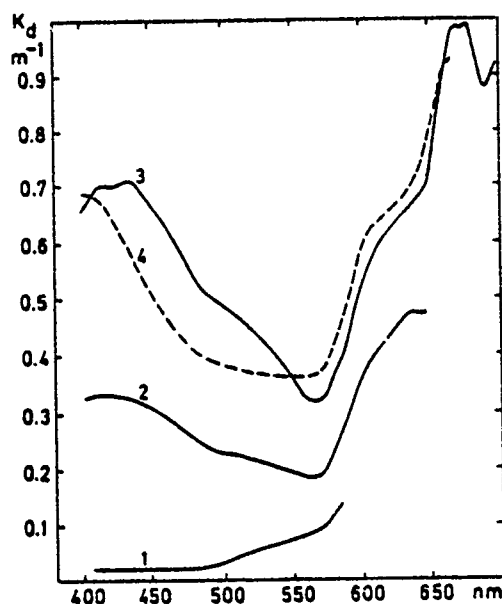
FIGURE 4: THE ATTENUATION COEFFICIENT Kd OF DOWNWARD IRRADIANCE

1 = the Sargasso Sea; 2 and 3 = the upwelling area off West Africa; 4 = close to the African coast (from Jerlov, 1976)
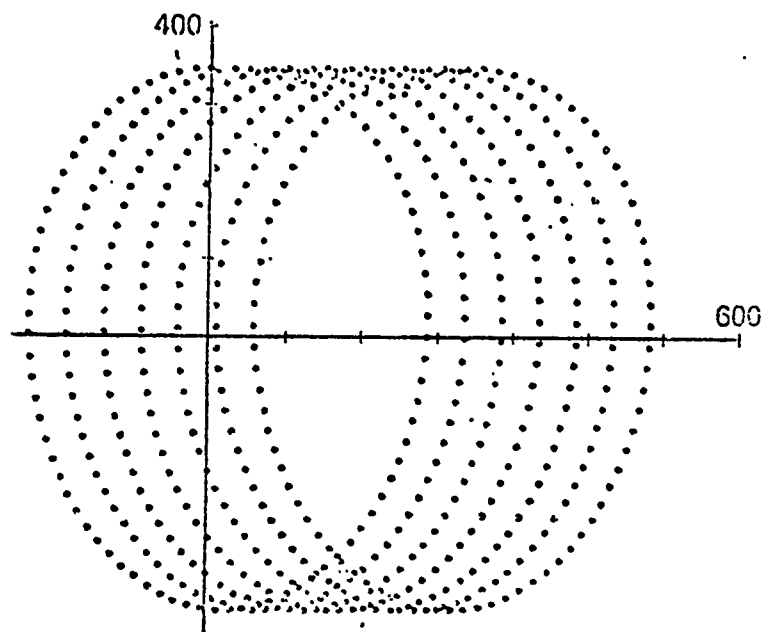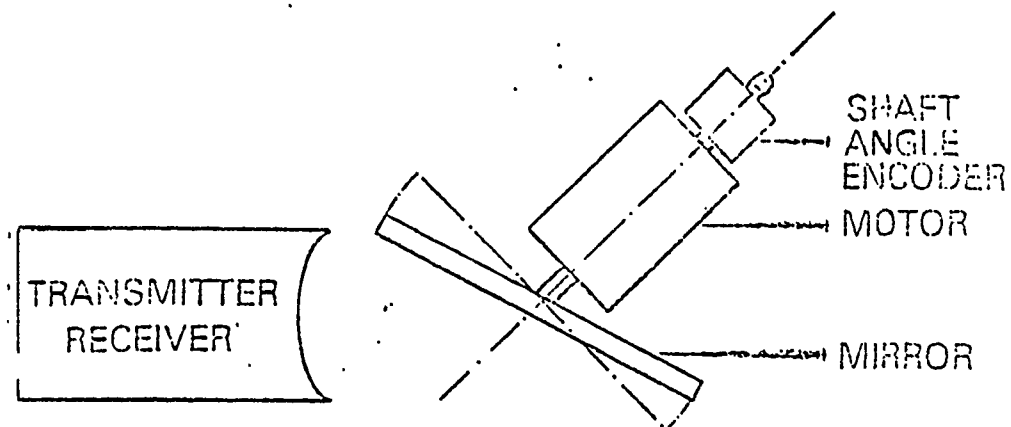
FIGURE 5: NUTATING MIRROR SCANNER SYSTEM AND TYPICAL
SCAN PATTERNS FOR THE HYDROGRAPHIC AIRBORNE
LASER SOUNDER (from NORDA, 1978)
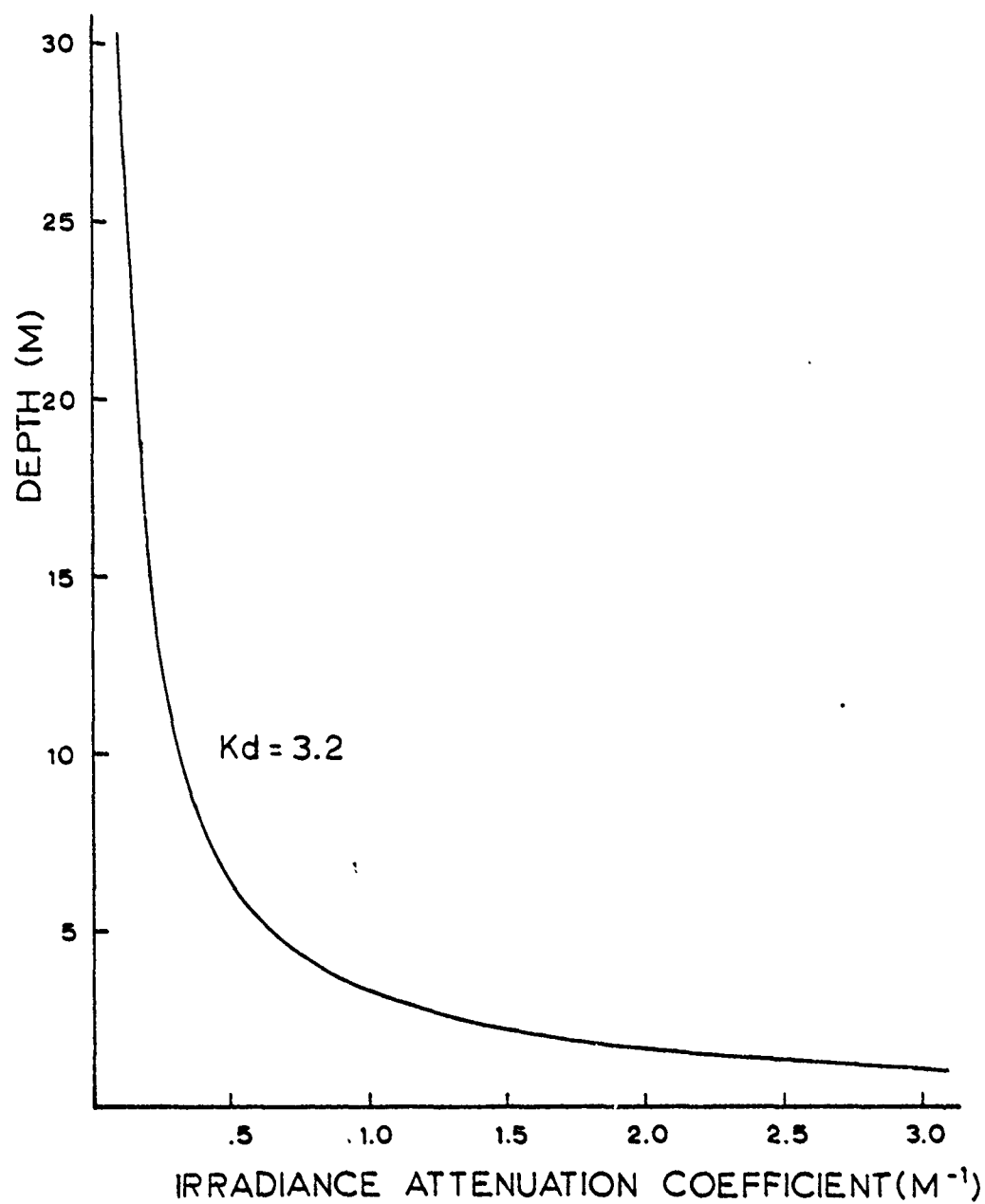
FIGURE 6: PENETRATION CAPABILITY OF A LASER
BATHYMETRY SYSTEM WITH Kd = 3.2
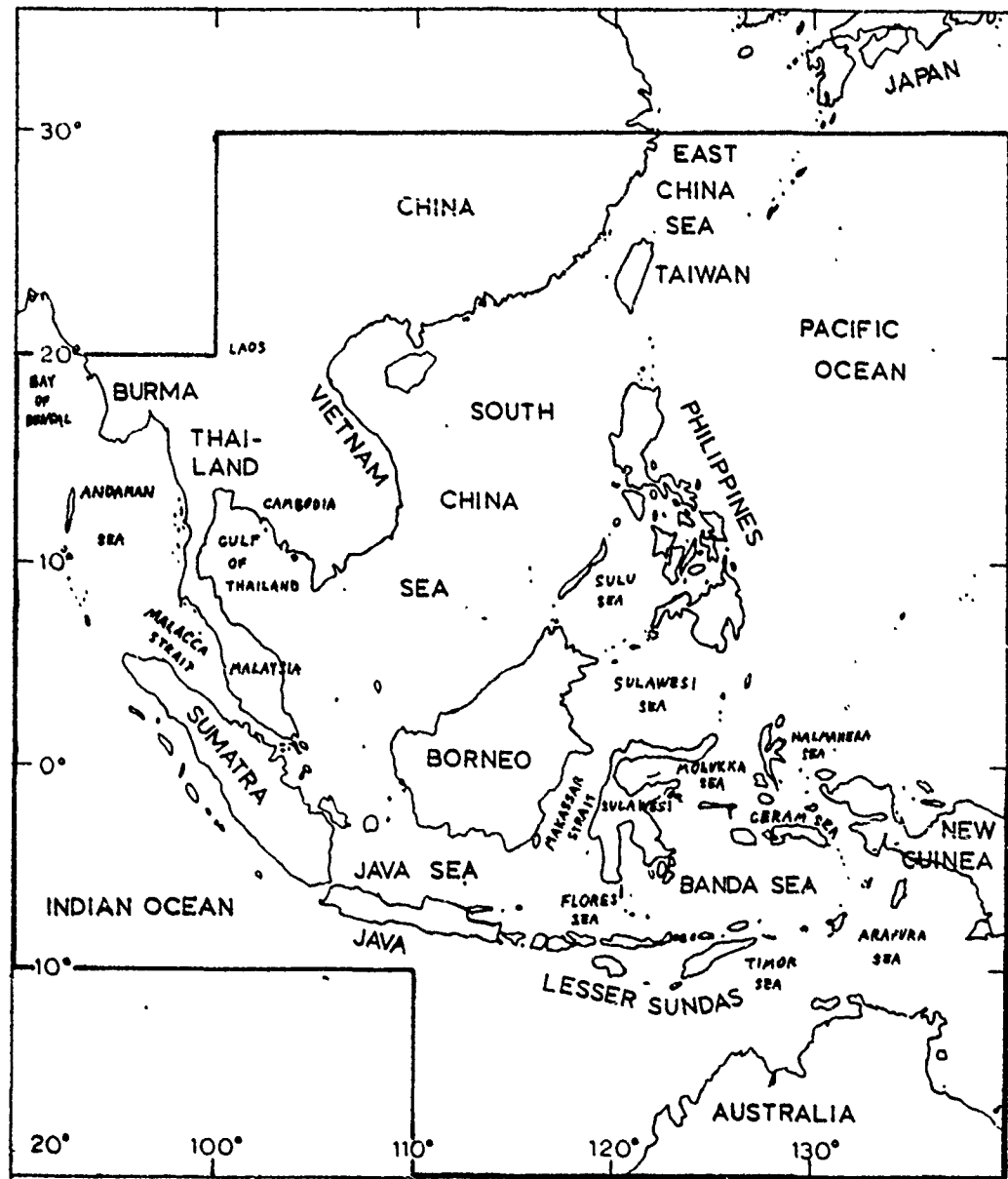
FIGURE 7:   AREA OF INVESTIGATION
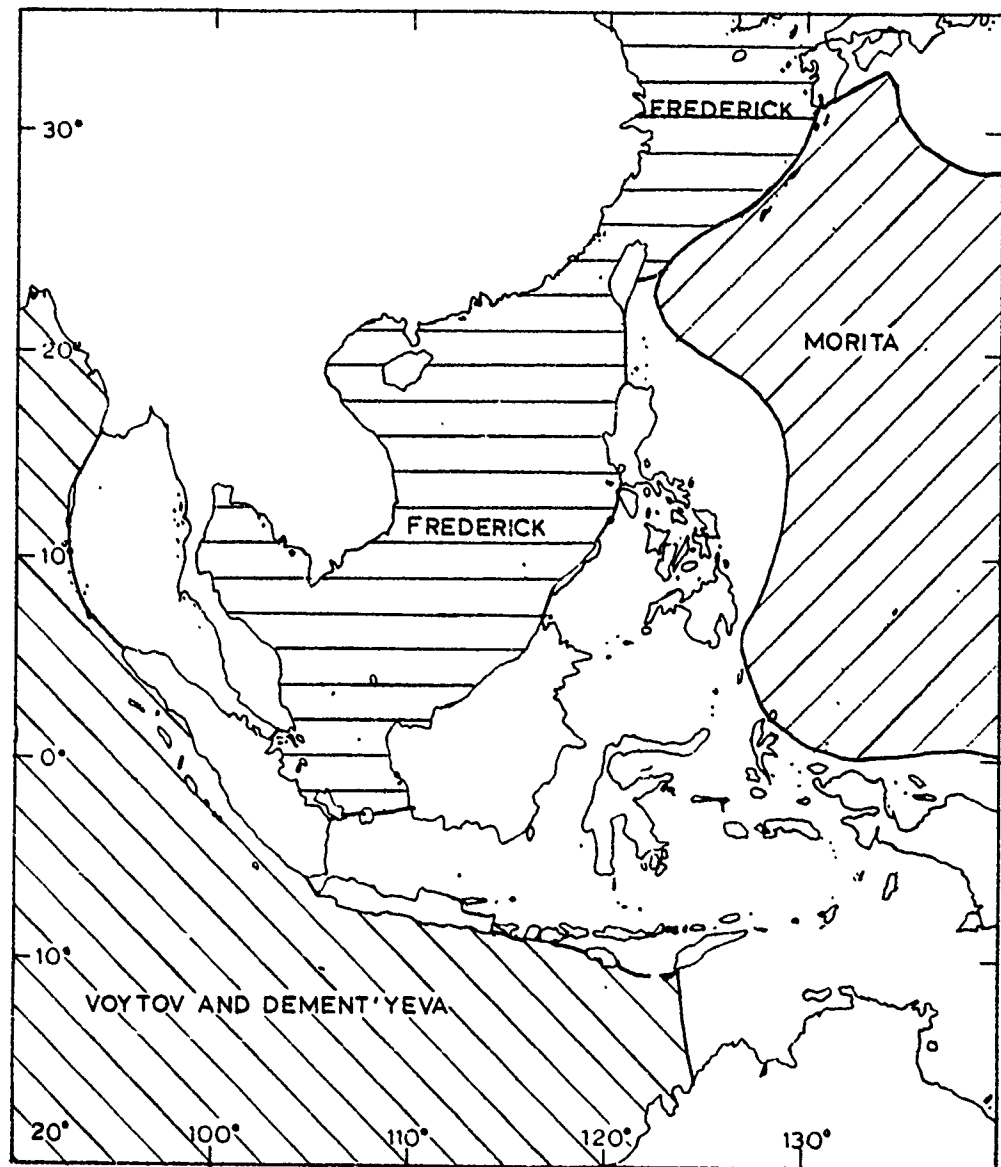
FIGURE 8:   LIMITS OF PREVIOUS INVESTIGATIONS

81
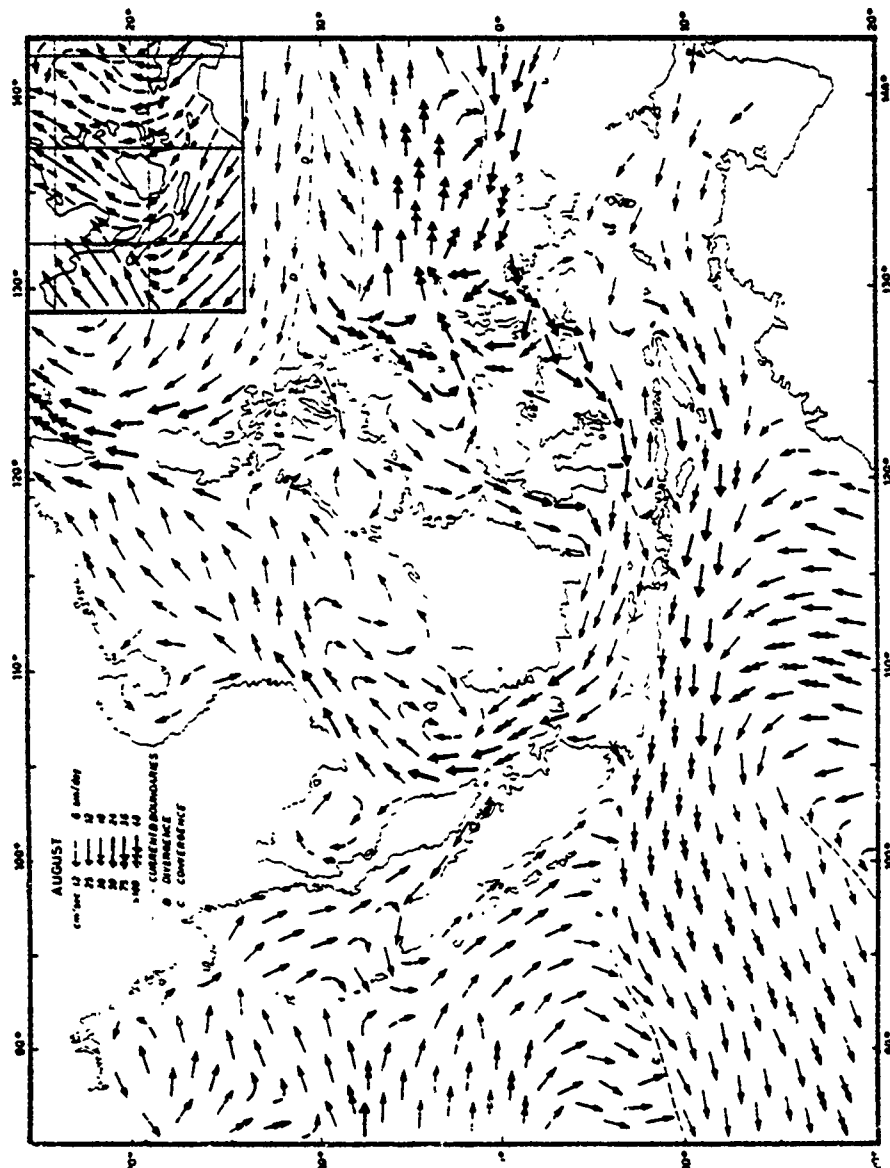
FIGURE 9: SURFACE CURRENTS AND WINDS (UPPER RIGHT HAND CORNER) IN AUGUST
(from Wyrtki, 1961)
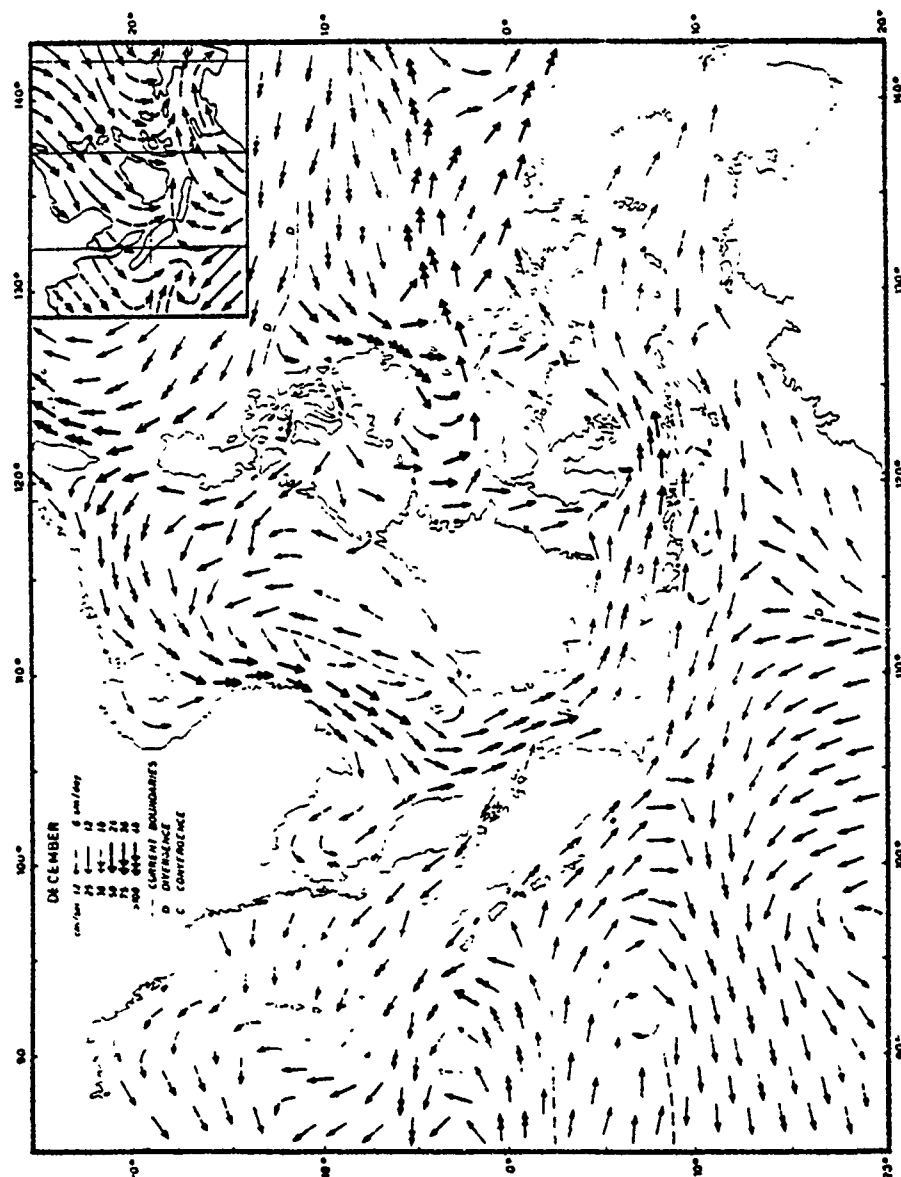
FIGURE 10: SURFACE CURRENTS AND WINDS (UPPER RIGHT HAND CORNER) IN DECEMBER
(from Wyrtki, 1961)
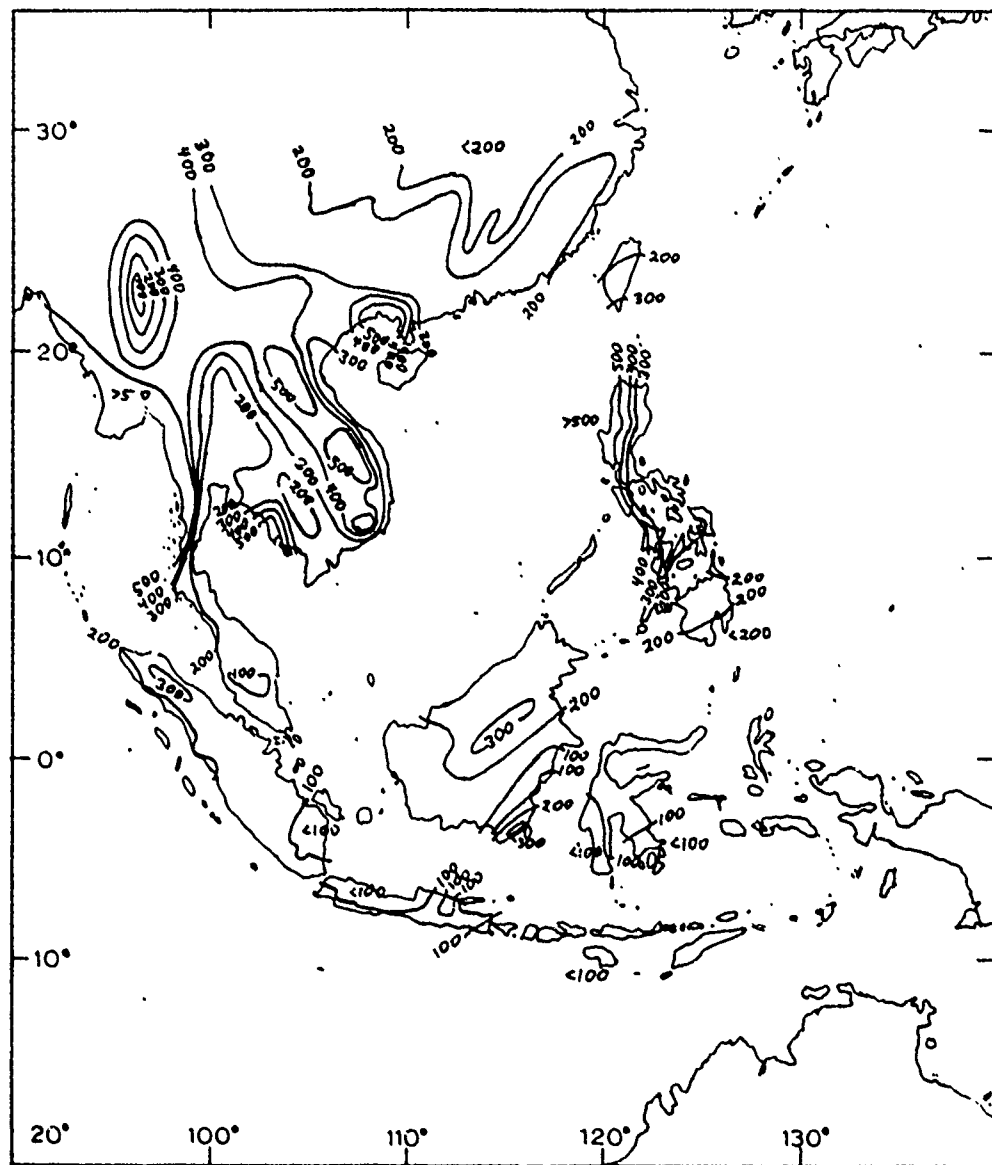
FIGURE 11: RAINFALL IN JULY IN MM
(FROM ATLAS OF SOUTH-EAST ASIA, 1964)
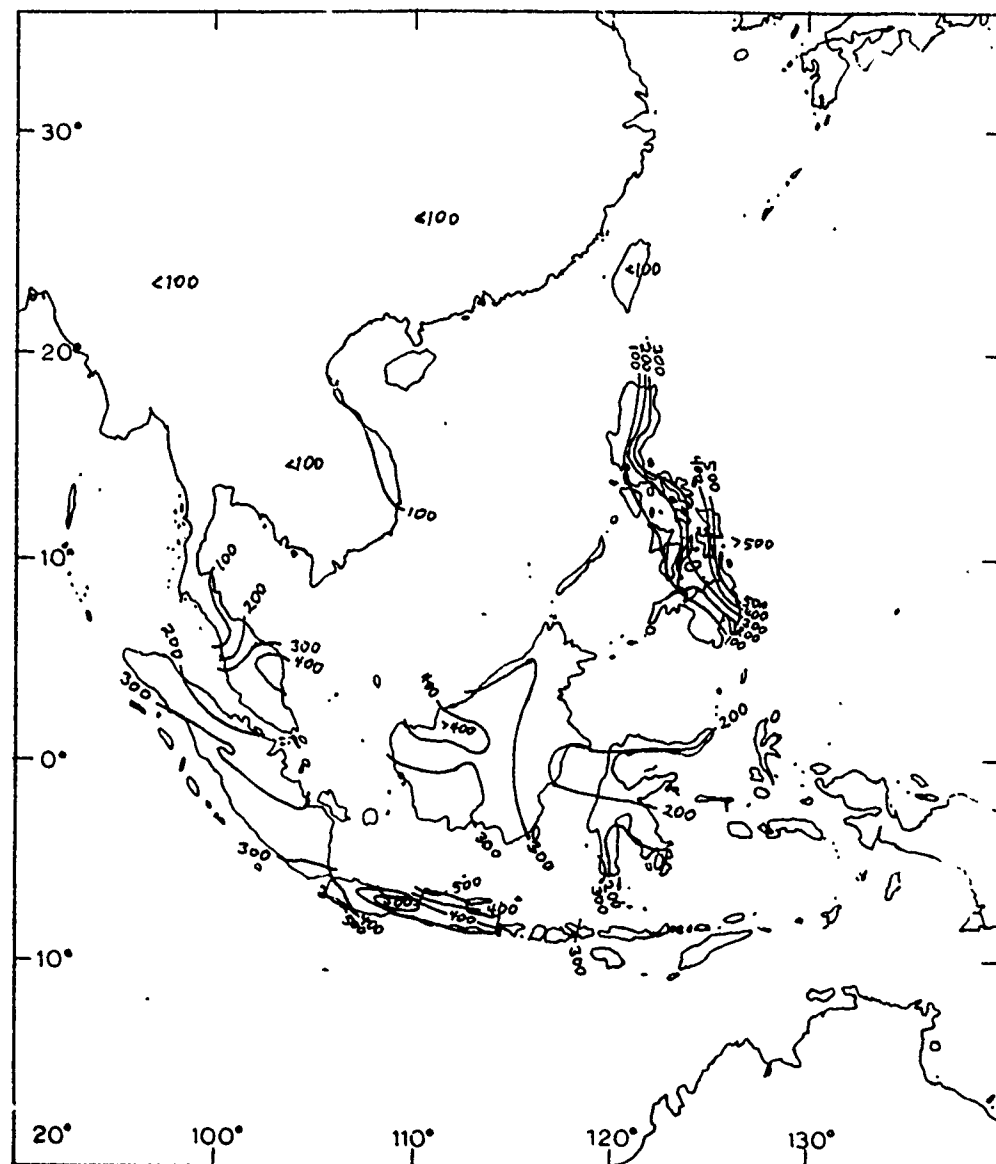
FIGURE 12:   RAINFALL IN JANUARY IN MM
(FROM ATLAS OF SOUTH-EAST ASIA, 1964)
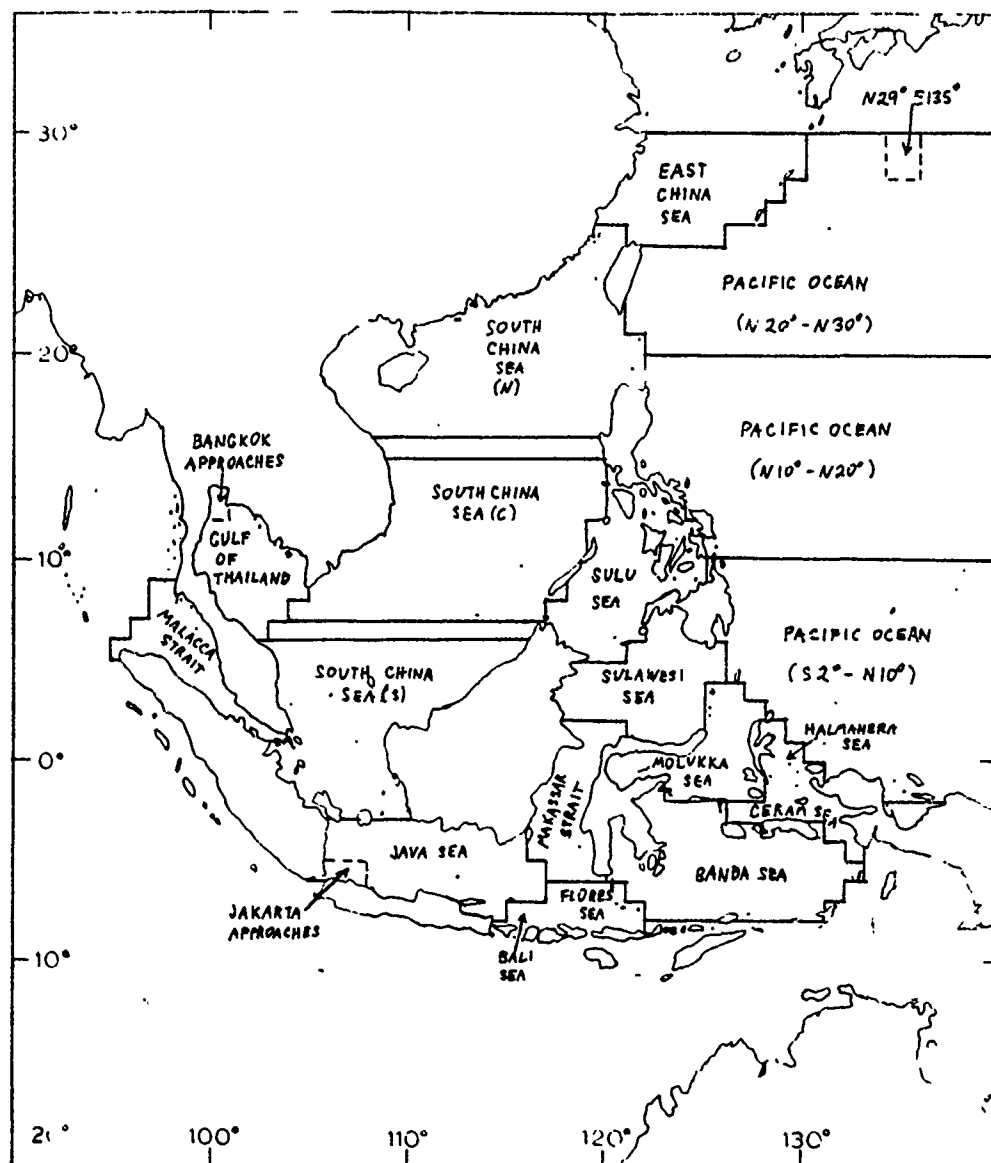
FIGURE 13:   BOUNDARIES OF THE SUBREGIONS USED IN THE
            ANALYSIS OF SEASONAL VARIATION OF TRANSPARENCY
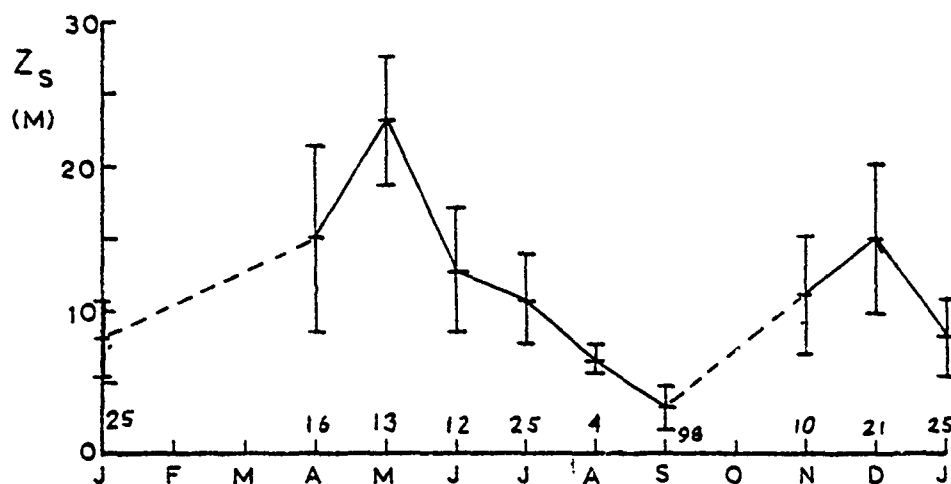
FIGURE 14 : JAKARTA APPROACHES

- SECCHI DEPTHS (METERS)

The number of data points in each month appears along
the abscissa.
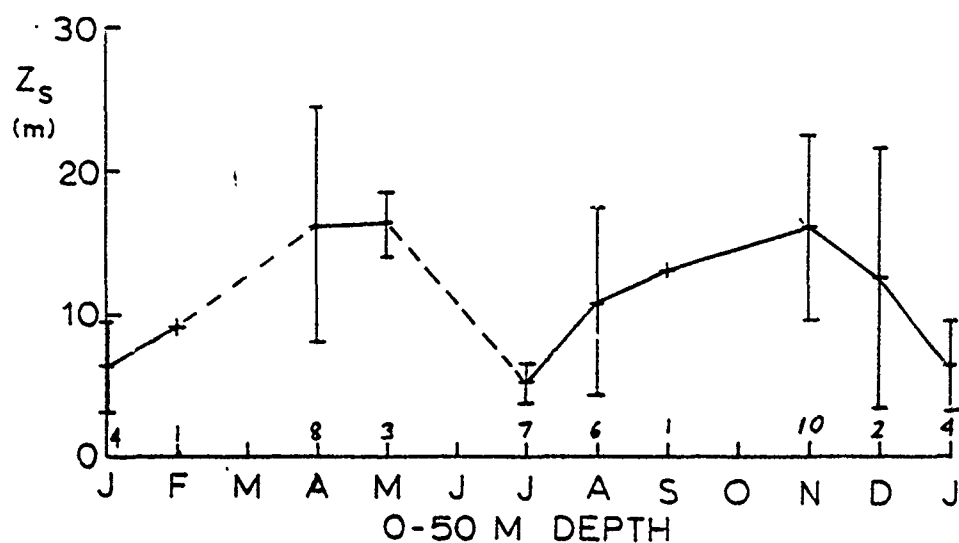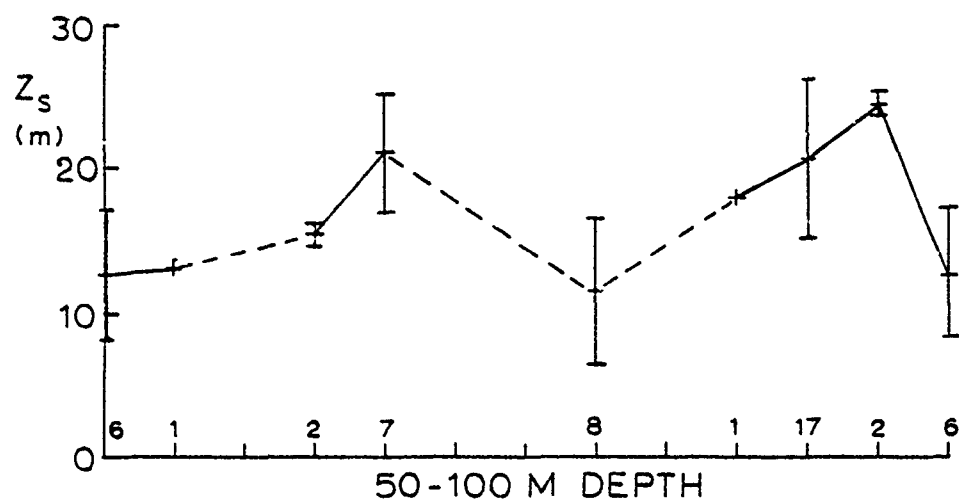
FIGURE 15 : JAVA SEA
(EXCLUDING JAKARTA APPROACHES)

Secchi depths (meters)

The number of data points in each
month appears along the abscissa.
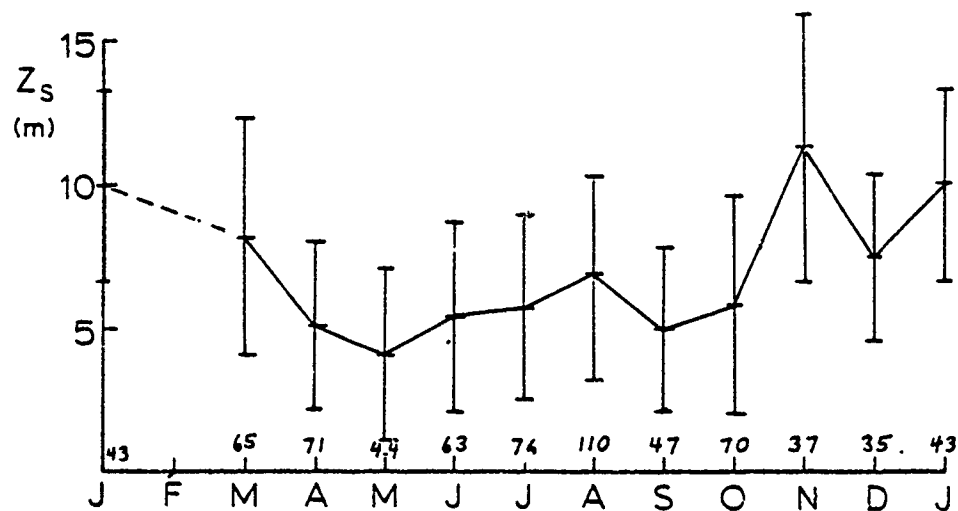
FIGURE 16 : BANGKOK APPROACHES

Secchi depths (meters)

The number of data points in each
month appears along the abscissa.

89
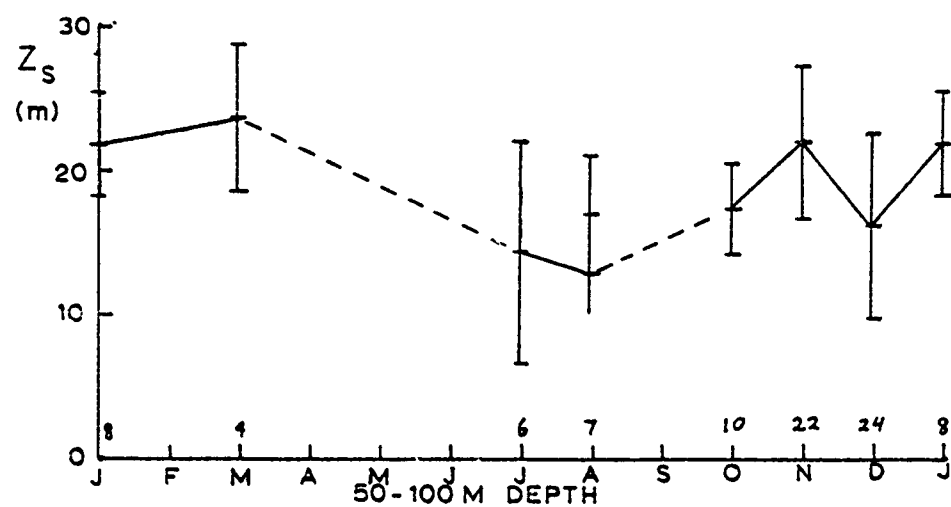
FIGURE 17 : GULF OF THAILAND

Secchi depths (meters)

The number of data points in each month appears along the abscissa.
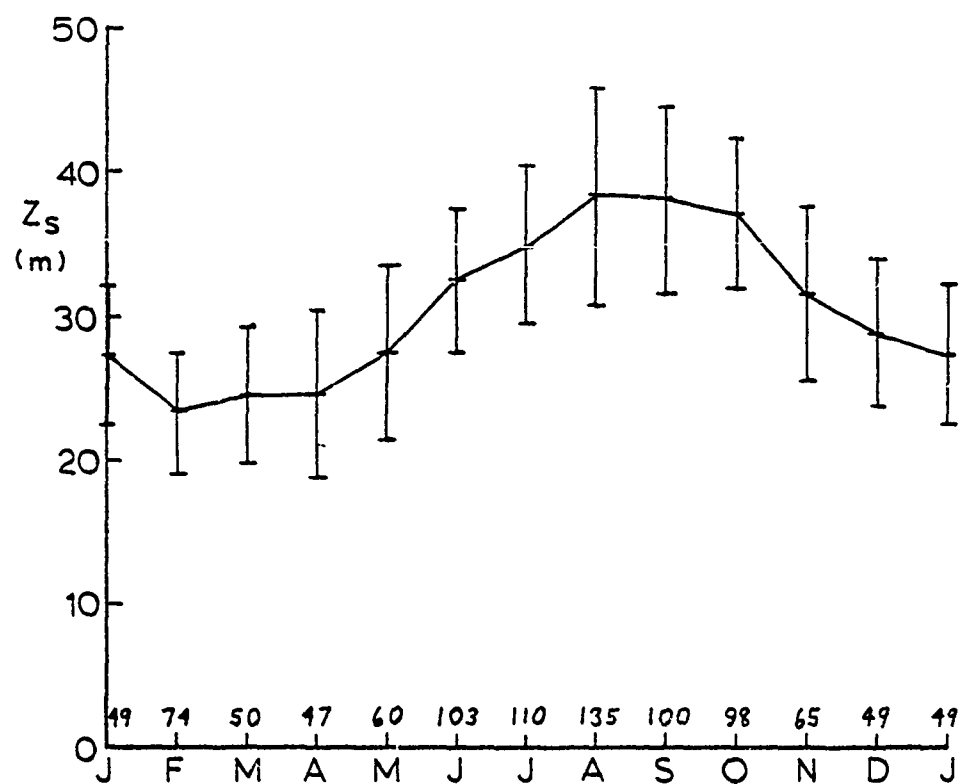
FIGURE 18 : SOUTH OF JAPAN
(N 29° E 135°)

Secchi depths (meters)

The number of data points in each
month appears along the abscissa.

91
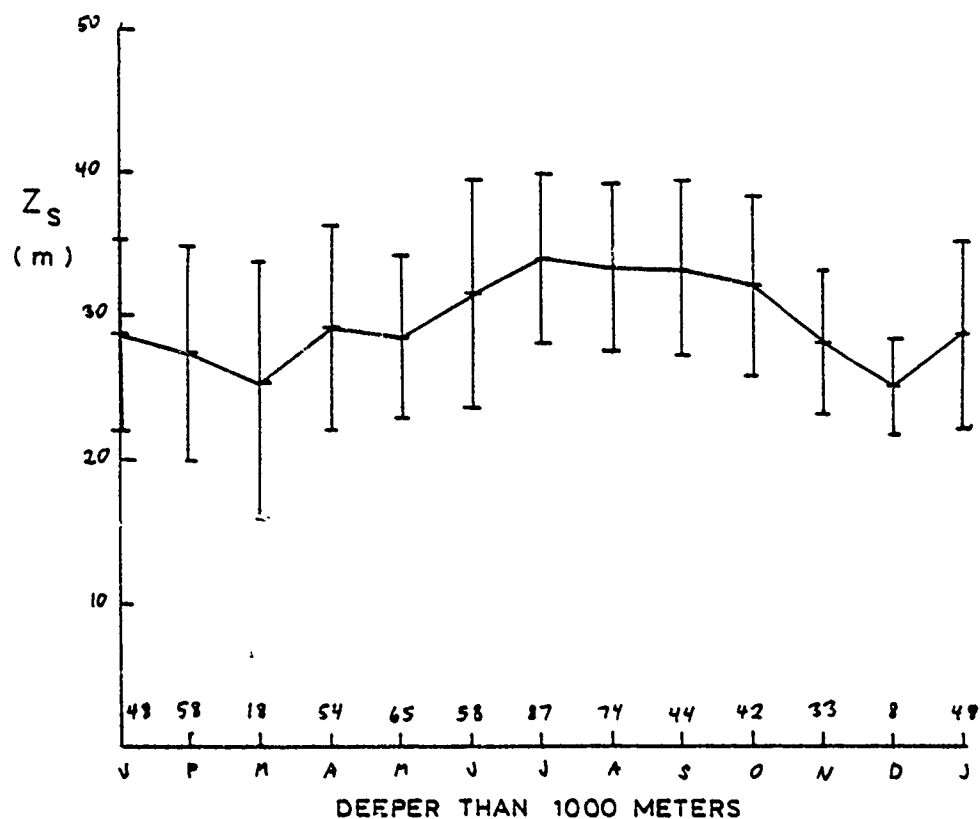
FIGURE 19 :   PACIFIC OCEAN (20°N - 30°N)

Secchi depths (meters)

The number of data points in each
month appears along the abscissa.

92
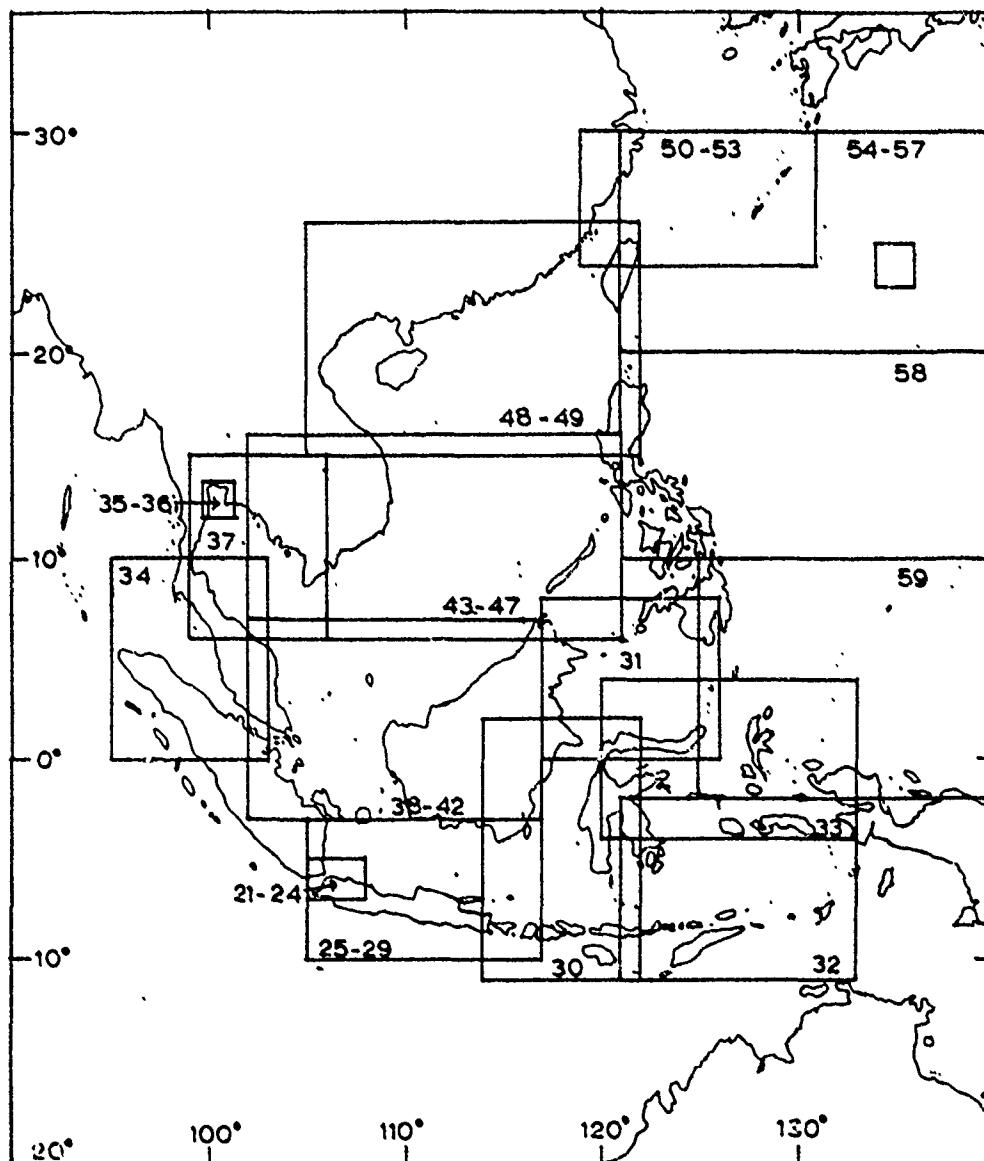
FIGURE 20: LIMITS OF CONTOUR CHARTS OF SECCHI DEPTHS
WITH FIGURE NUMBERS OF CHARTS INDICATED

93
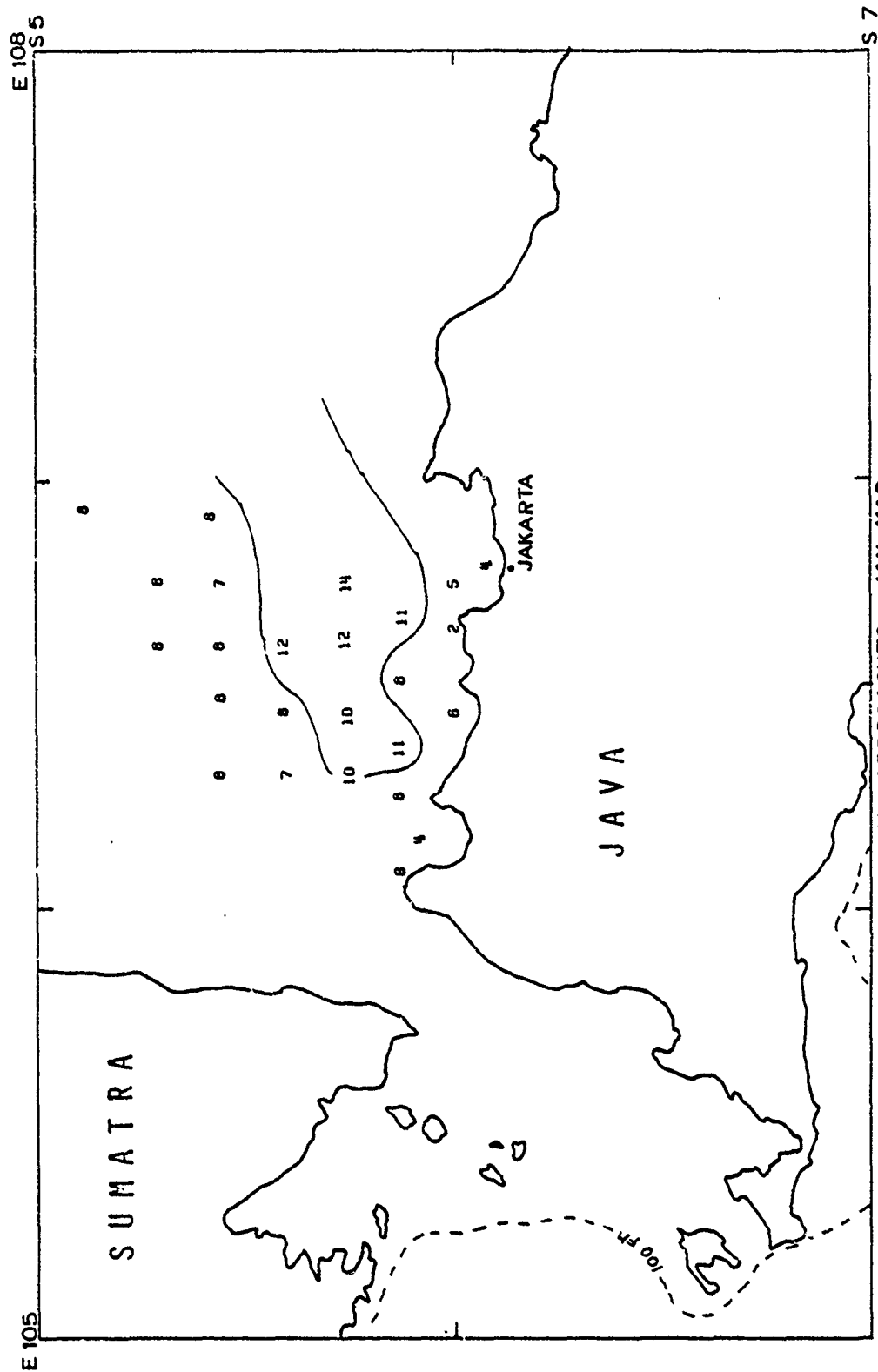
FIGURE 21: SECCHI DEPTHS, JAKARTA APPROACHES, JAN-MAR

94
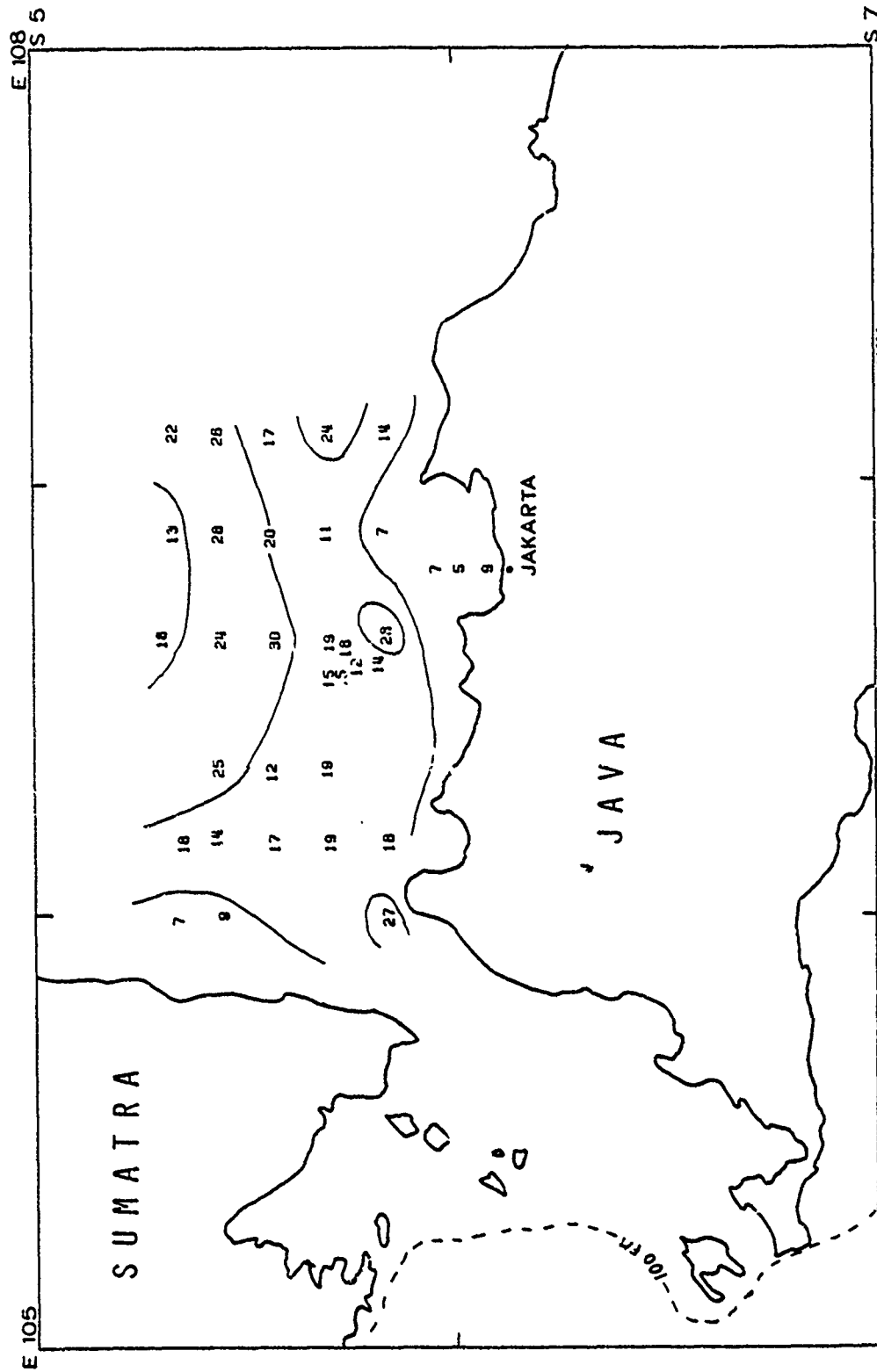
FIGURE 22 : SECCHI DEPTHS, JAKARTA APPROACHES, APP.-JIII

95
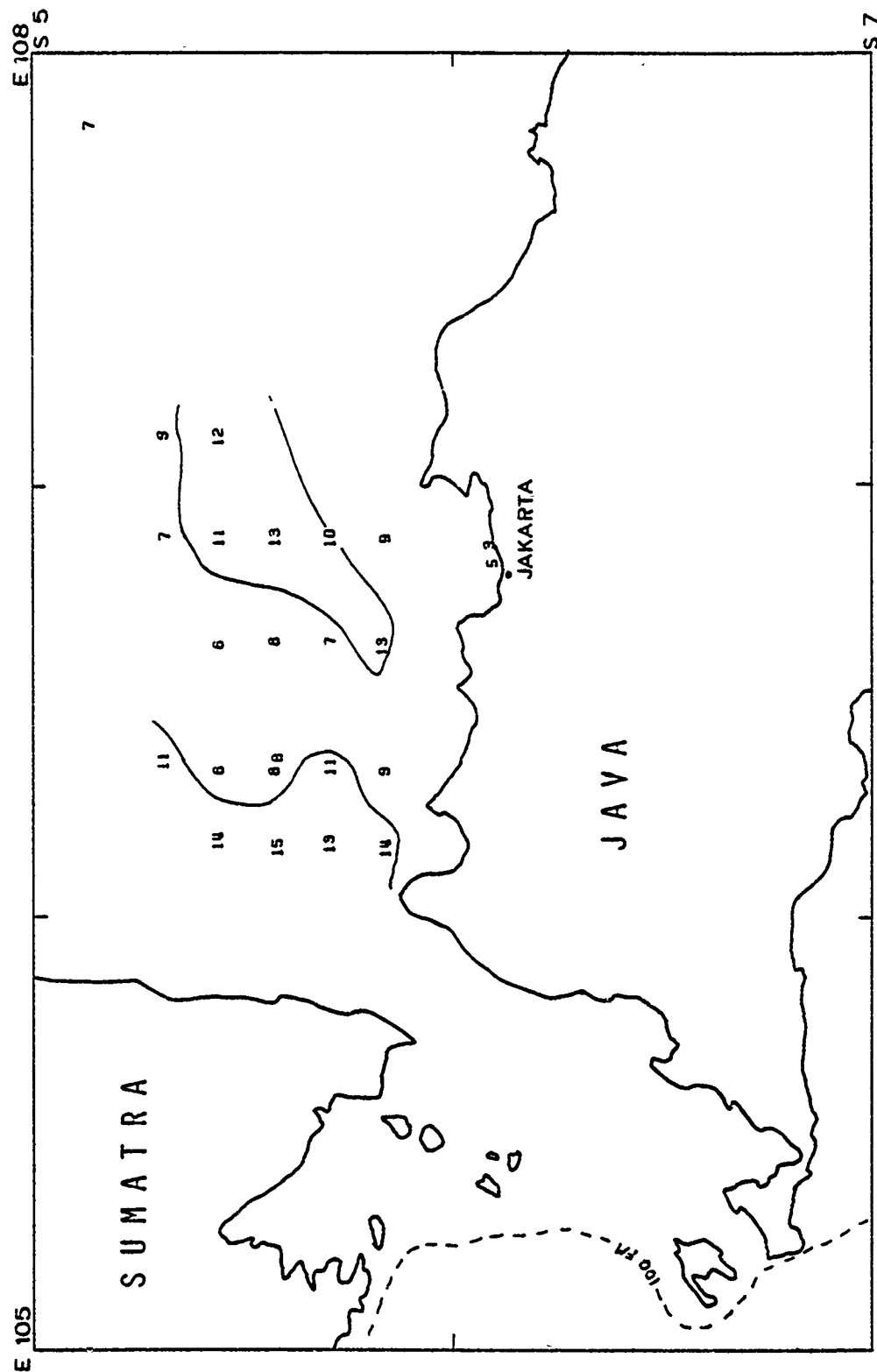
FIGURE 23 : SECCHI DEPTHS, JAKARTA APPROACHES, JUL-SEP

96
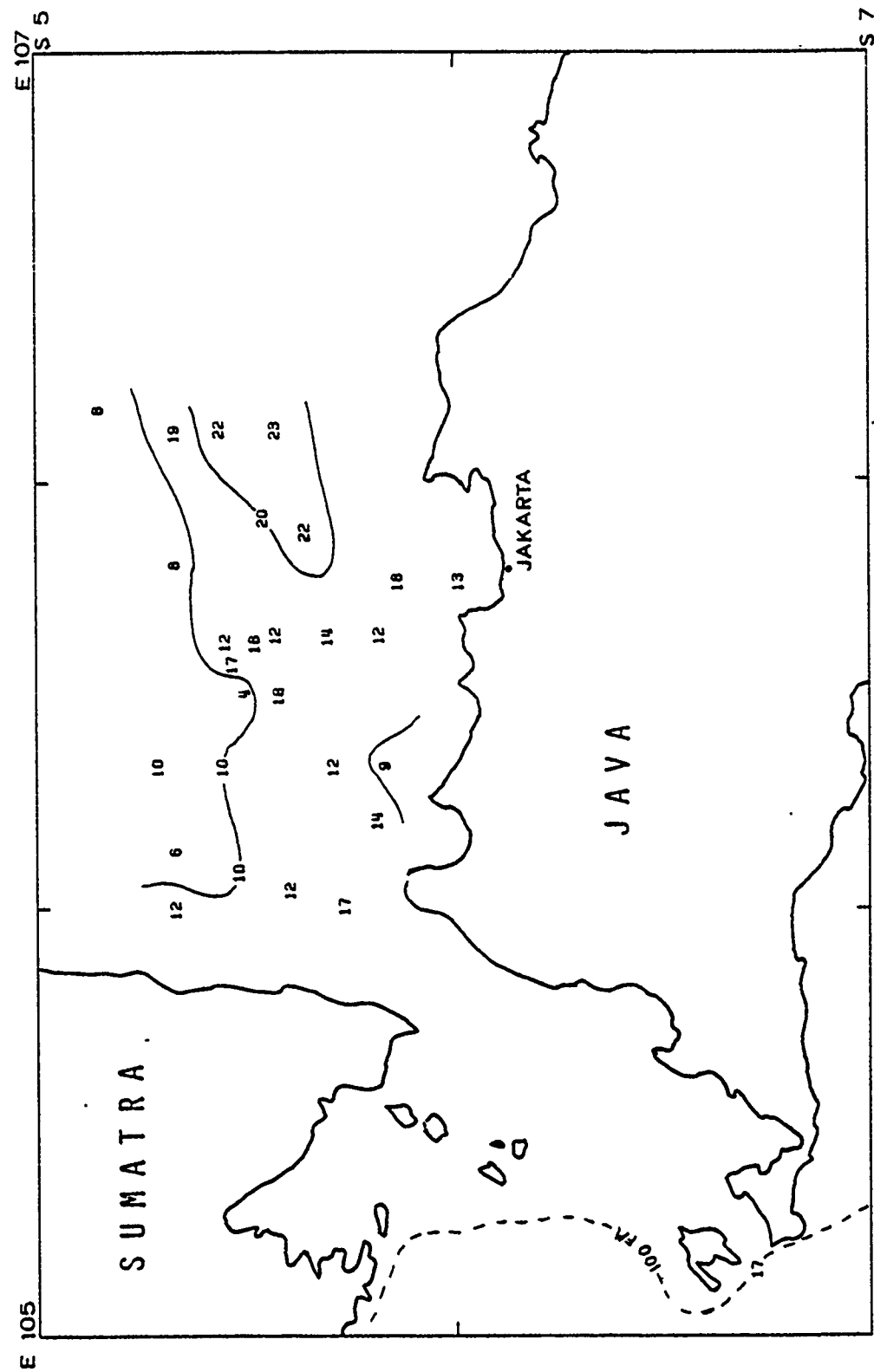
FIGURE 24 : SECCHI DEPTHS, JAKARTA APPROACHES, OCT–DEC
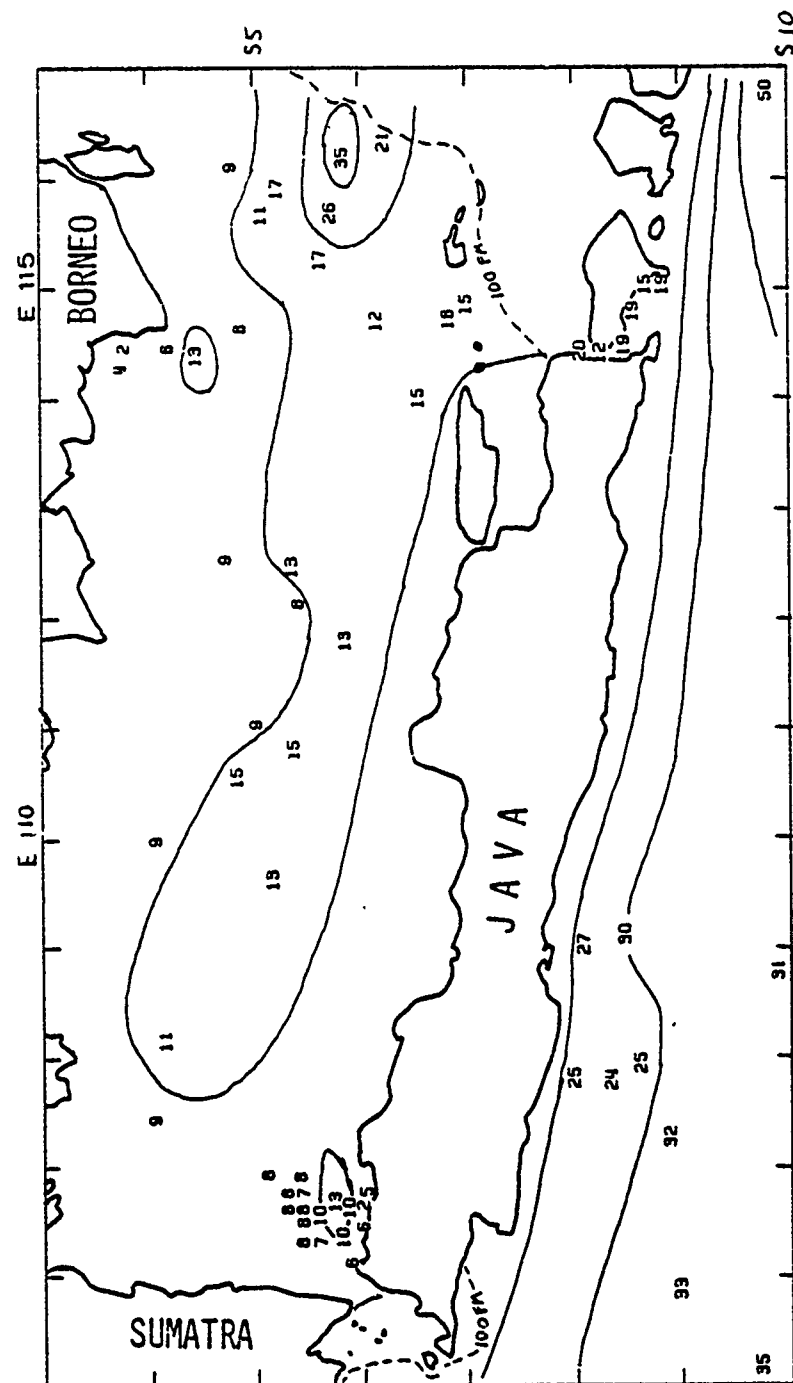
FIGURE 25 : SECCHI DEPTHS, JAVA SEA, JAN-MAR
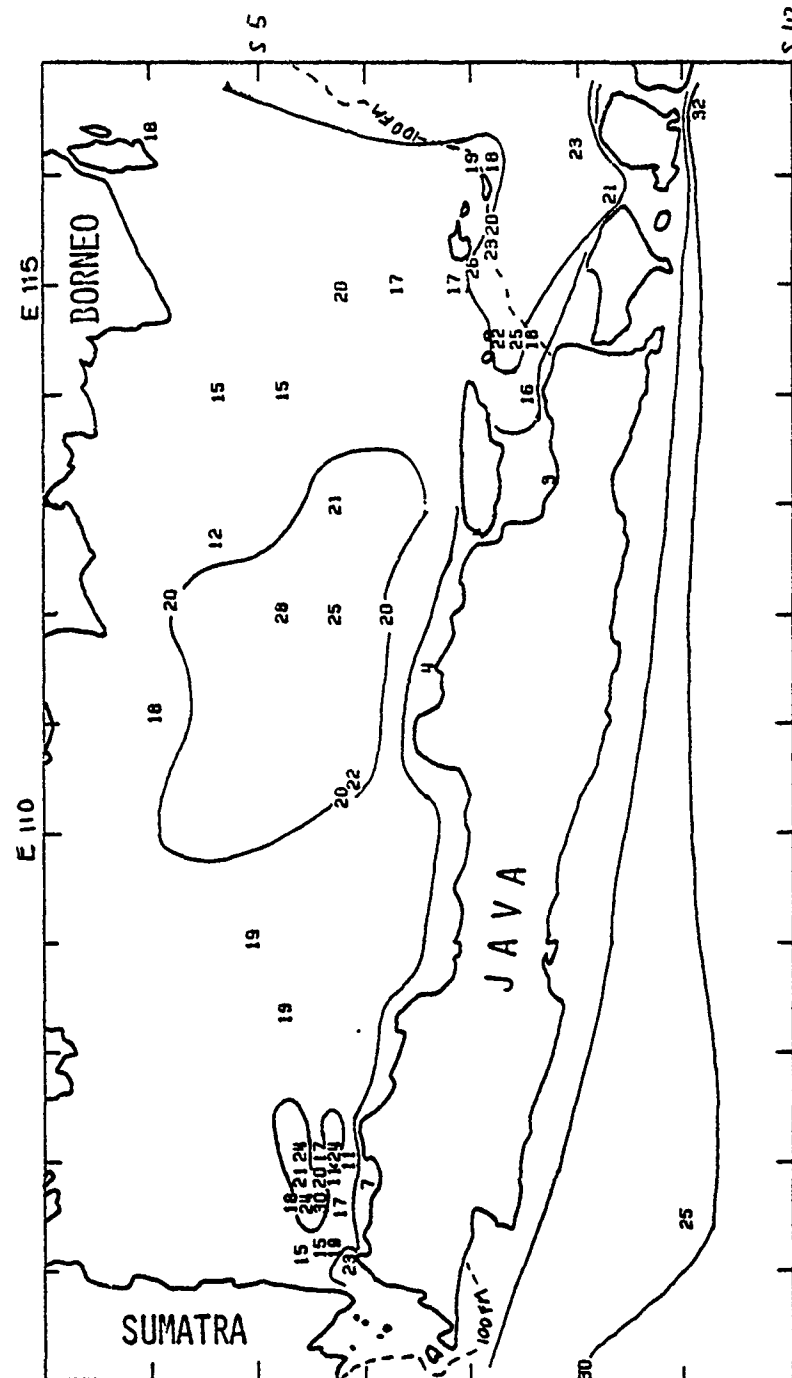
FIGURE 26 : SECCHI DEPTHS, JAVA SEA, APR-JUN
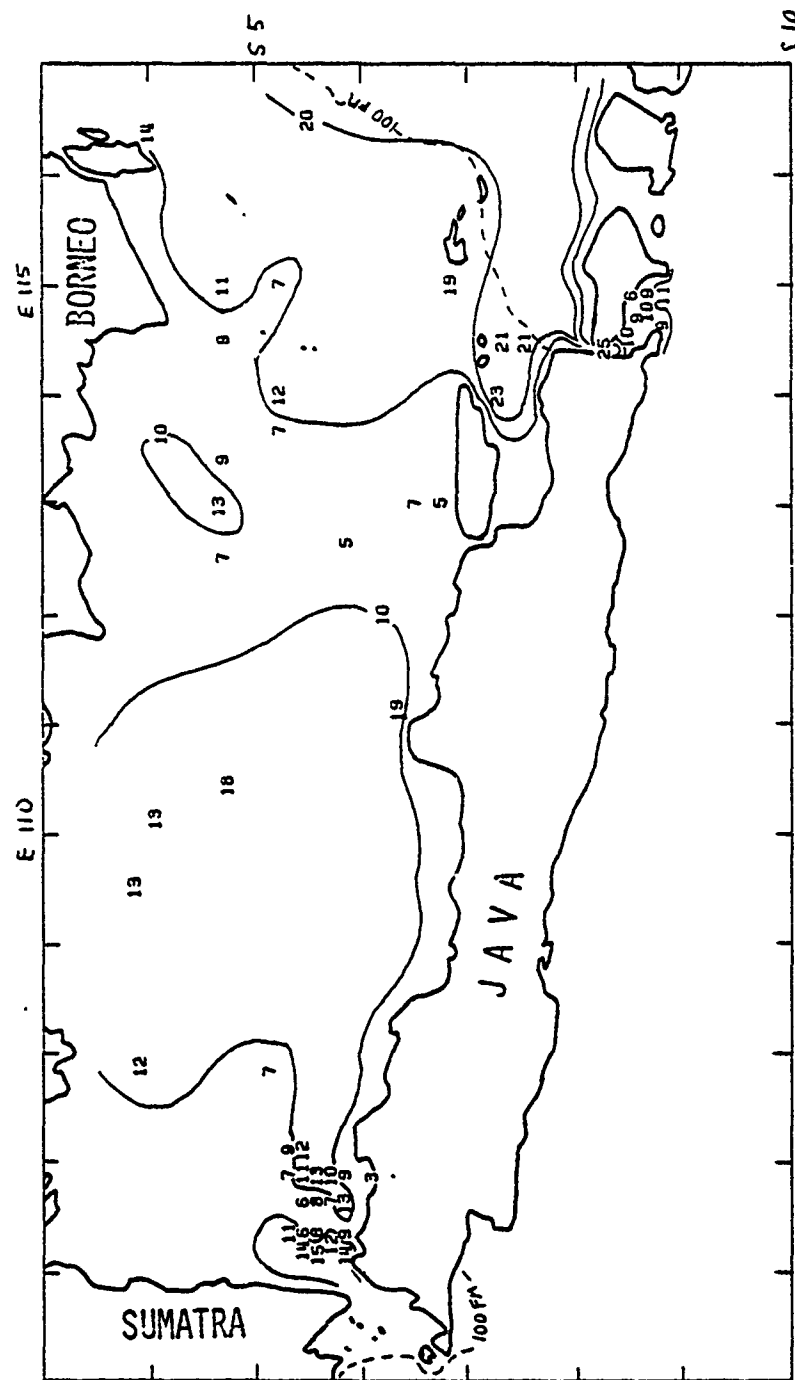
FIGURE 27 : SECCHI DEPTHS, JAVA SEA, JUL-SEP
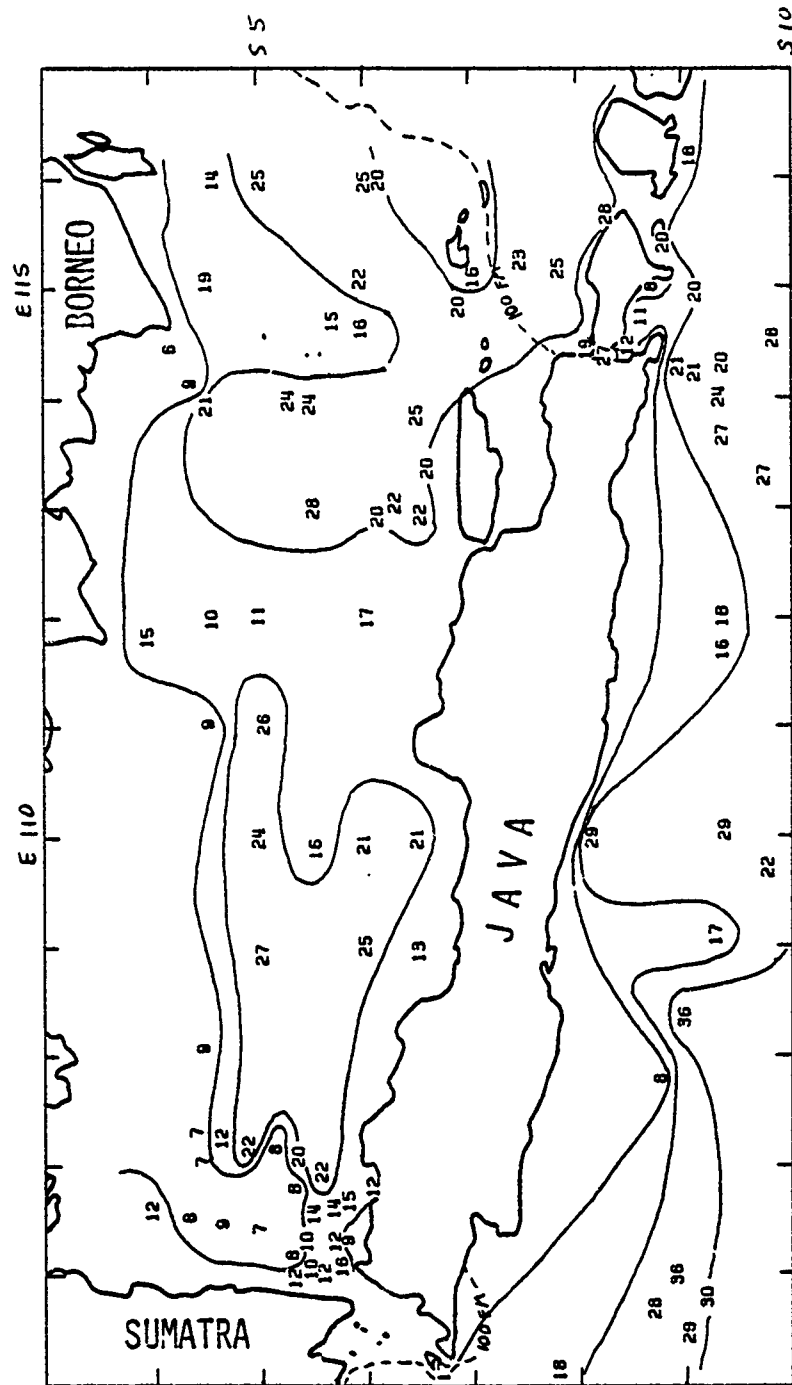
FIGURE 28 : SECCHI DEPTHS, JAVA SEA, OCT-DEC

101
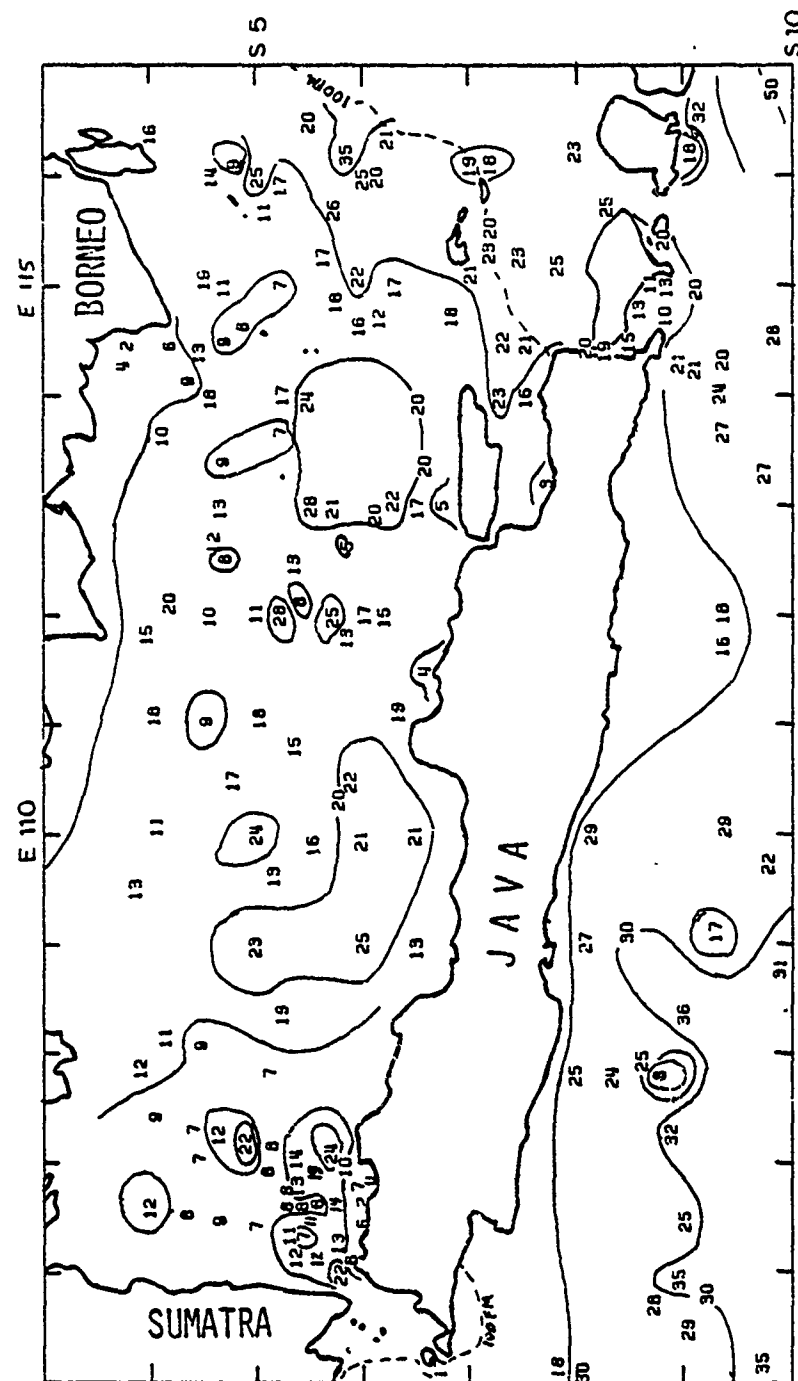
FIGURE 29 : SECCHI DEPTHS, JAVA SEA, ENTIRE YEAR
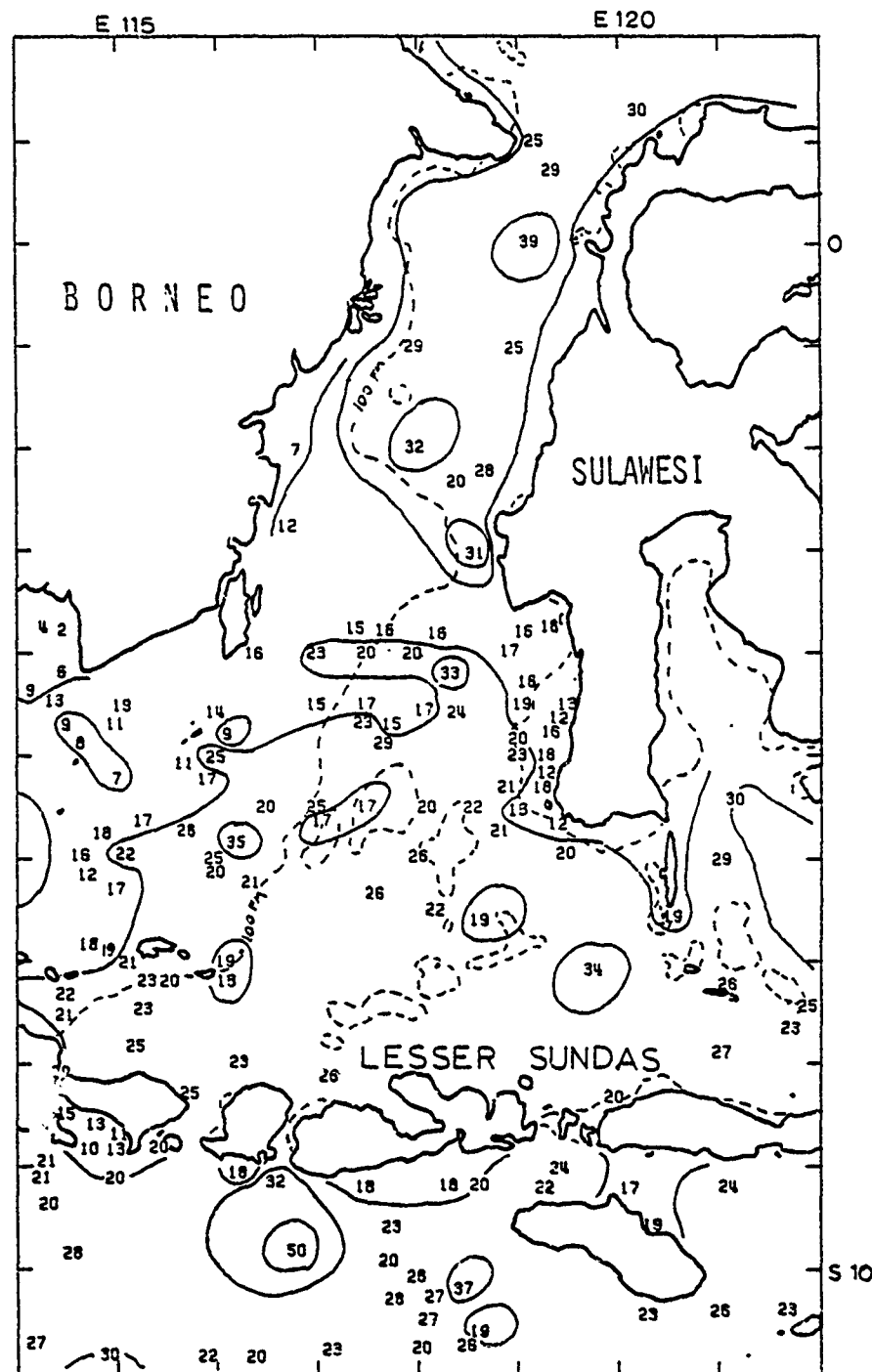
FIGURE 30 : SECCHI DEPTHS, MAKASSAR STRAIT, FLORES SEA
AND BALI SEA, ENTIRE YEAR
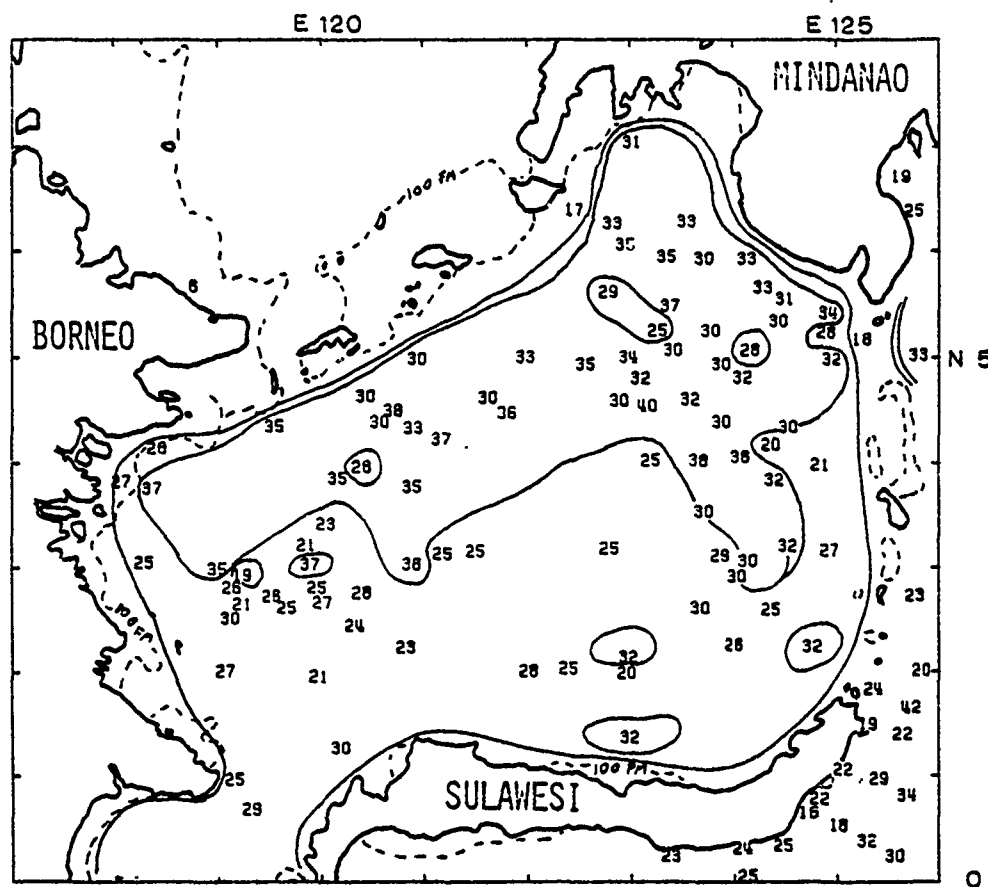
FIGURE 31 : SECCHI DEPTHS, SULAWESI SEA, ENTIRE YEAR
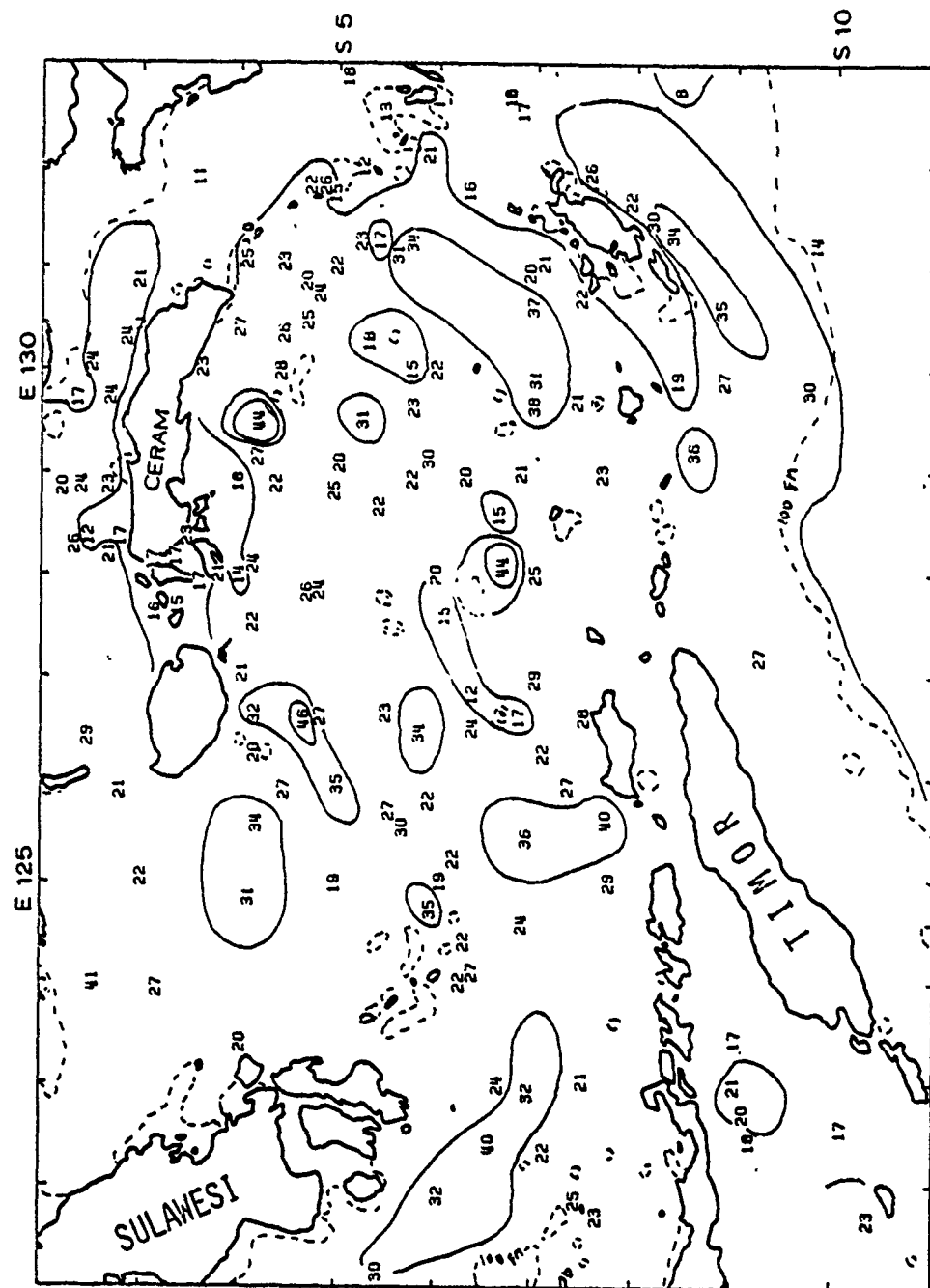
FIGURE 32 : SECCHI DEPTHS, BANDA SEA, ENTIRE YEAR
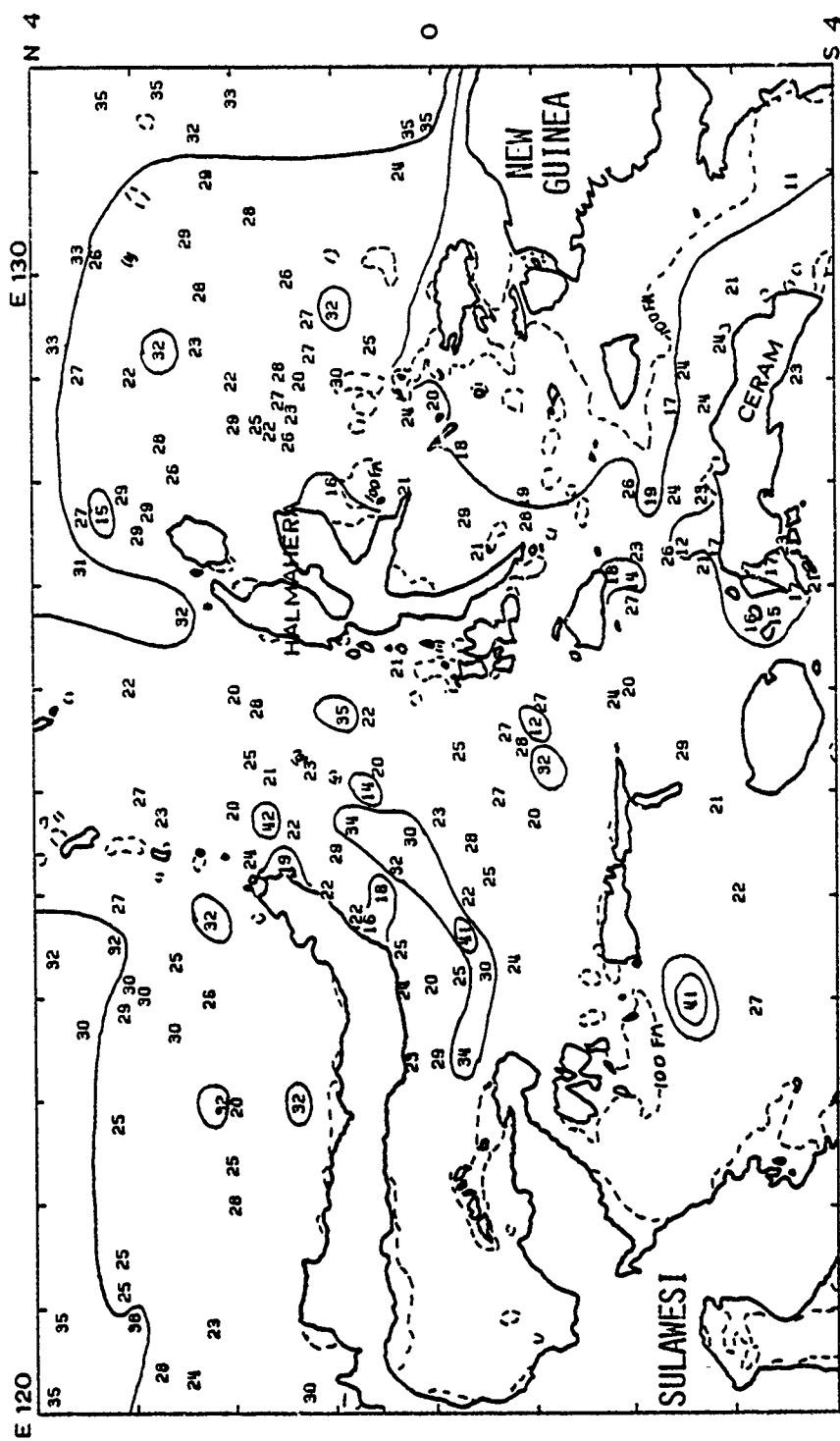
FIGURE 33 : SECCHI DEPTHS, MOLUKKA, HALMAHERA, AND CERAM SEAS, ENTIRE YEAR
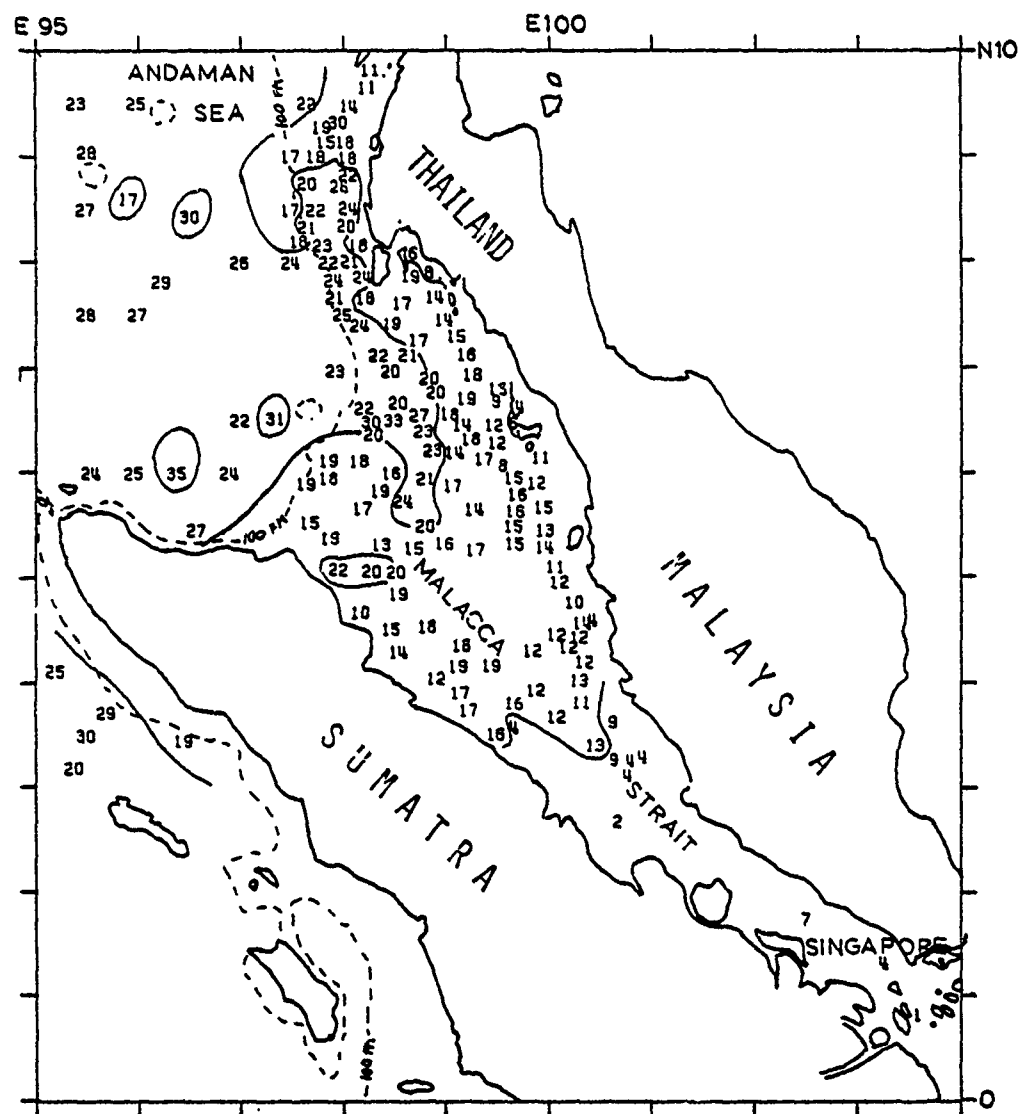
FIGURE 34: SECCHI DEPTHS, MALACCA STRAIT, DEC-APR

FIGURE 35 : SECCHI DEPTHS, BANGKOK APPROACHES
        APR-OCT
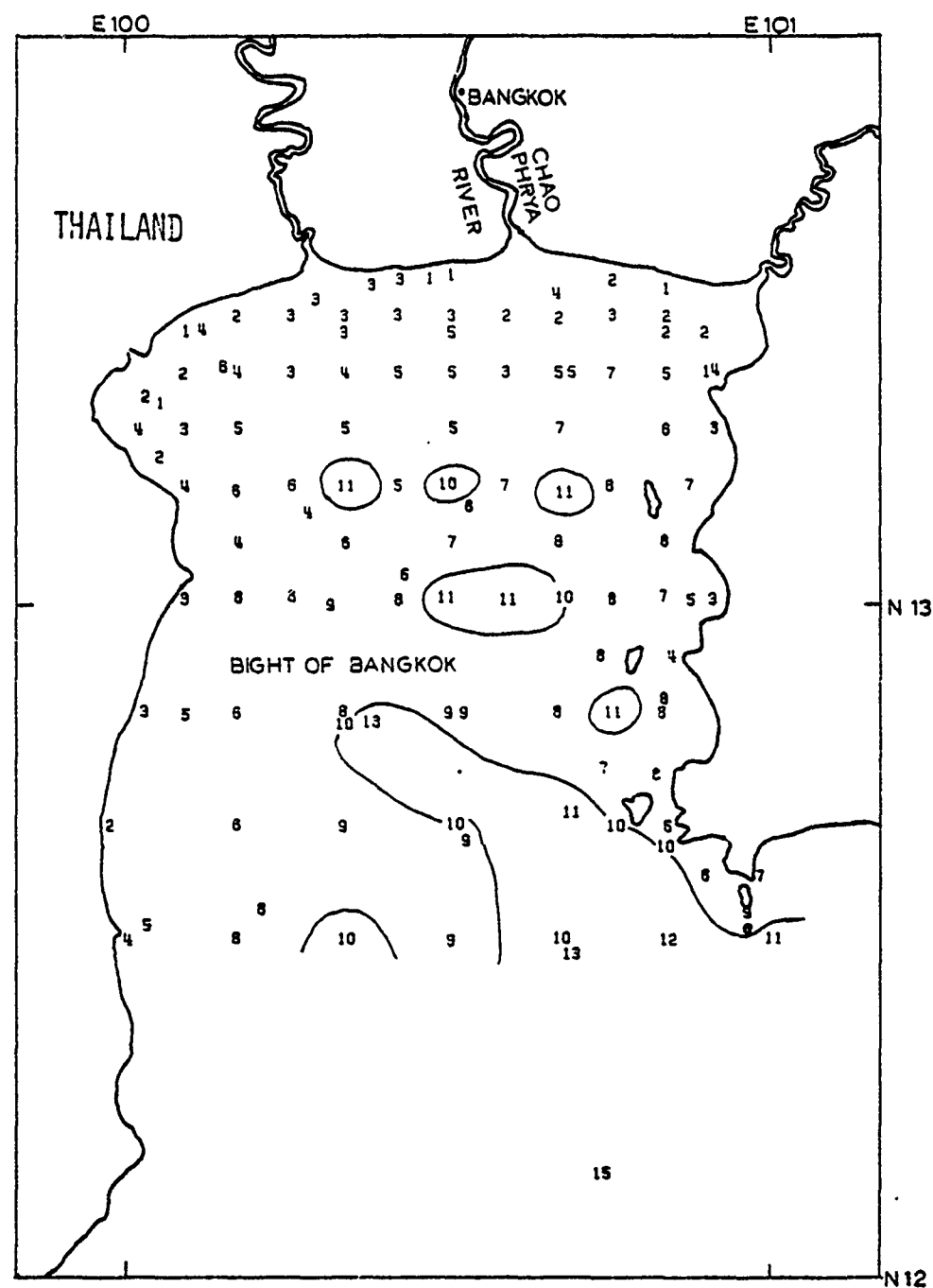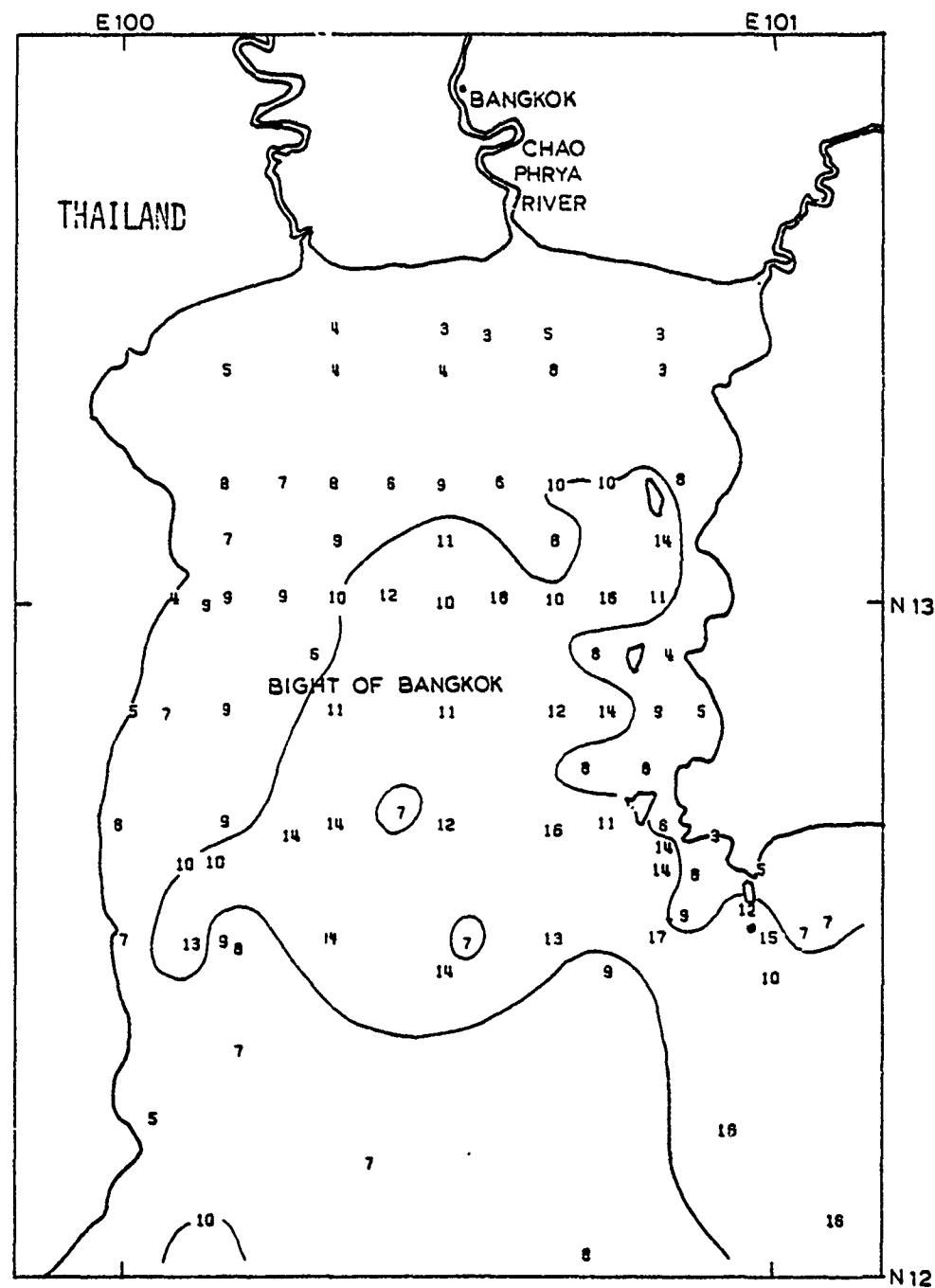
FIGURE 36 : SECCHI DEPTHS, BANGKOK APPROACHES,
NOV-MAR
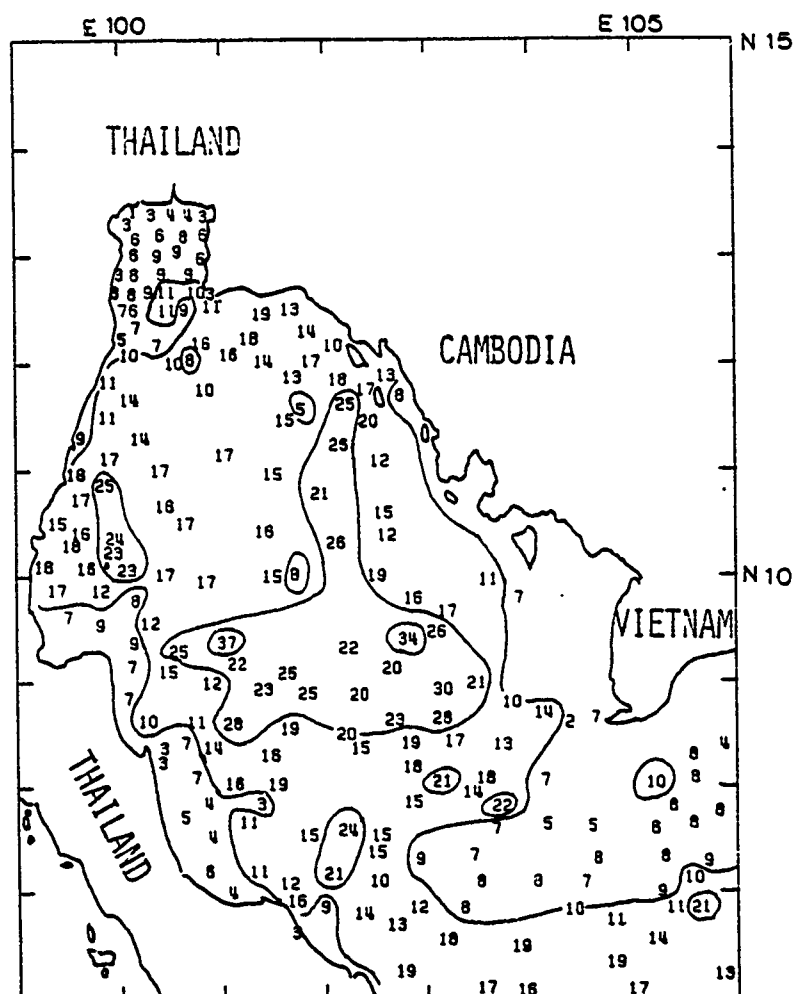
FIGURE 37 : SECCHI DEPTHS, GULF OF THAILAND, ENTIRE YEAR
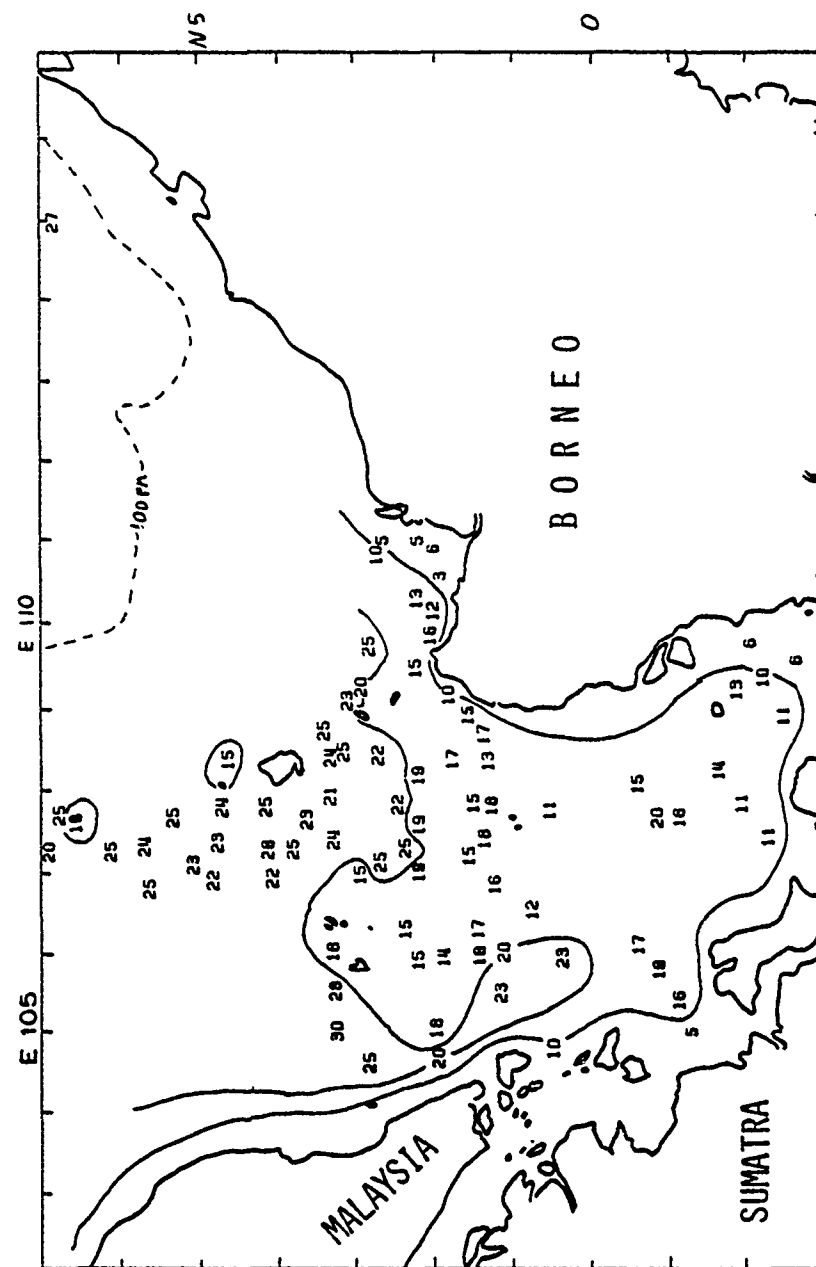
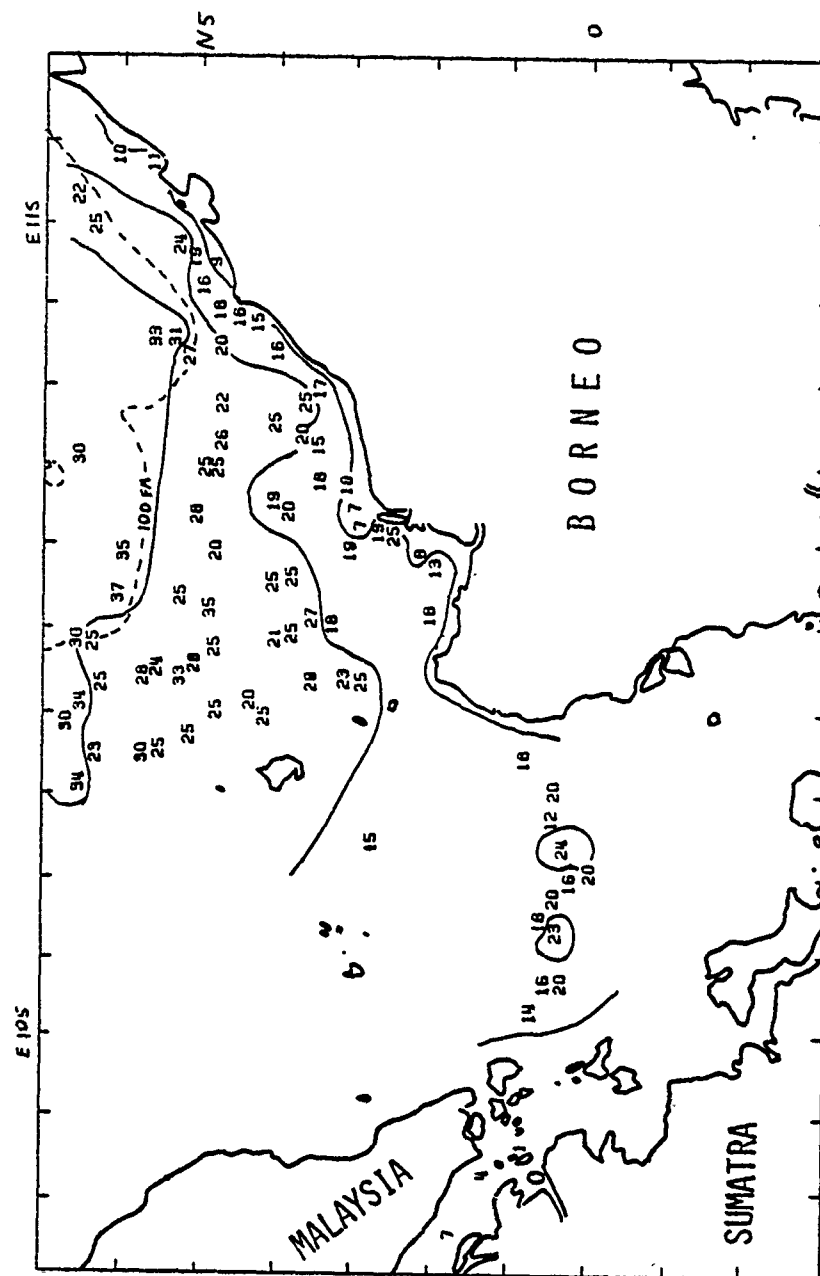FIGURE 38 : SECCHI DEPTHS, SOUTH CHINA SEA (SOUTHERN SECTION), JAN-MAR

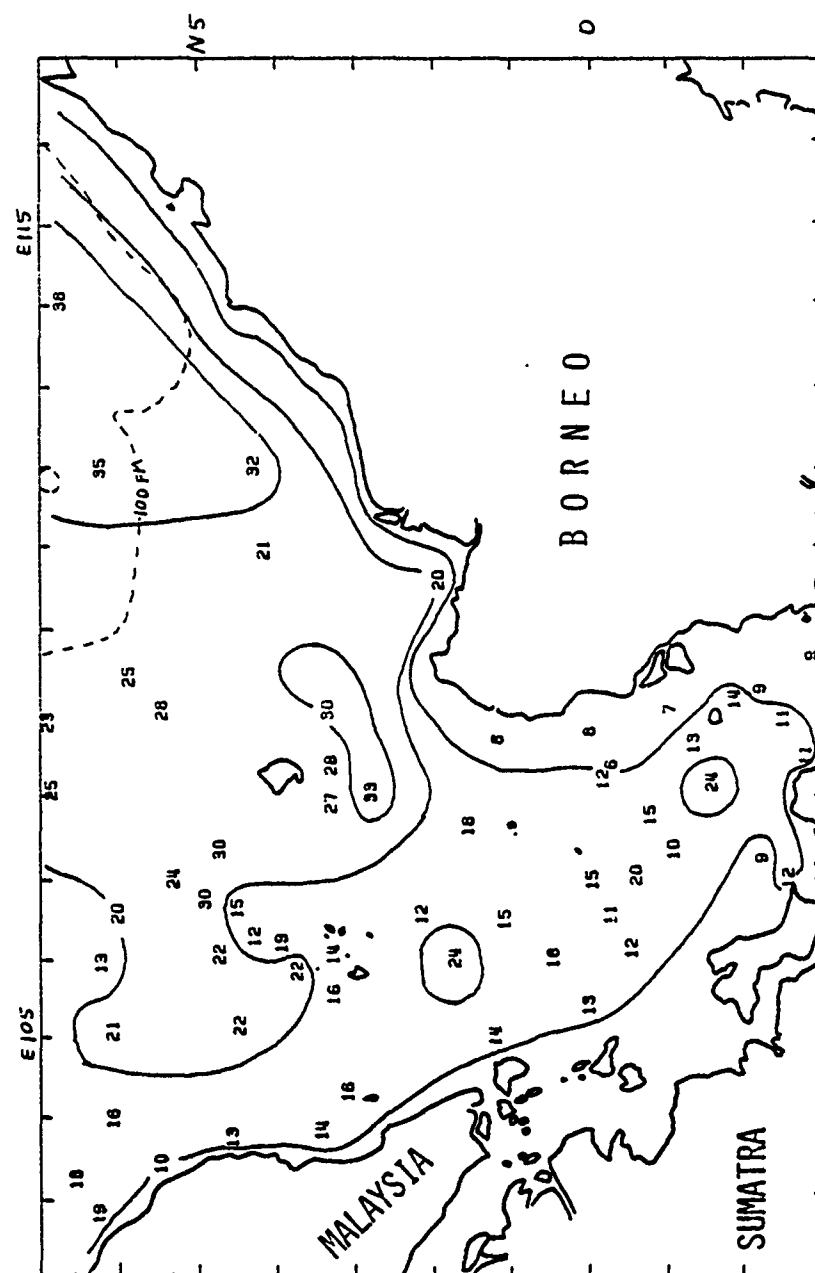FIGURE 39 : SECCHI DEPTHS, SOUTH CHINA SEA (SOUTHERN SECTION), APR-JUN

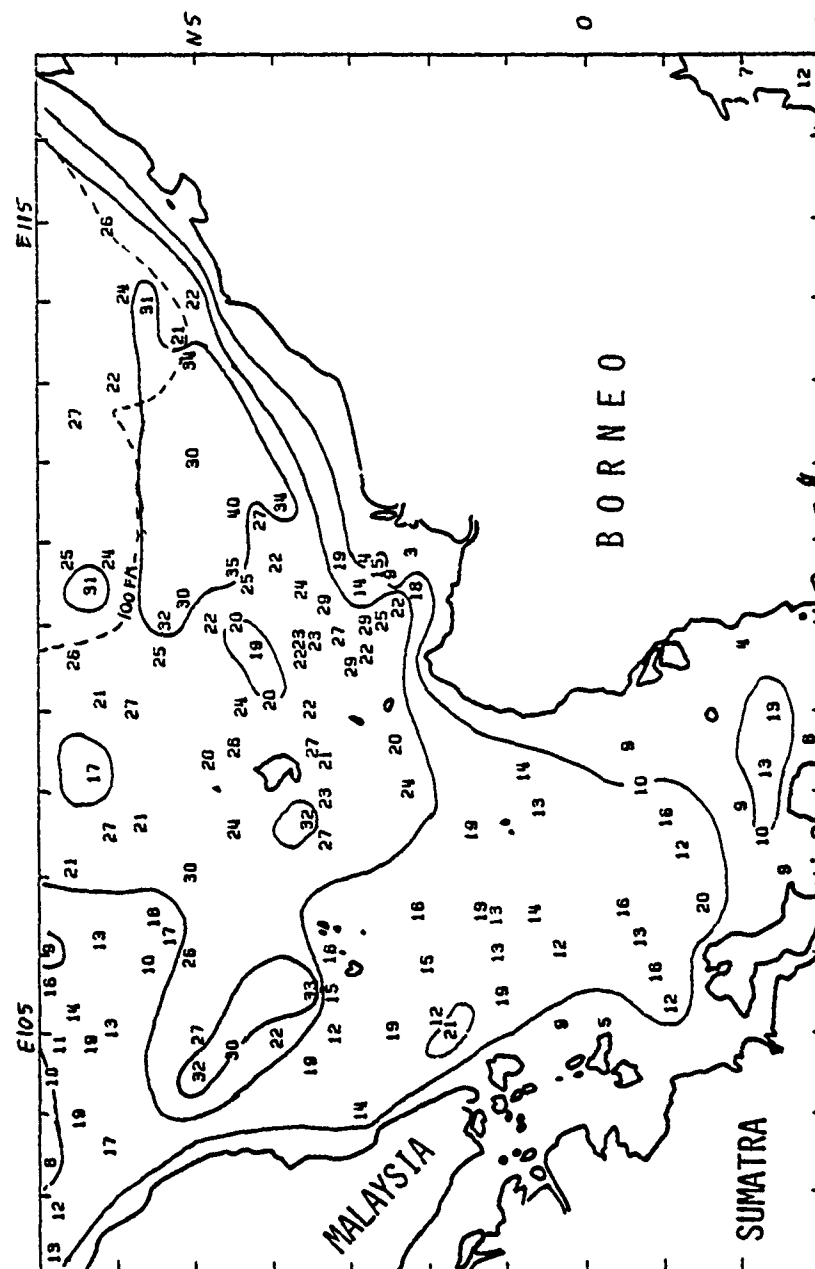FIGURE 40 : SECCHI DEPTHS, SOUTH CHINA SEA (SOUTHERN SECTION), JUL-SEP

113

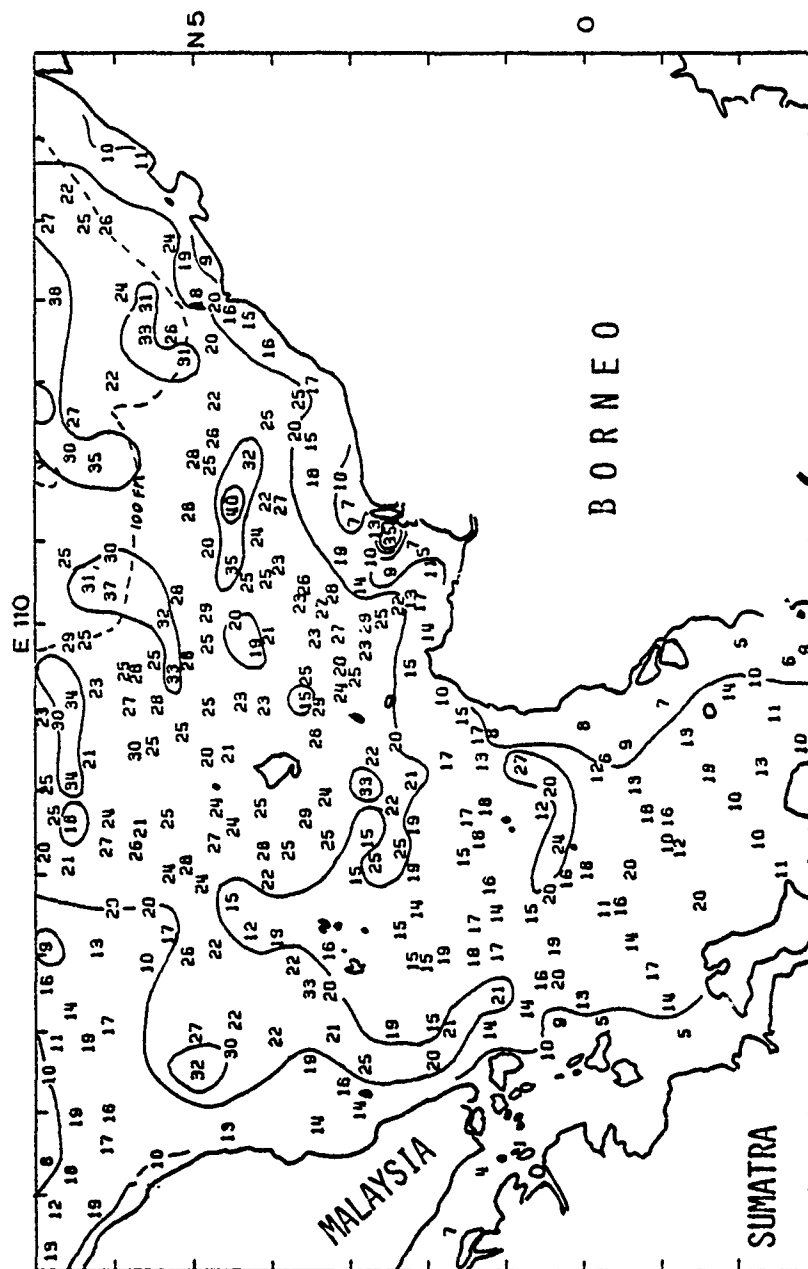FIGURE 41 :SECCHI DEPTHS, SOUTH CHINA SEA (SOUTHERN SECTION), OCT-DEC

114

FIGURE 42 : SECCHI DEPTHS, SOUTH CHINA SEA (SOUTHERN SECTION), ENTIRE YEAR

N5

0
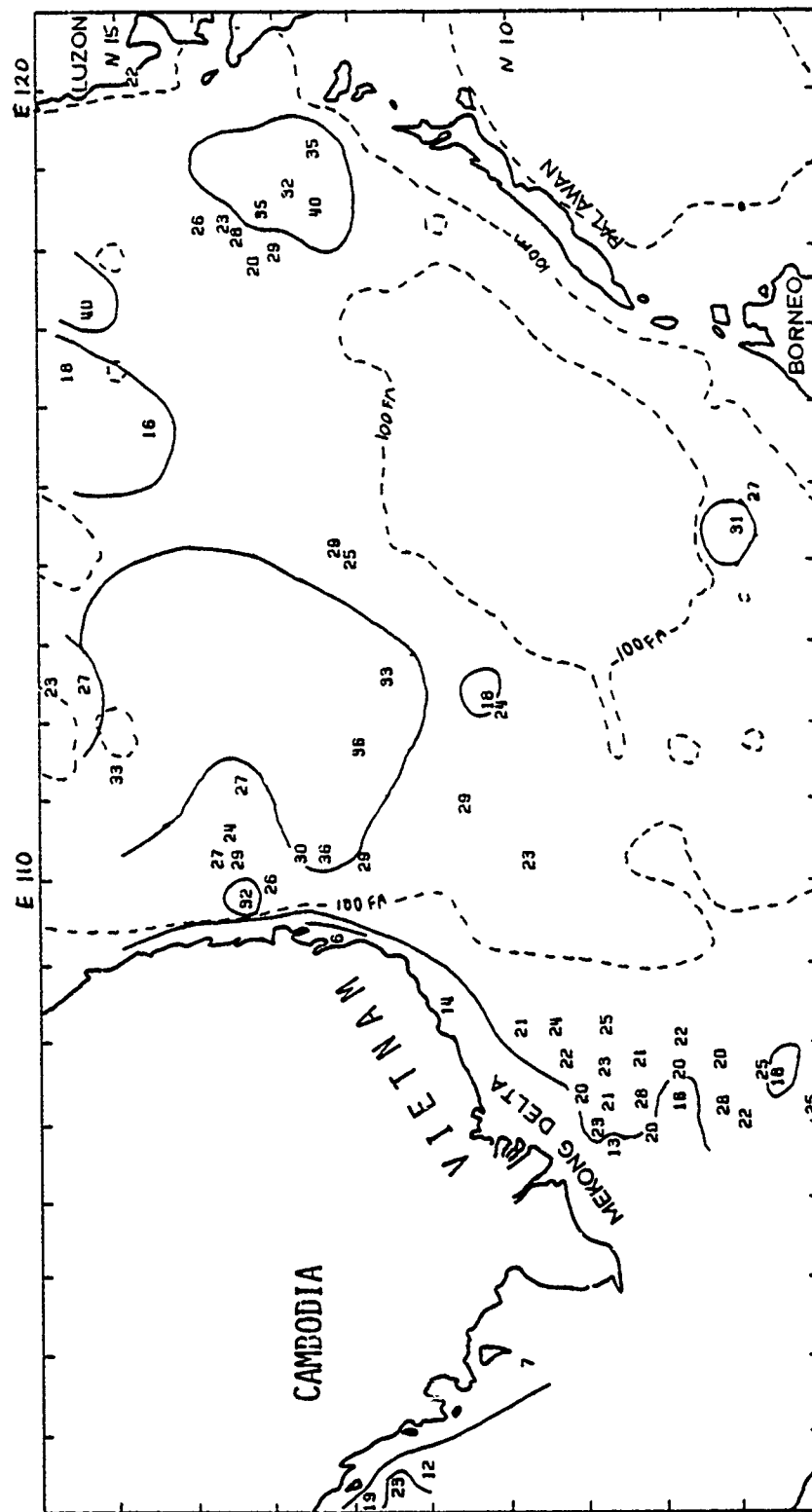
E 110

BORNEO

MALAYSIA

SUMATRA

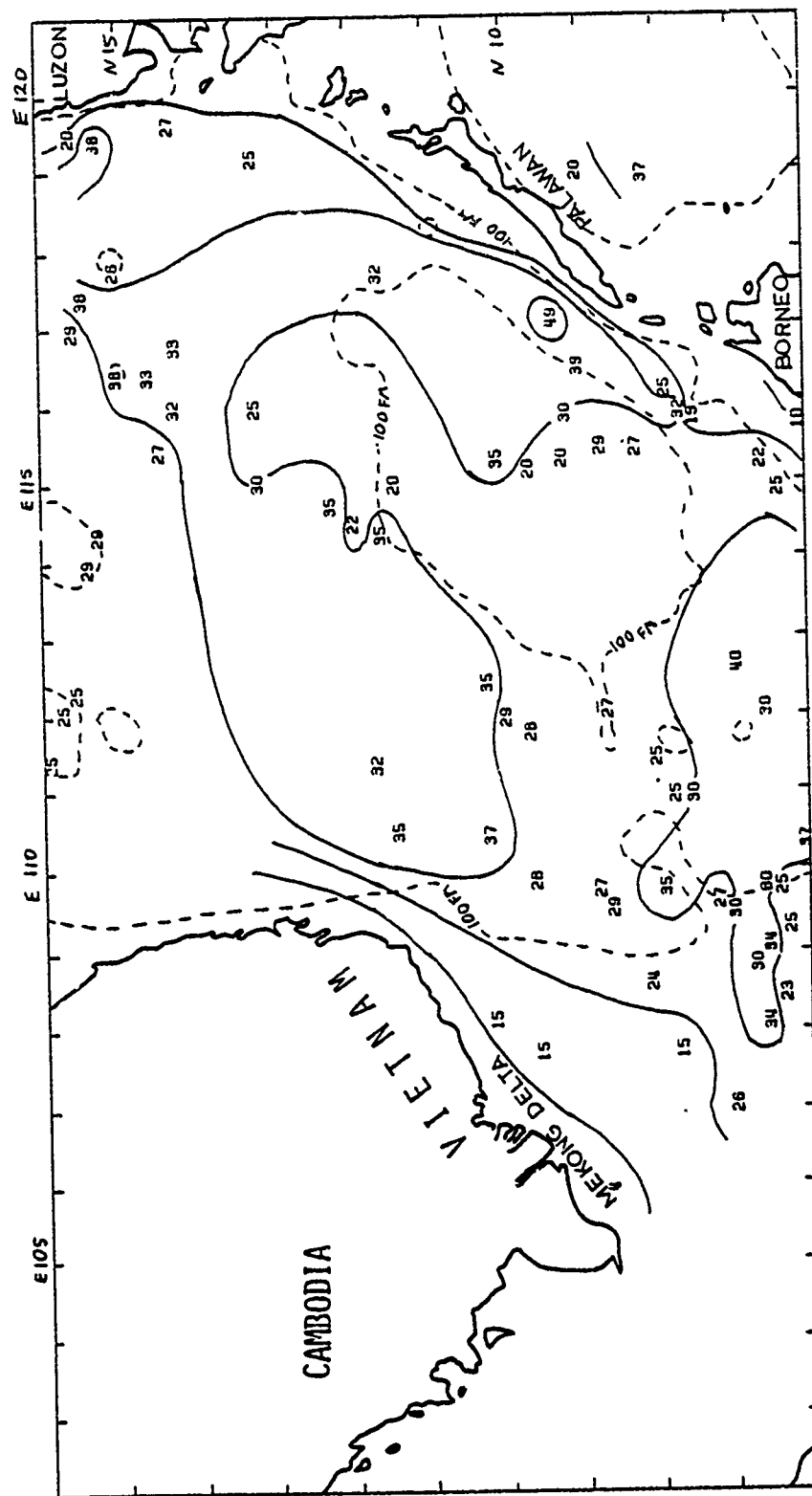FIGURE 43 : SECCHI DEPTHS, SOUTH CHINA SEA (CENTRAL SECTION), JAN-MAR

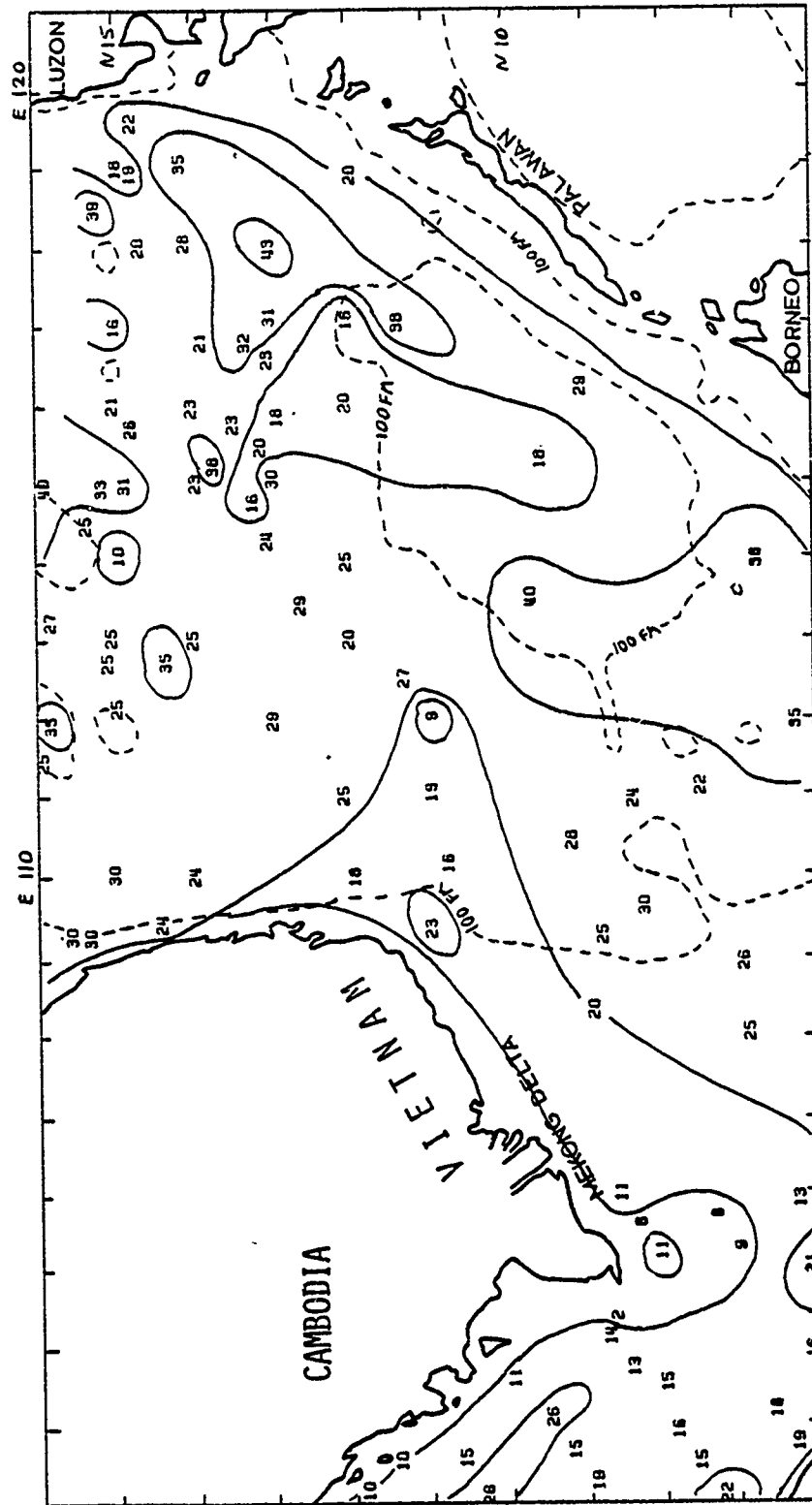FIGURE 44 : SECCHI DEPTHS, SOUTH CHINA SEA (CENTRAL SECTION), APR-JUN

117

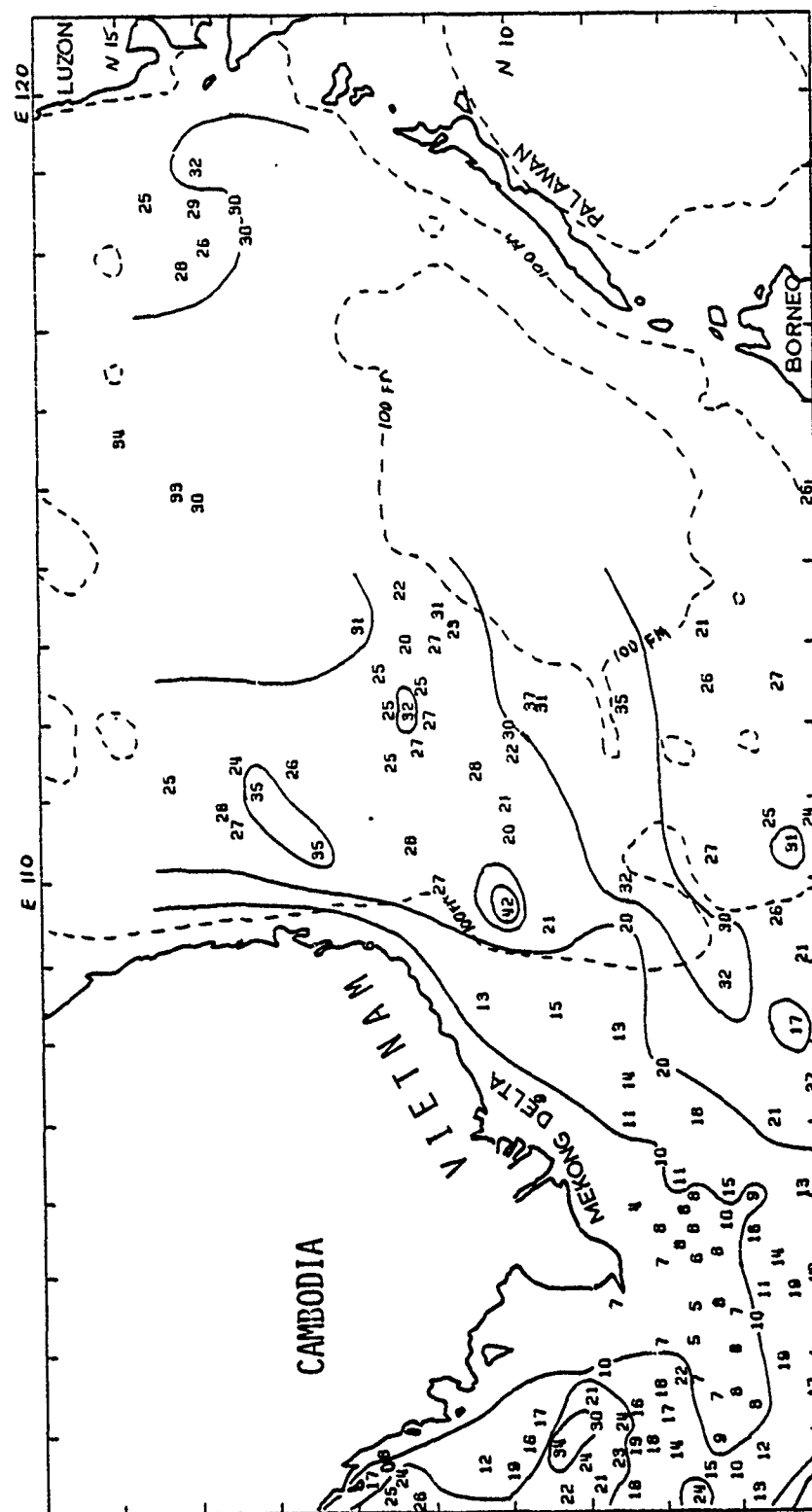FIGURE 45 : SECCHI DEPTHS, SOUTH CHINA SEA (CENTRAL SECTION), JUL-SEP

FIGURE 46 : SECCHI DEPTHS, SOUTH CHINA SEA (CENTRAL SECTION), OCT-DEC

FIGURE 47 : SECCHI DEPTHS, SOUTH CHINA SEA (CENTRAL SECTION), ENTIRE YEAR
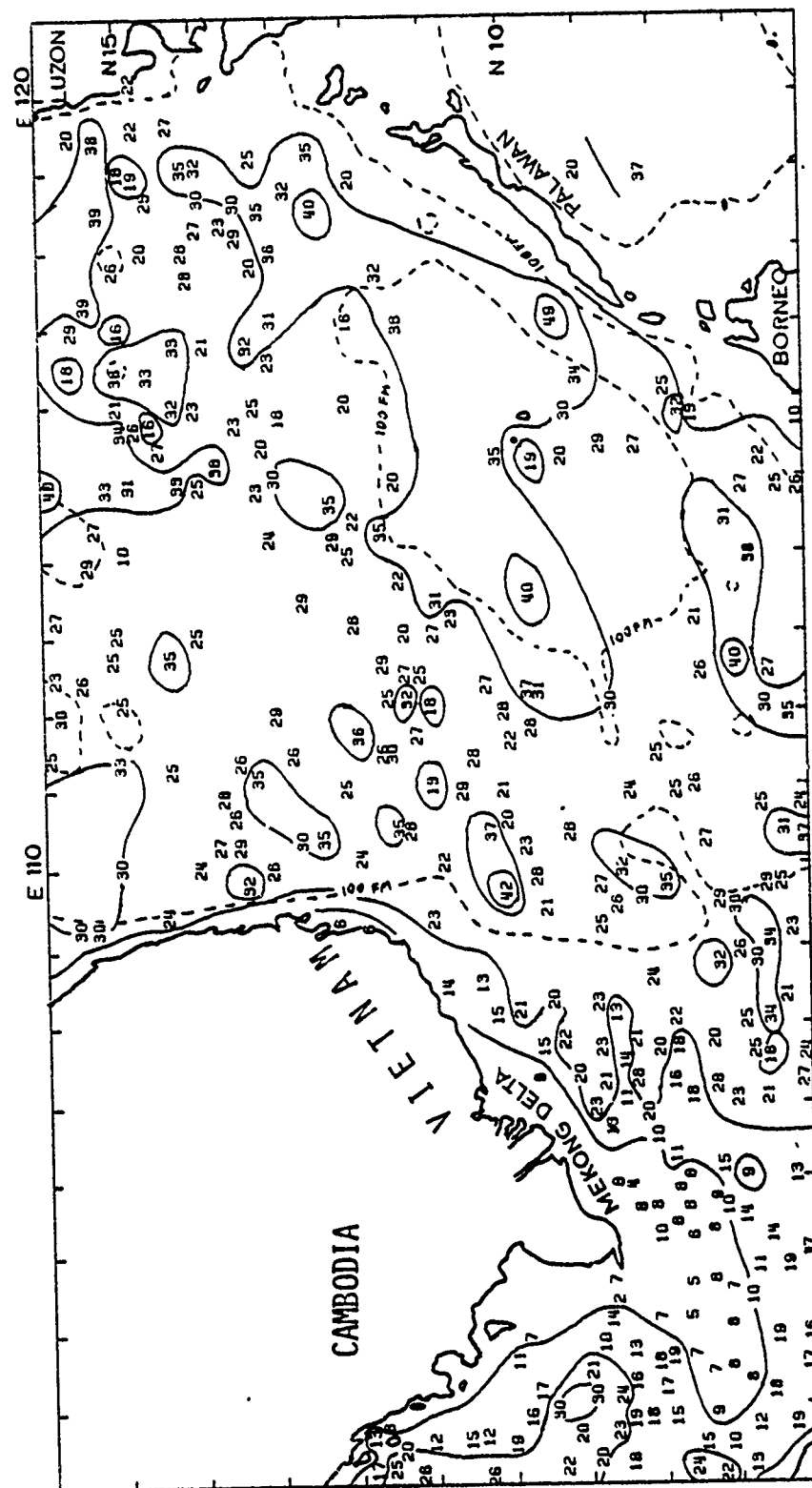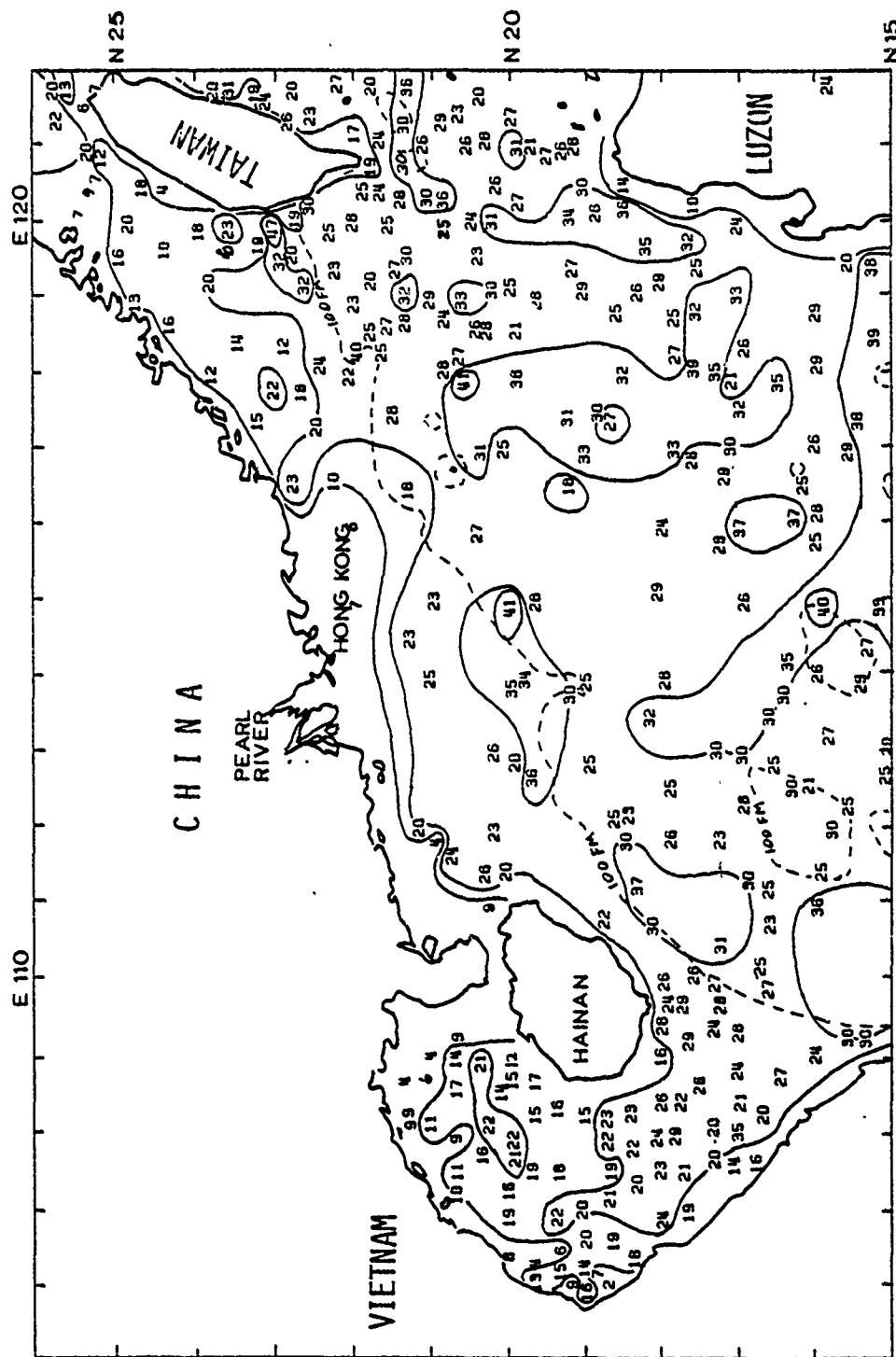
FIGURE 48 : SECCHI DEPTHS, SOUTH CHINA SEA (NORTHERN SECTION), APR-NOV

121
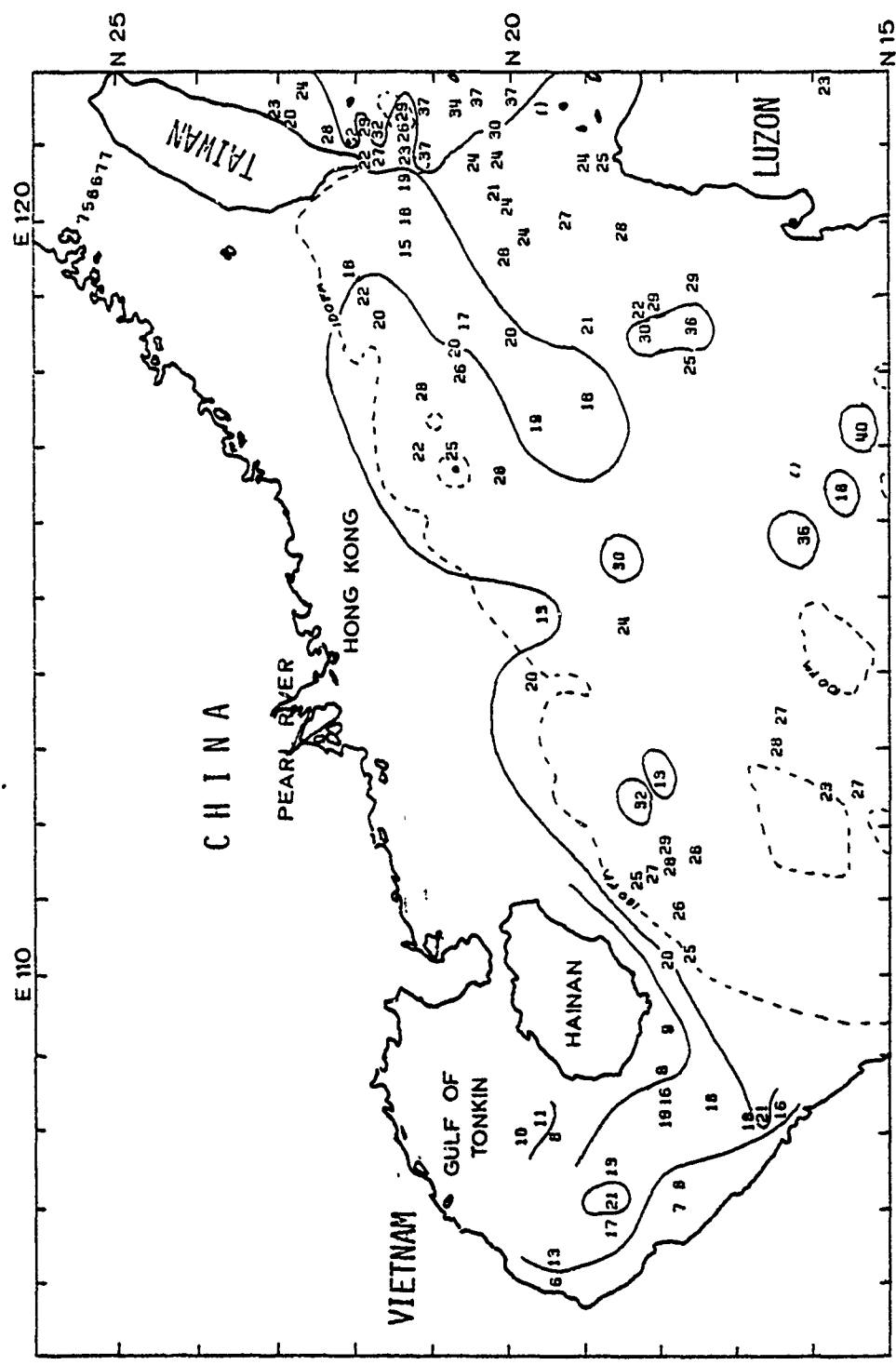
FIGURE 49 : SECCHI DEPTHS, SOUTH CHINA SEA (NORTHERN SECTION), DEC-MAR
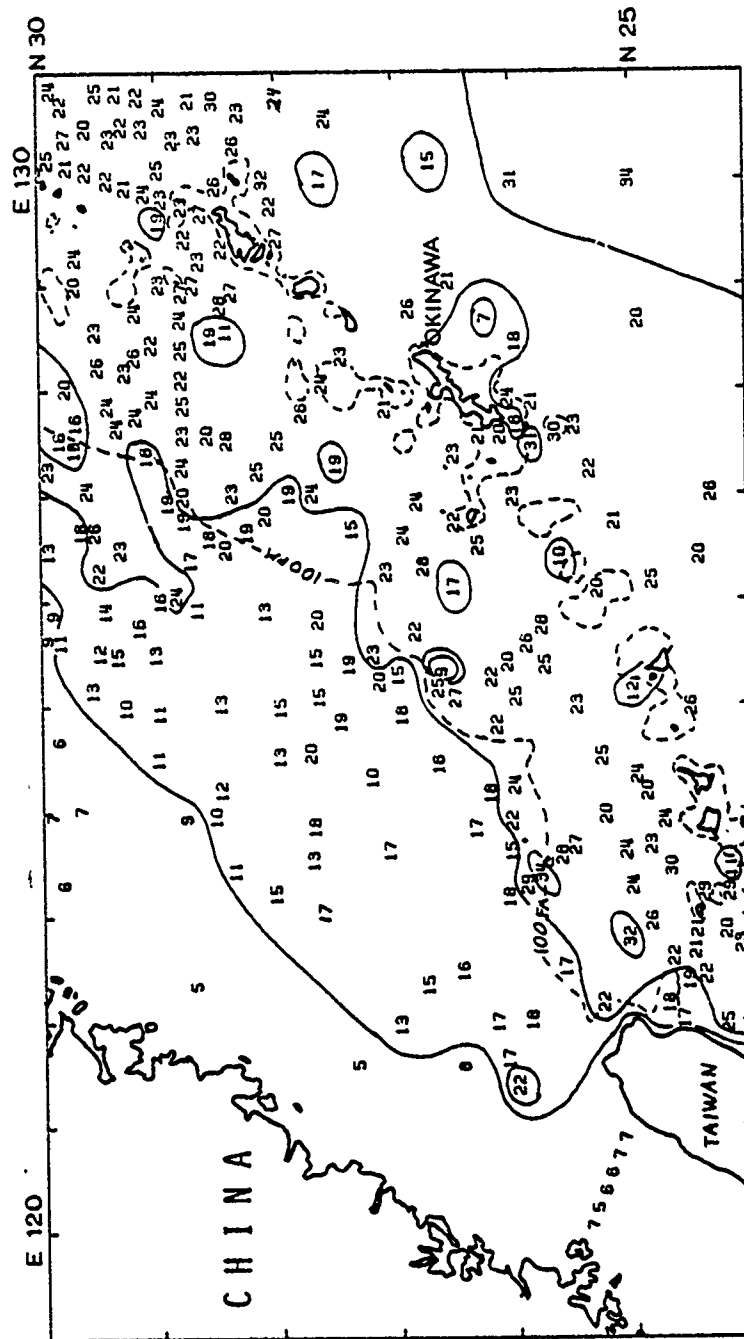
FIGURE 50 : SECCHI DEPTHS, EAST CHINA SEA, JAN-MAR

123
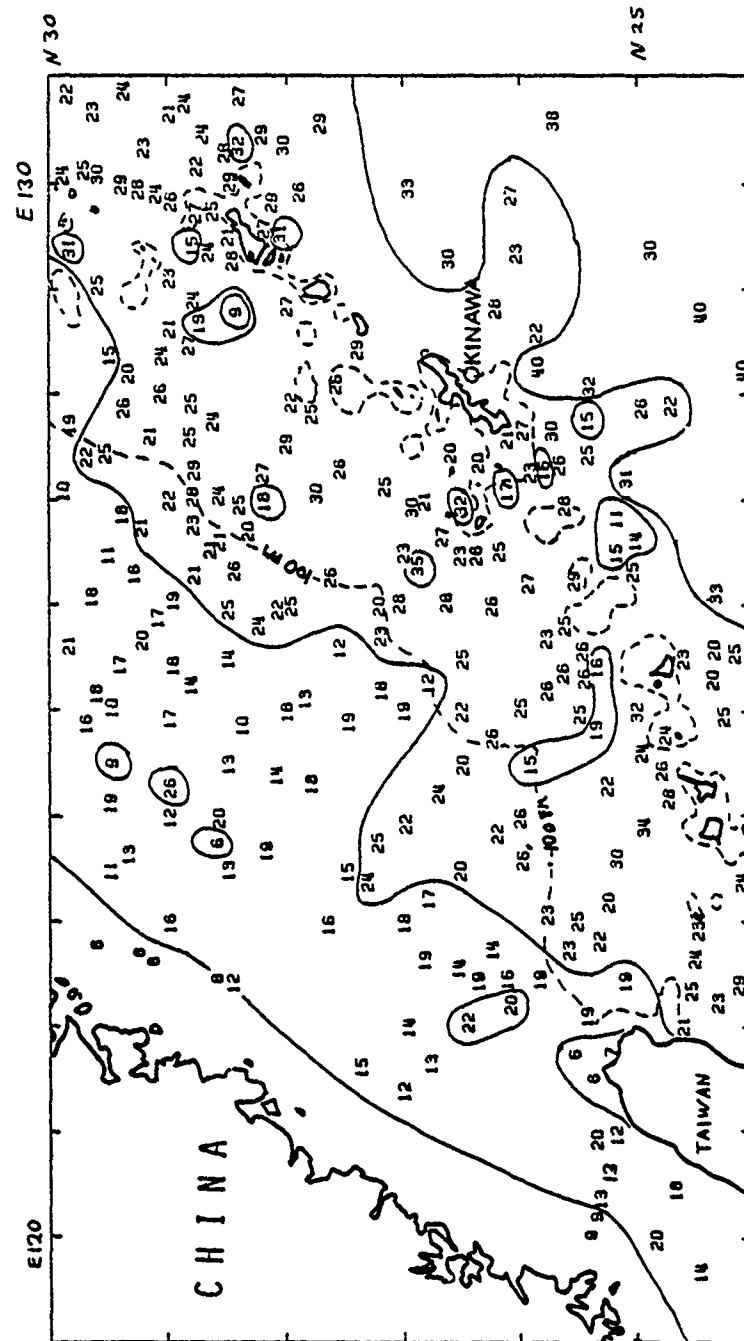
FIGURE 51 : SECCHI DEPTHS, EAST CHINA SEA, APR.-JUN
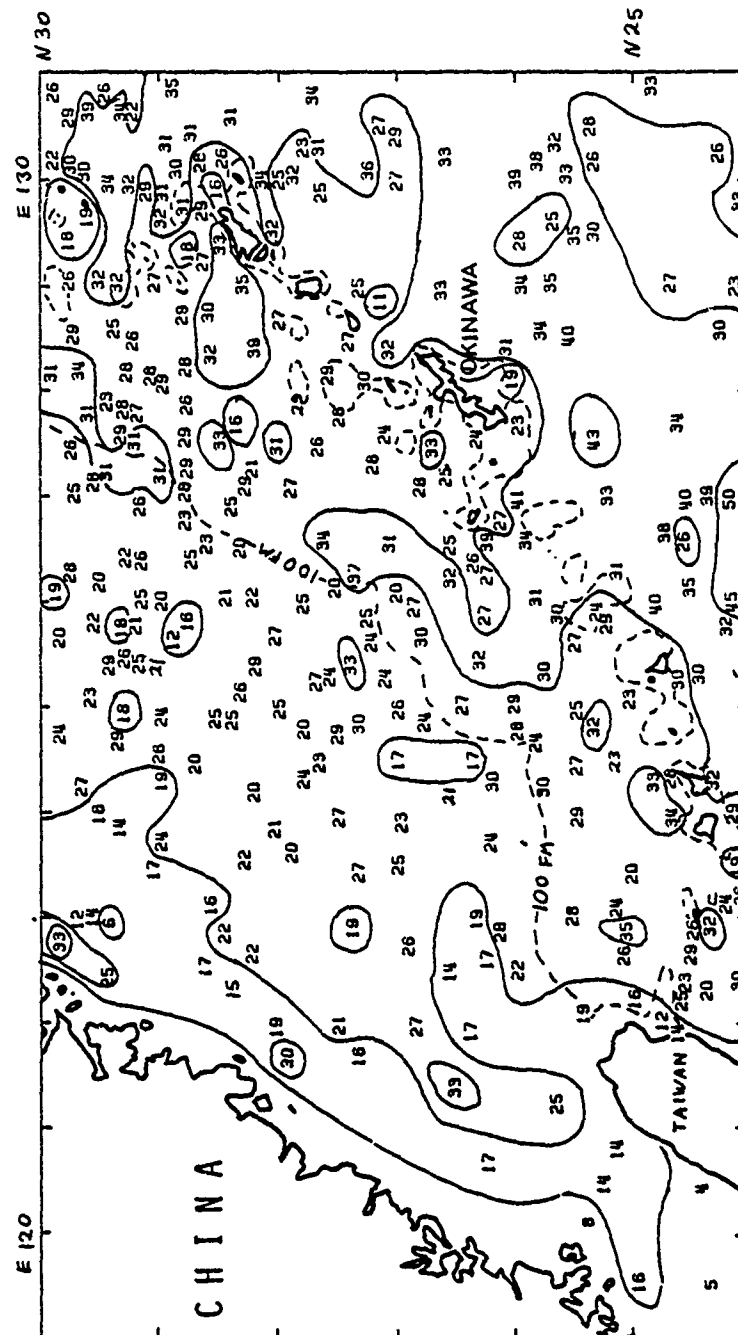
FIGURE 52 : SECCHI DEPTHS, EAST CHINA SEA, JUL-SEP
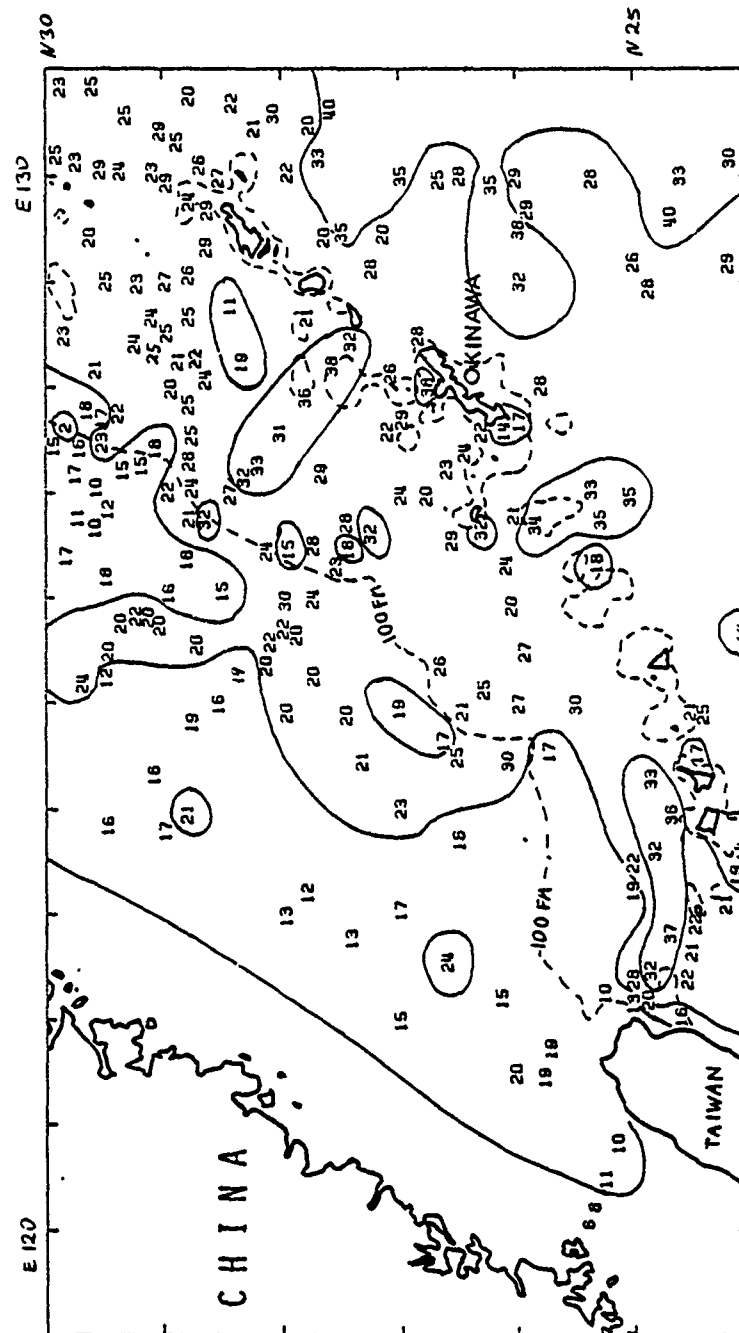
FIGURE 53 : SECCII DEPTIIS, EAST CHINA SEA, OCT-DEC
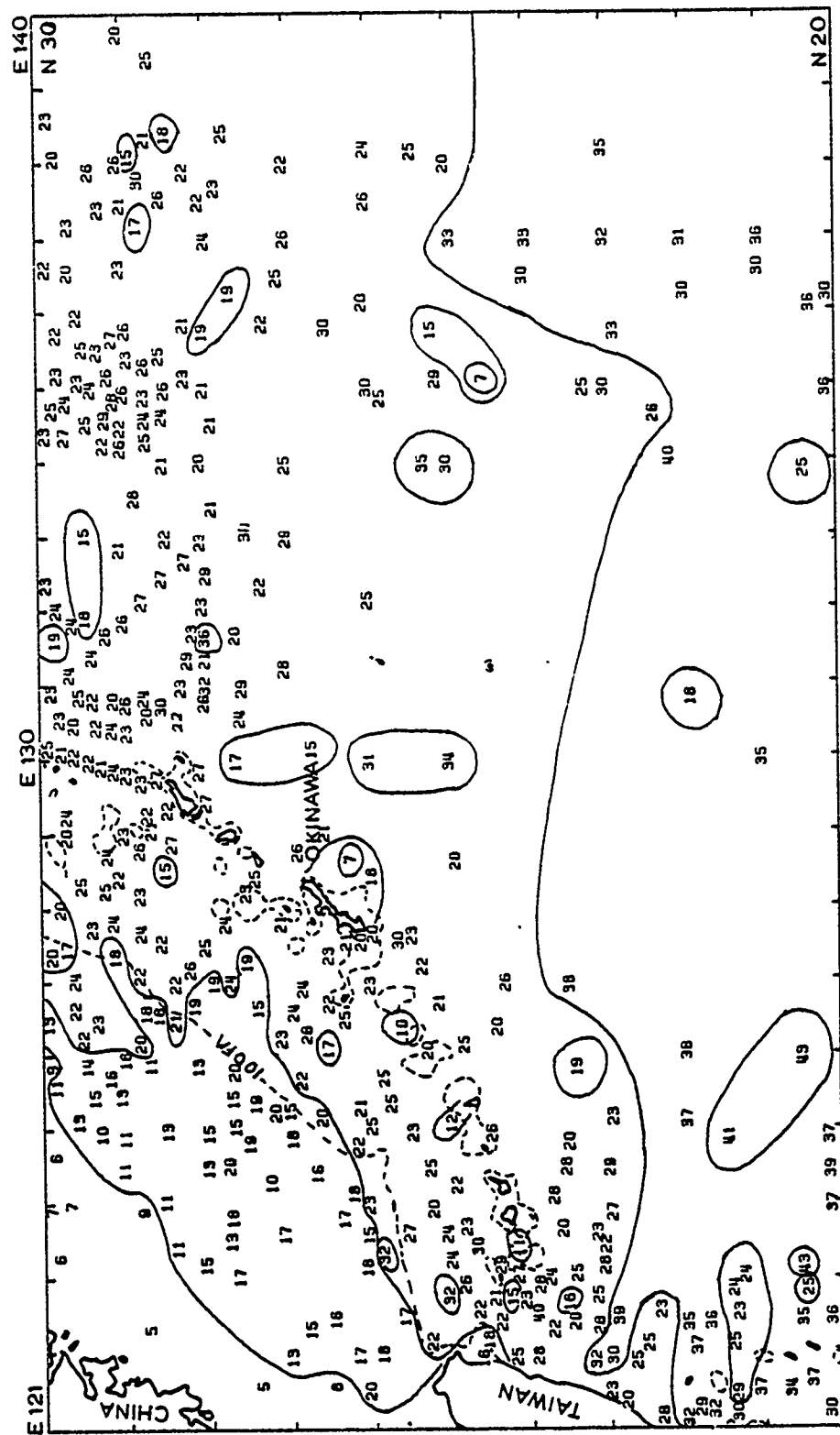
FIGURE 54 : SECCHI DEPTHS, PHILIPPINE SEA AND PACIFIC OCEAN (20°N-30°N), JAN-MAR
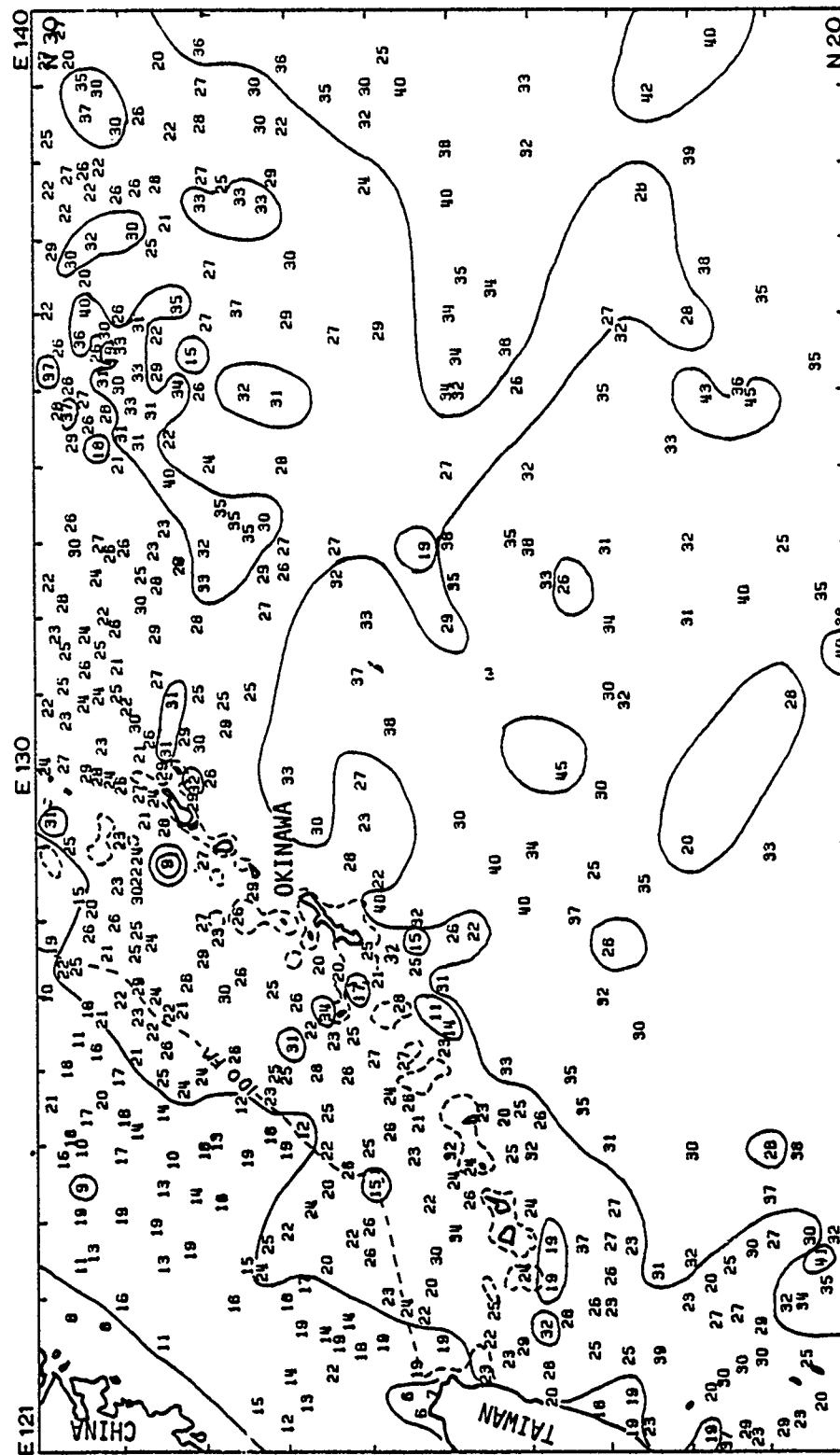
FIGURE 55 : SECCHI DEPTHS, PHILIPPINE SEA AND PACIFIC OCEAN (20°N - 30°N), APR-JUN

FIGURE 56 : SECCHI DEPTHS, PHILIPPINE SEA AND PACIFIC OCEAN (20°N - 30°N), JUL-SEP
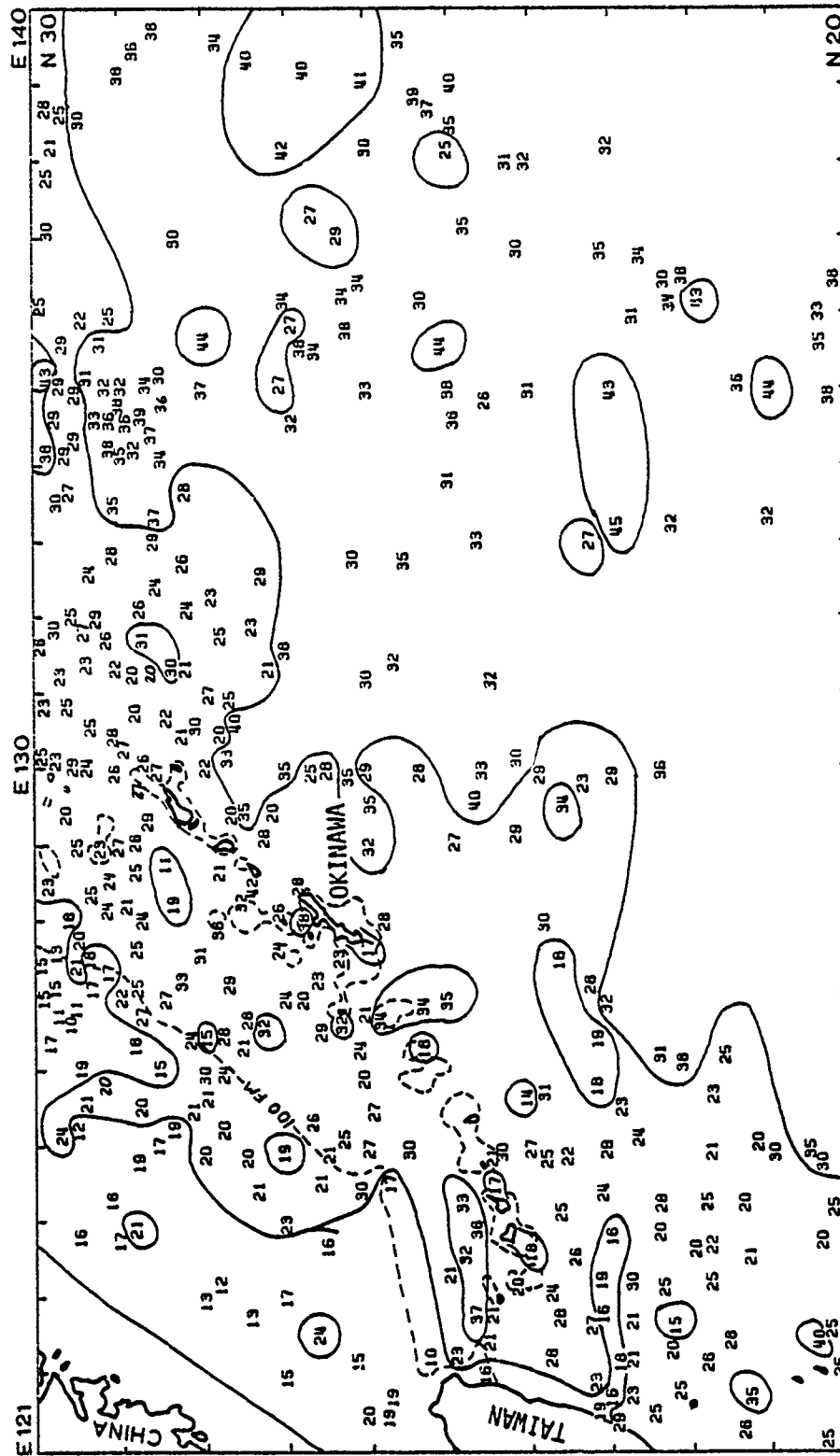
FIGURE 57 : SECCHI DEPTHS, PHILIPPINE SEA AND PACIFIC OCEAN (20°N - 30°N), OCT-DEC
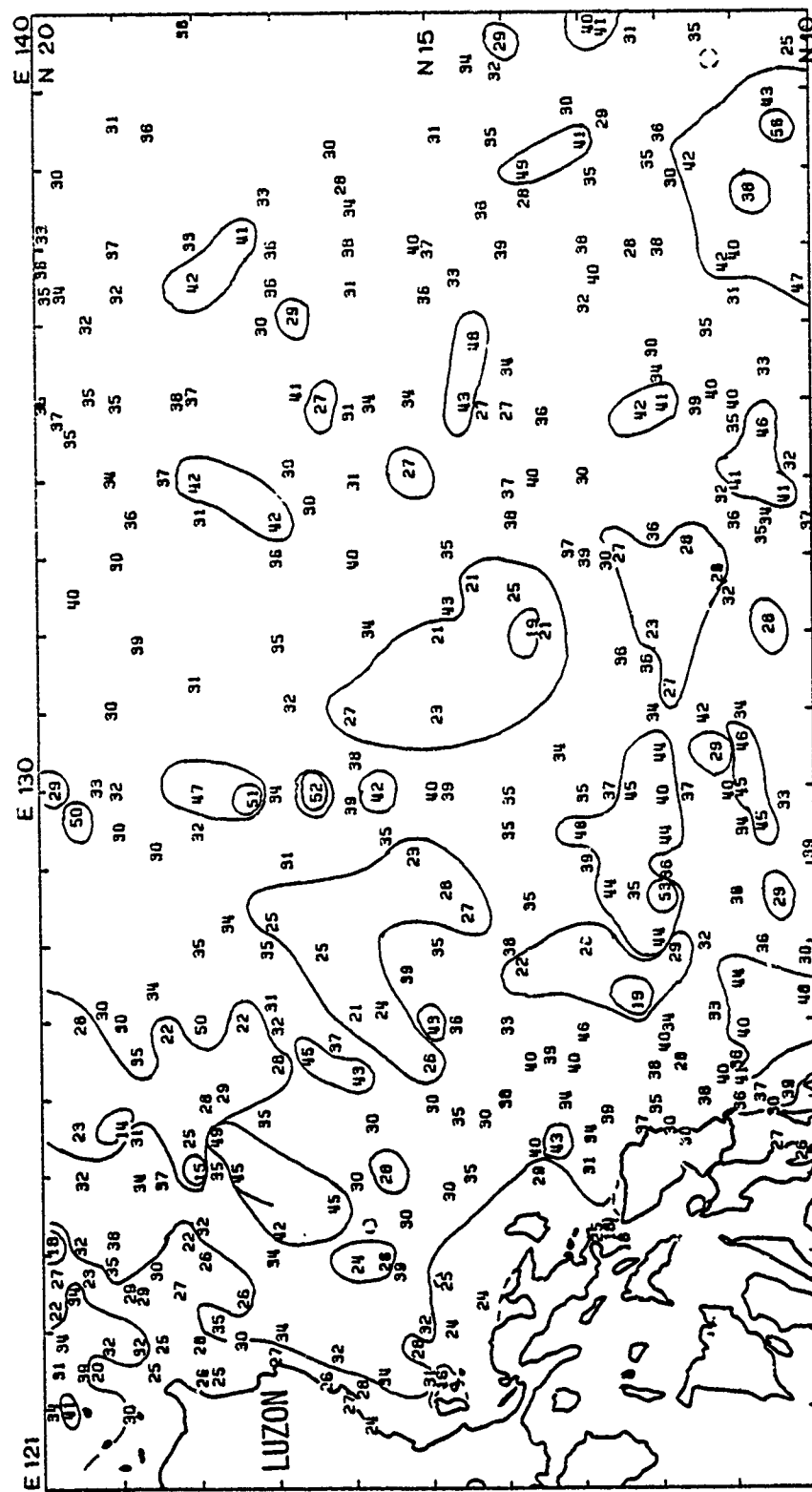
FIGURE 58 : SECCHI DEPTHS, PHILIPPINE SEA AND PACIFIC OCEAN (10°N – 20°N), ENTIRE YEAR.
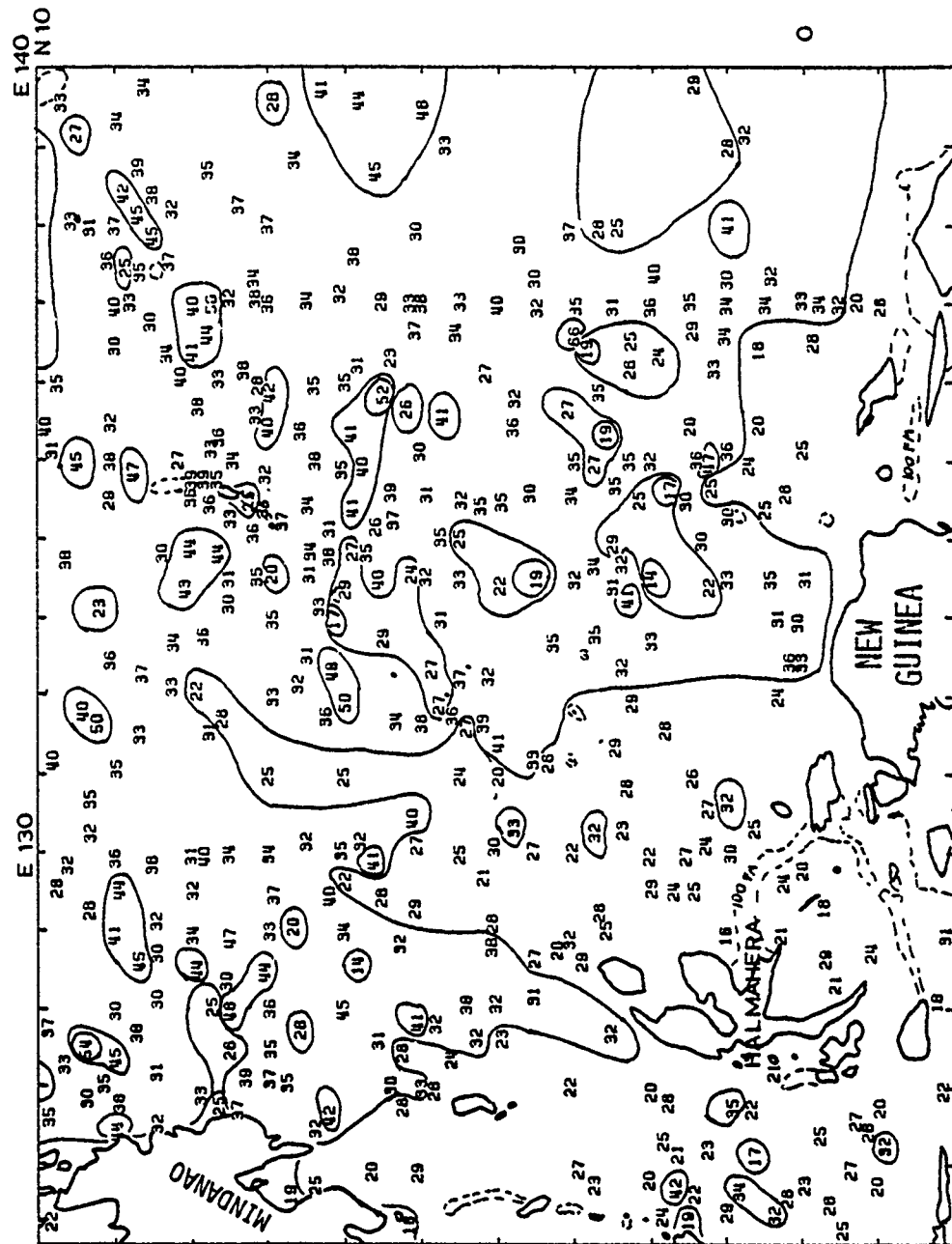
FIGURE 59 : SECCHI DEPTHS, PHILIPPINE SEA AND PACIFIC OCEAN (2°S – 10°N), ENTIRE YEAR

Legend:
- ▨ <10m
- ▦ 10-20m
- ▥ 20-30m
- ▤ 30-40m
- ▦ >40m
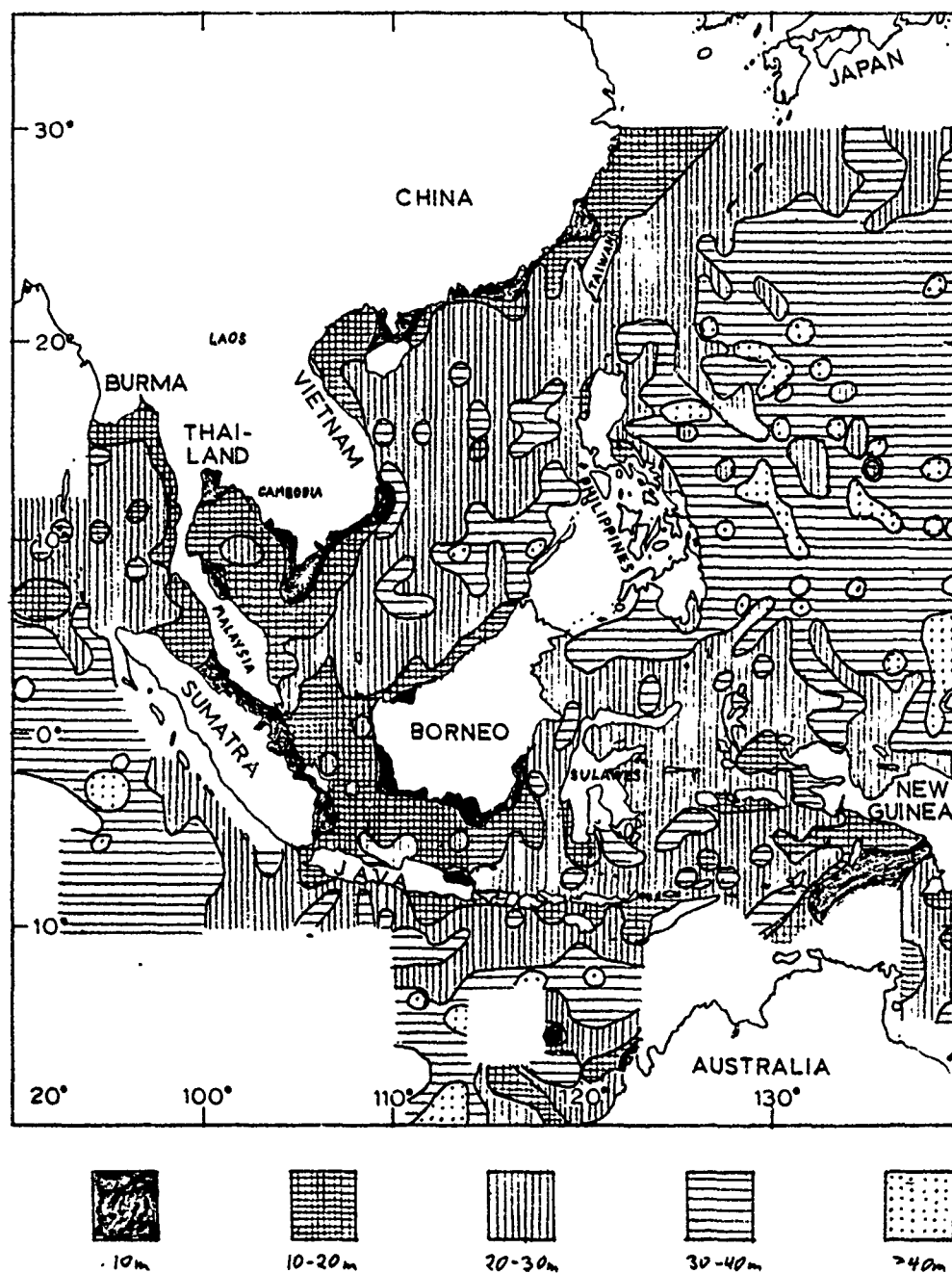
FIGURE 60 : SECCHI DEPTHS, SOUTHEAST ASIAN
AND INDONESIAN WATERS
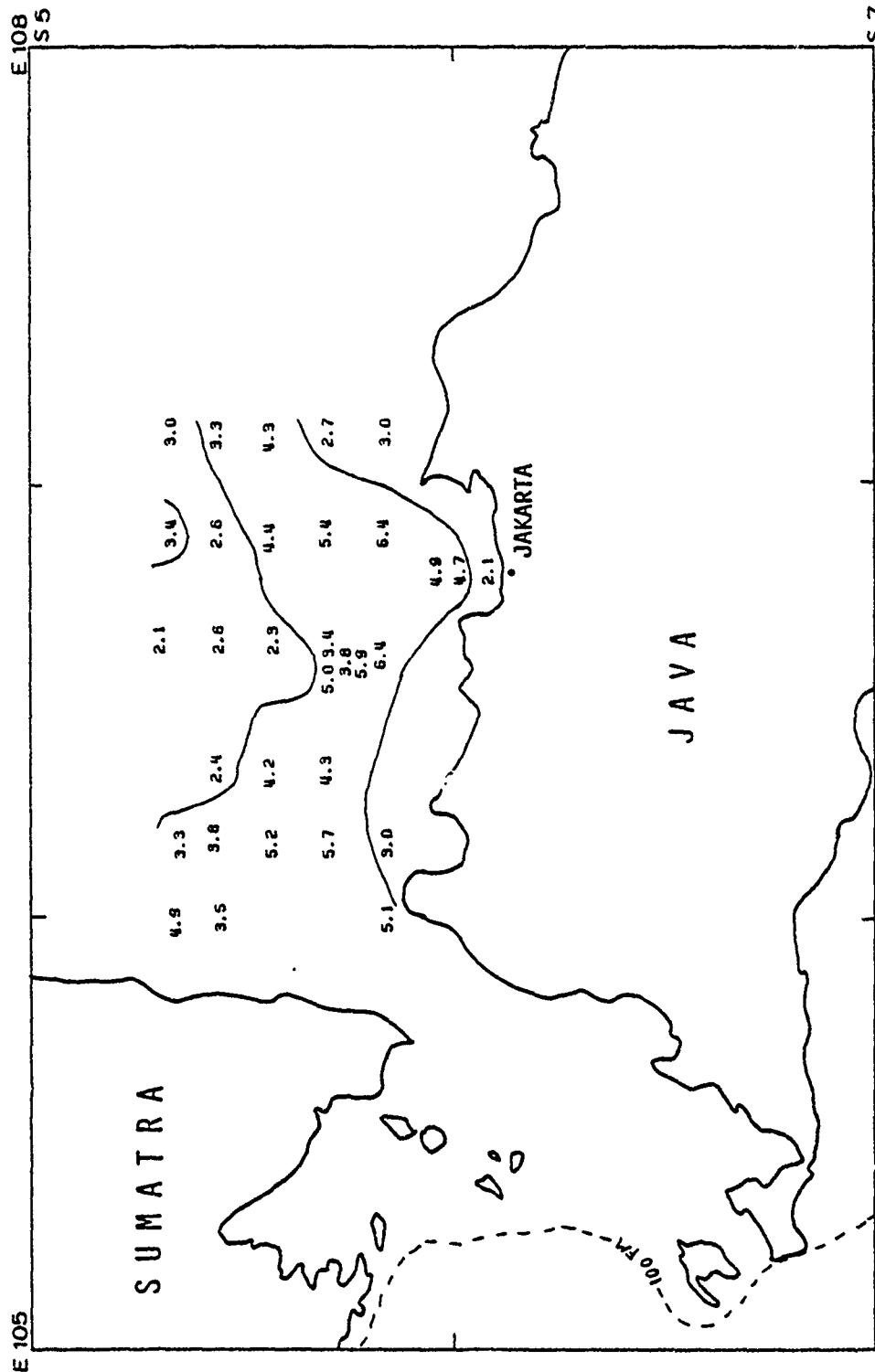
FIGURE 61 : KD VALUES, JAKARTA APPROACHES, APR–JUN
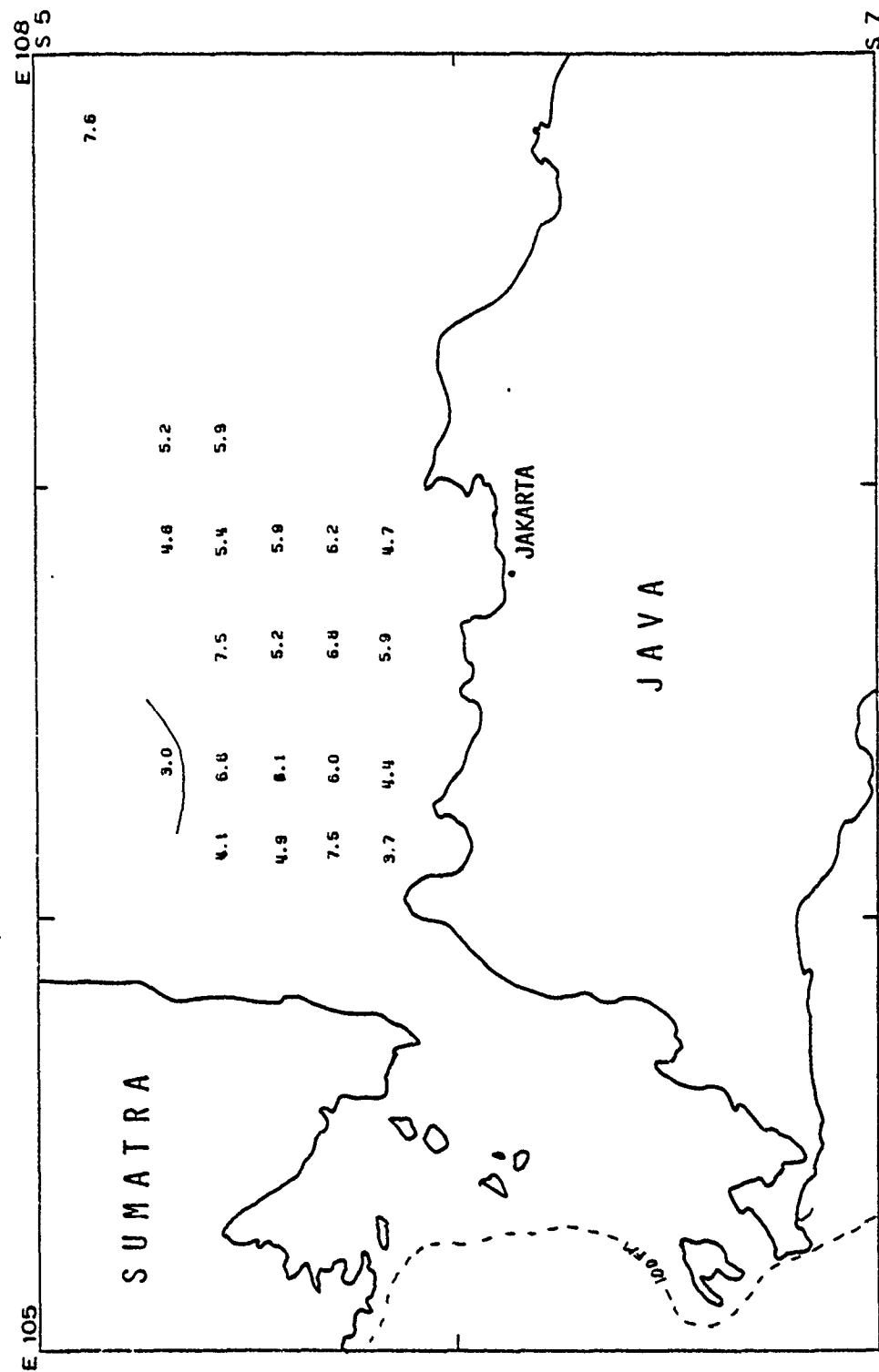
FIGURE 52 : KD VALUES, JAKARTA APPROACHES, JUL-SEP

135
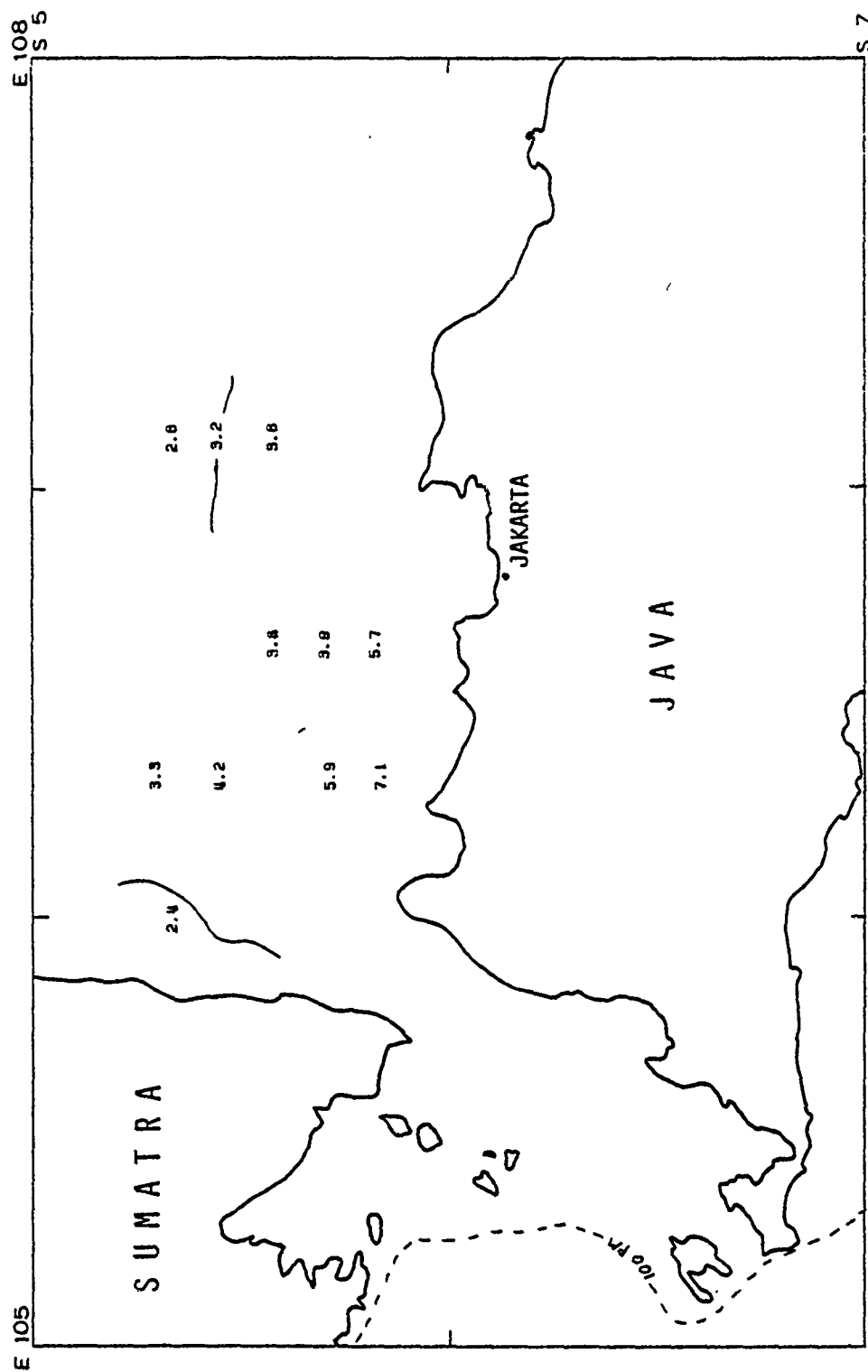
FIGURE 53 : KD VALUES, JAKARTA APPROACHES, OCT-DEC
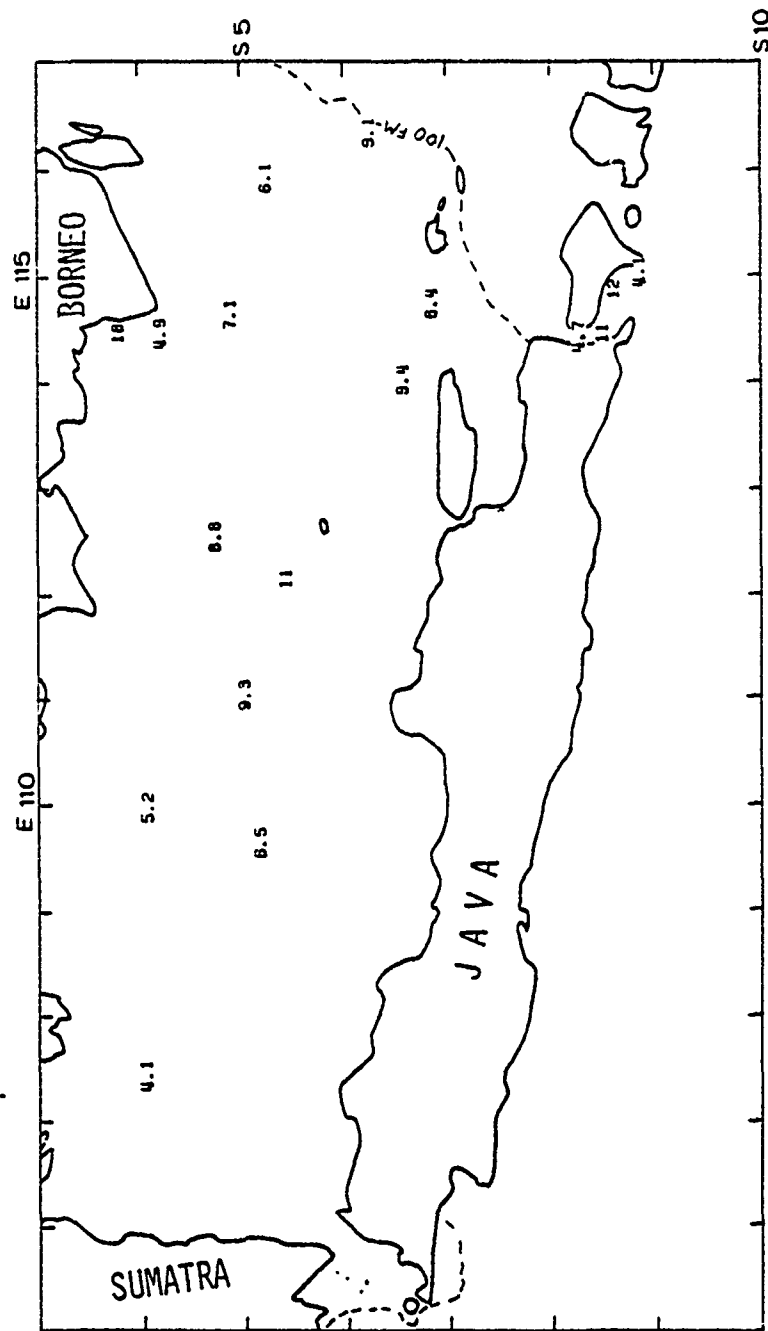
FIGURE 64: KD VALUES, JAVA SEA, JAN-MAR

FIGURE 65 : KD VALUES, JAVA SEA, APR-JUN
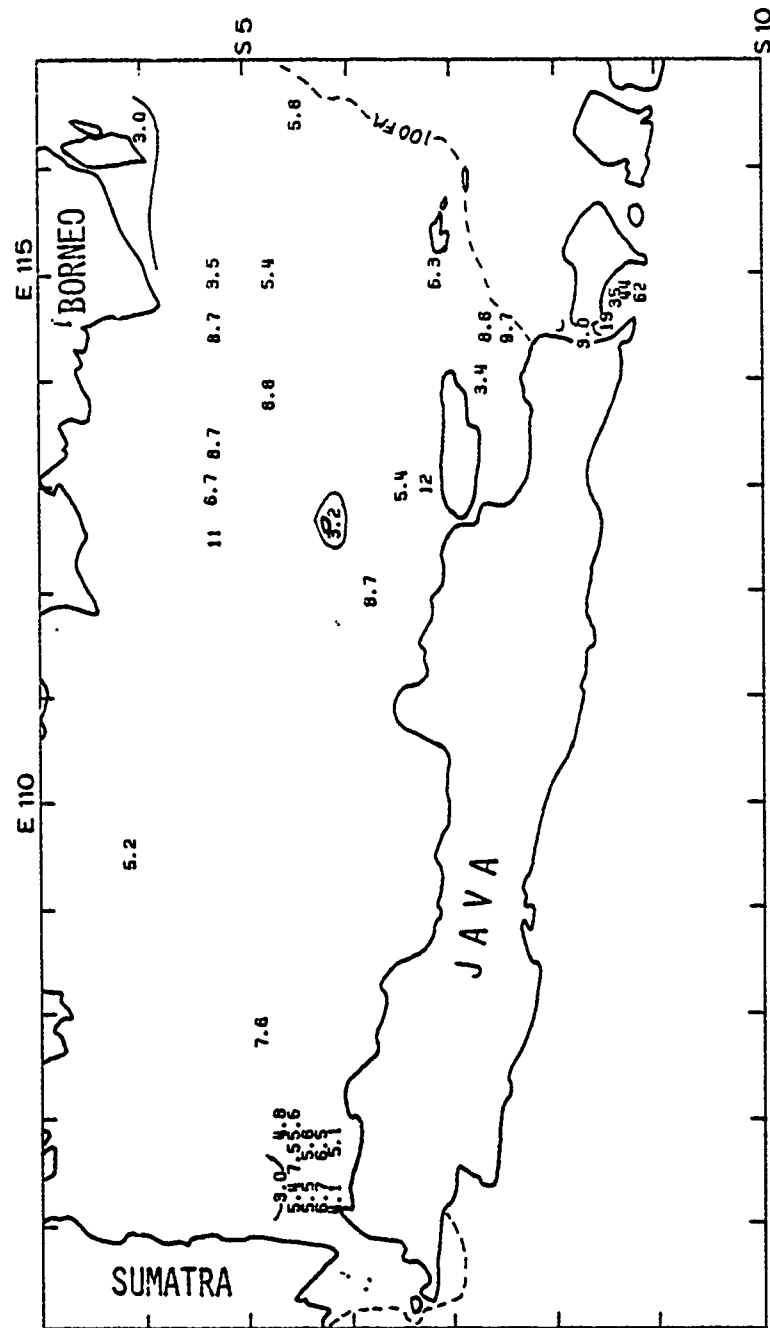
FIGURE 66 : KD VALUES, JAVA SEA, JUL-SEP
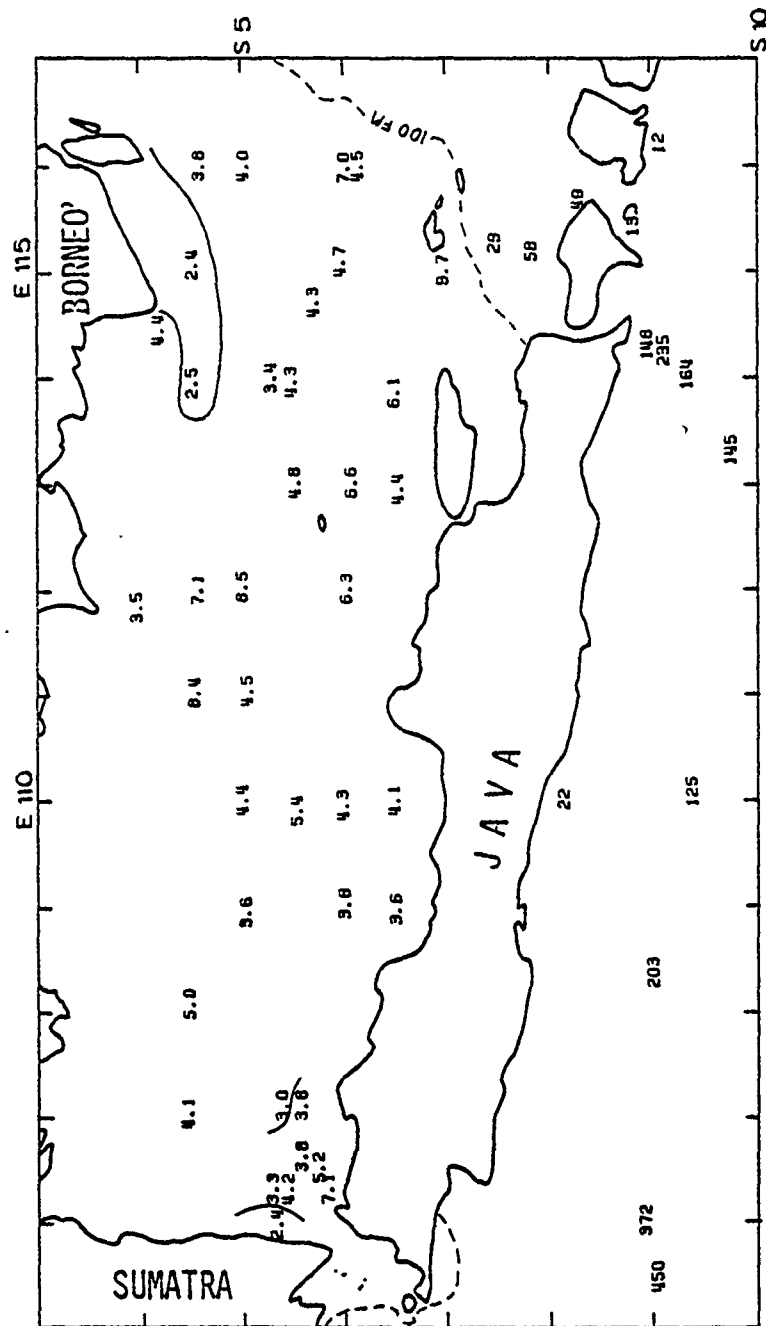
FIGURE 67 : KD VALUES, JAVA SEA, OCT-DEC
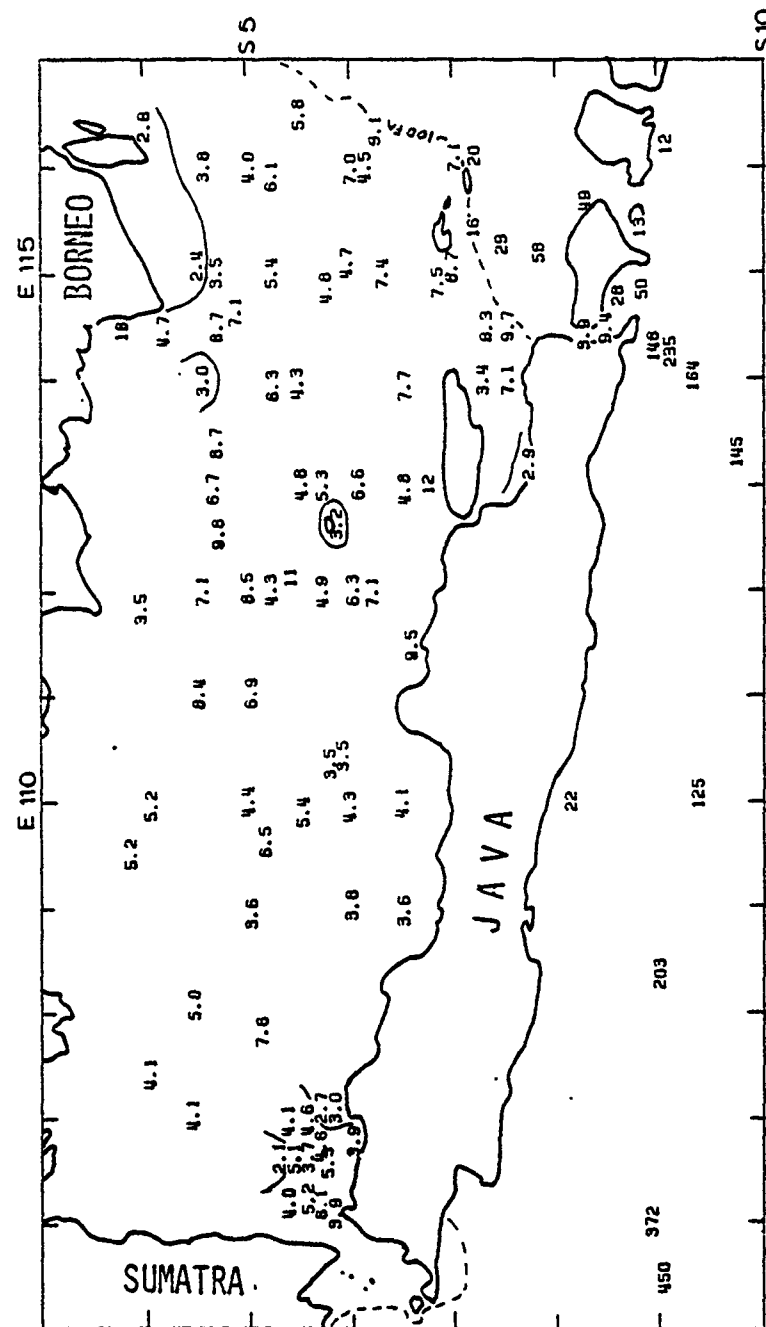
FIGURE 68: KD VALUES, JAVA SEA, ENTIRE YEAR
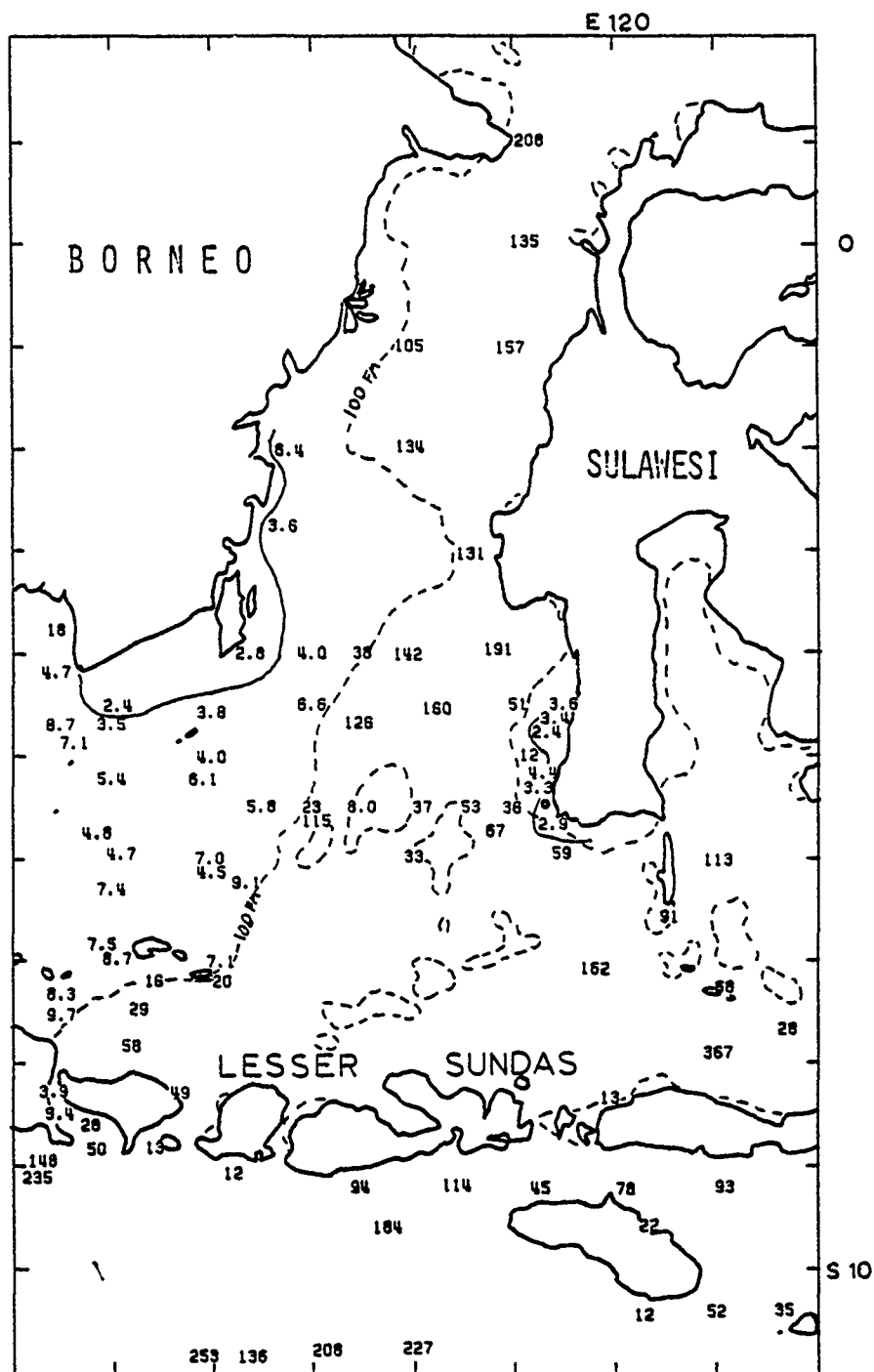
FIGURE 69 : KD VALUES, MAKASSAR STRAIT, FLORES SEA
AND BALI SEA, ENTIRE YEAR

142

FIGURE 70: KD VALUES, MALACCA STRAIT, DEC-APR

143
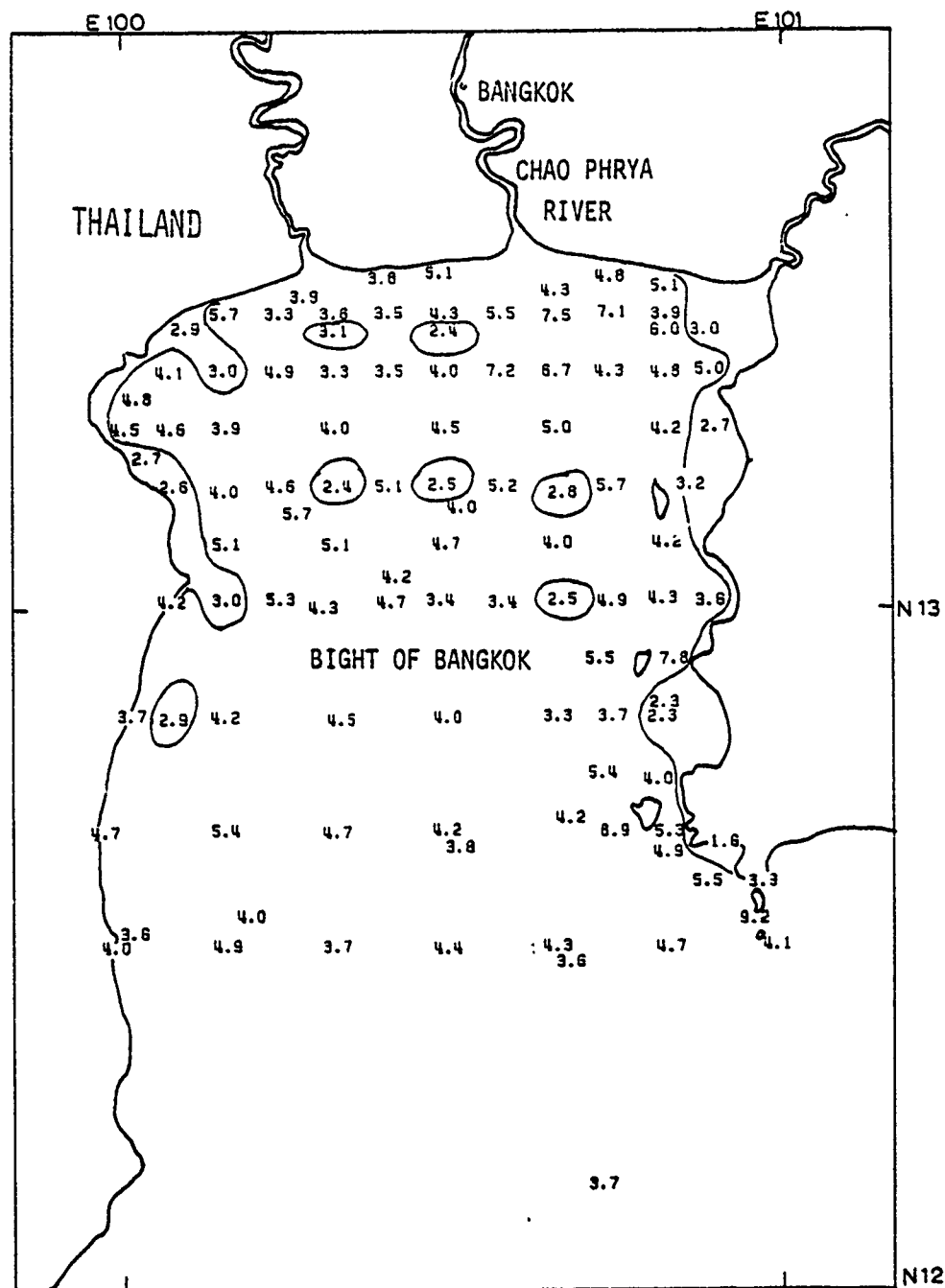
FIGURE 71 : KD VALUES, BANGKOK APPROACHES,
APR-OCT

144
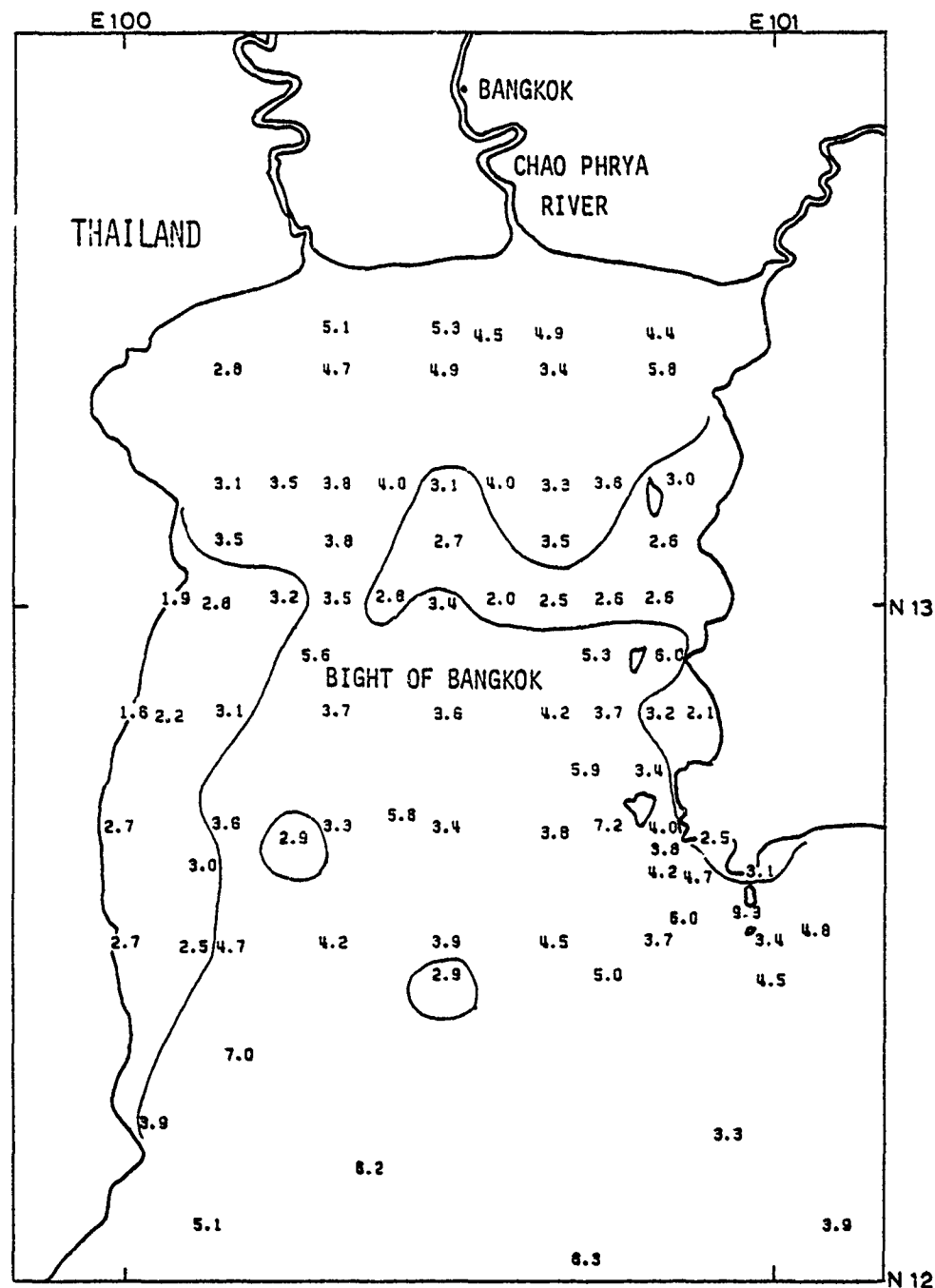
FIGURE 72 : KD VALUES, BANGKOK APPROACHES, NOV-MAR

145
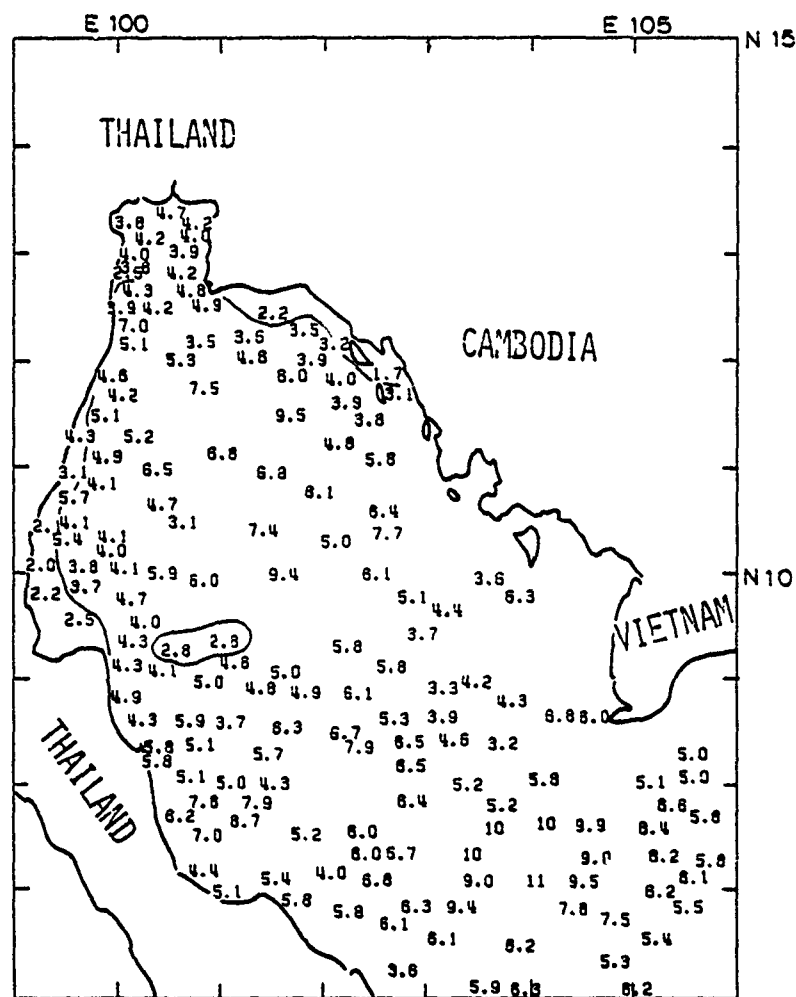
FIGURE 73 : KD VALUES, GULF OF THAILAND, ENTIRE YEAR
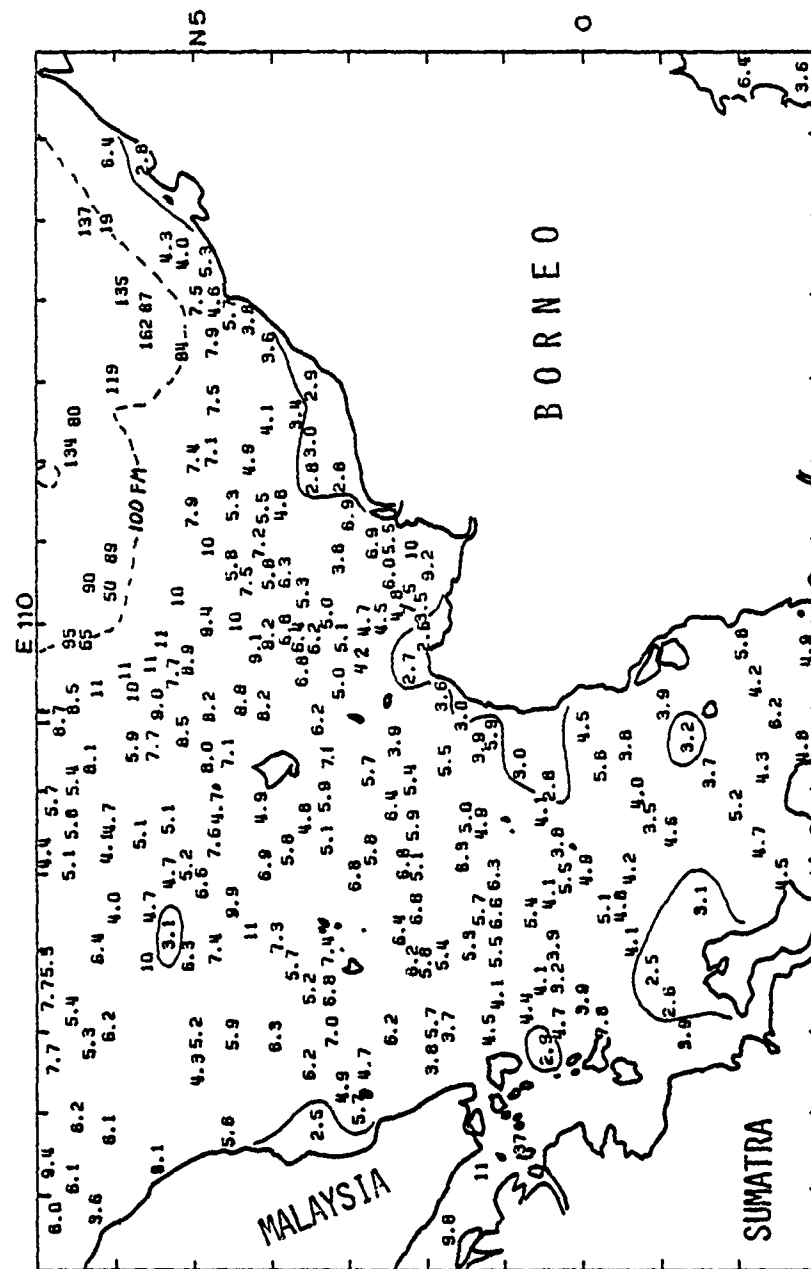
FIGURE 74 : KD VALUES, SOUTH CHINA SEA (SOUTHERN SECTION), ENTIRE YEAR

147

FIGURE 75 : KD VALUES, SOUTH CHINA SEA (CENTRAL SECTION), ENTIRE YEAR
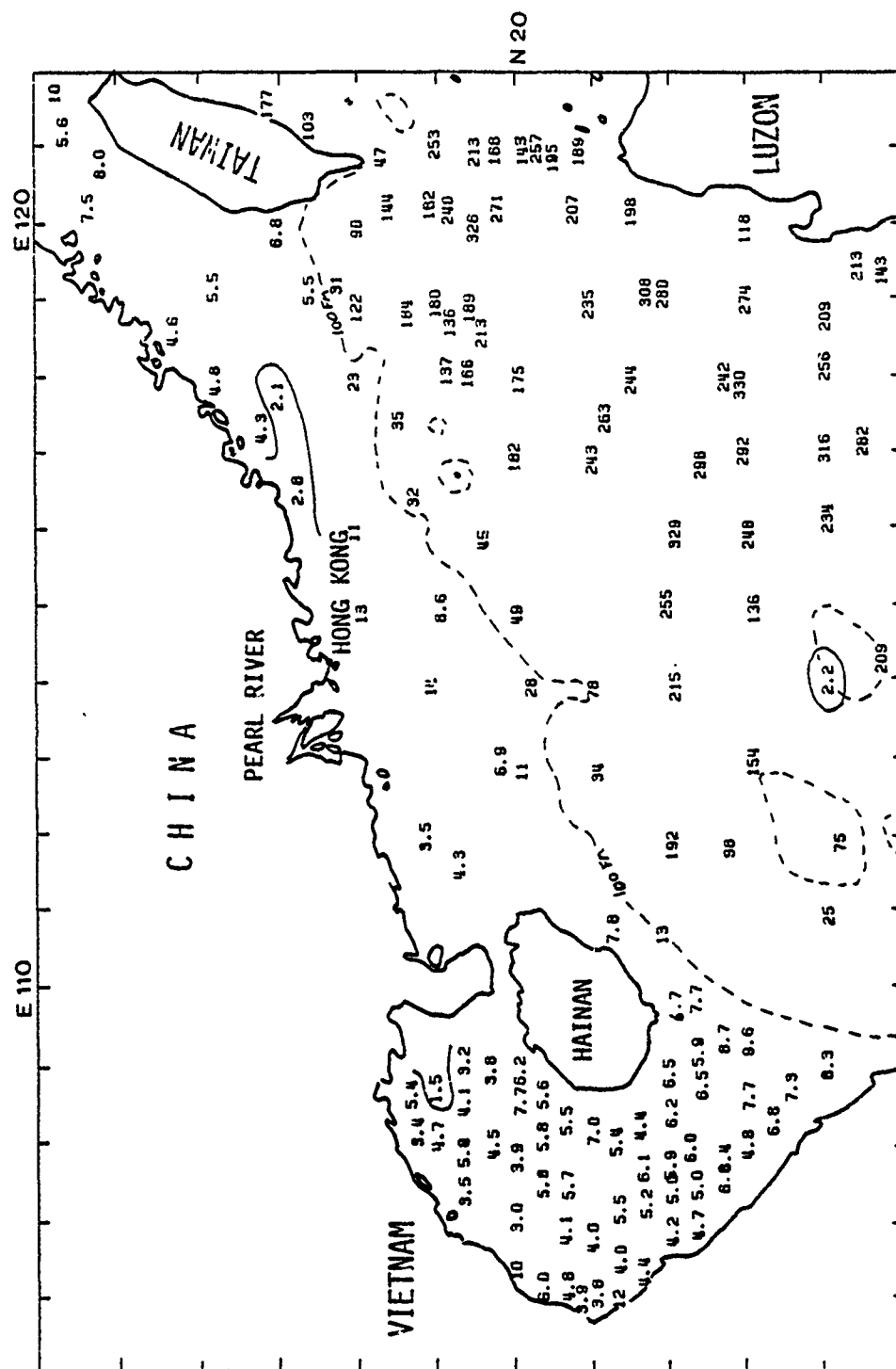
FIGURE 76 : KD VALUES, SOUTH CHINA SEA (NORTHERN SECTION), APR-NOV
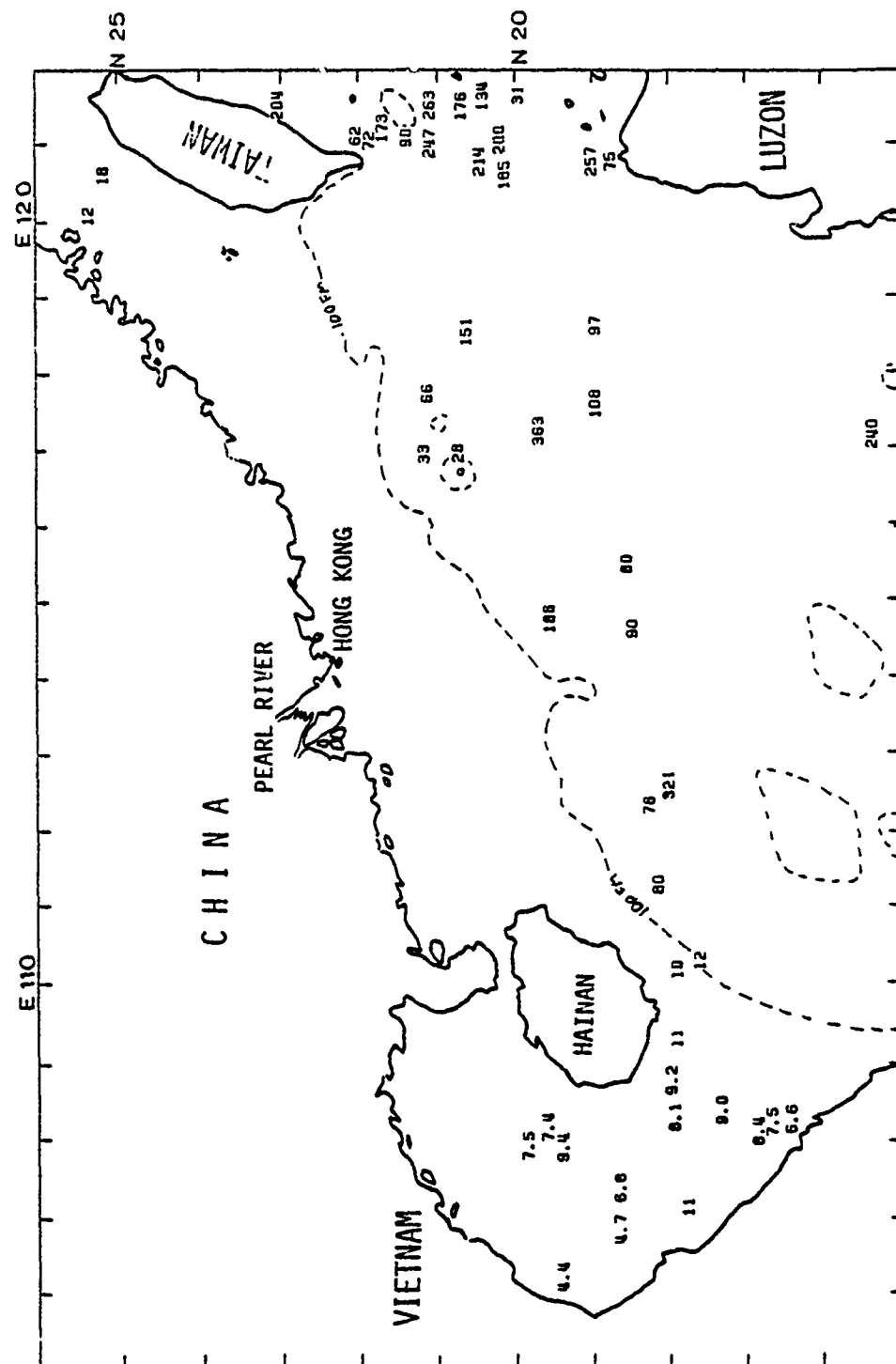
FIGURE 77 : KD VALUES, SOUTH CHINA SEA (NORTHERN SECTION), DEC-MAR

150
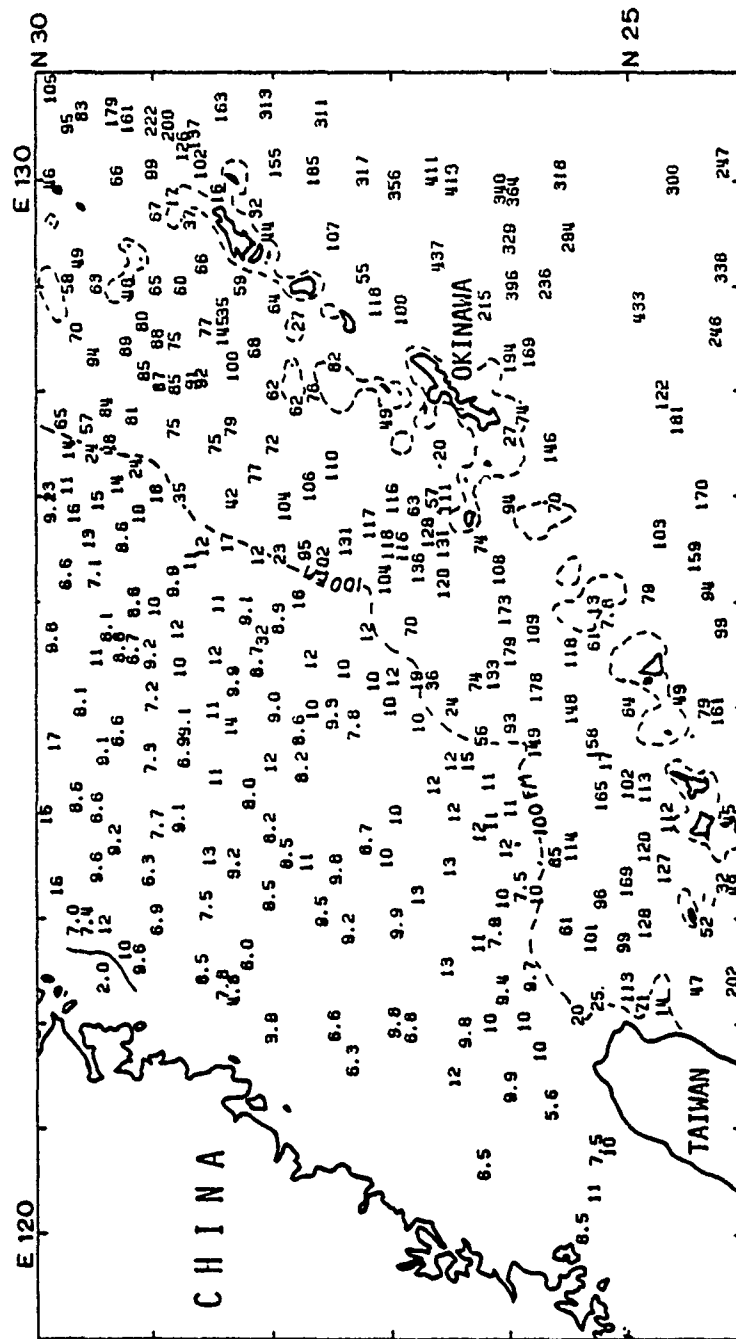
FIGURE 78 : KD VALUES, EAST CHINA SEA, ENTIRE YEAR

REFERENCES

1. *Atlas of South-East Asia*, Introduction by D. G. E. Hall, Macmillan and Co., London, St. Martin's Press, New York, 1964.

2. Ball, T. F. and LaFond, E. C., *Shallow Water Turbidity Studies*, U. S. Navy Electronic Laboratory, San Diego, Research and Development Report 1129, 26 p., 1962.

3. Brown, P. J., *Correlation Coefficients Calculated on a World Wide Basis Between Observed Secchi Depths and Other Simultaneously Measured Standard Oceanographic Parameters*, M. S. Thesis, U. S. Naval Postgraduate School, Monterey, 123 p., 1973. (AD-769, 427)

4. Byrnes, H. J., *Operating Scenario for a Hydrographic Airborne Laser Sounder*, Naval Ocean Research and Development Activity, Bay St. Louis, Mississippi, 29 p., 1978.

5. Chan, K. M., "The Seasonal Variation of Hydrological Properties in the Northern South China Sea," *The Kuroshio*, ed. by J. C. Marr, East-West Center Press, Honolulu, 143-162, 1970.

6. Cialdi, A. and Secchi, P. A., "On the Transparency of the Sea," translated by A. Collier, *Limnology and Oceanography*, 13(3), 391-394, 1968.

7. *Data Report of CSK* (Cooperative Study of the Kuroshio), No. 337, 1977.

8. *Data Report of CSK*, No. 357, 1977.

9. *Data Report of CSK*, No. 368, 1977.

10. *Data Report of CSK*, No. 372, 1977.

11. *Data Report of CSK*, No. 414, 1979.

12. Environmental Data Service, ESSA, *World Weather Records 1951-1960*, Vol. 6, Washington, 605 p., 1968.

13. Environmental Data Service, ESSA, *World Weather Records 1951-1960*, Vol. 4, Washington, 576 p., 1967.

14. Fairbridge, R. W., ed., *The Encyclopedia of Oceanography*, Reinhold, New York, 1021 p., 1966.

15. Frederick, M. A., _An Atlas of Secchi Disc Transparency Measurements and Forel-Ule Color Codes for the Oceans of the World_, M. S. Thesis, U. S. Naval Postgraduate School, Monterey, 188 p., 1970. (AD-718, 333)

16. Gordon, H. R., "One-parameter Characterization of the Ocean's Inherent Optical Properties for Remote Sensing," _Applied Optics_, 16 (10), 2627, 1977.

17. Graham, J. J., "Secchi Disc Observations and Extinction Coefficients in the Central and Eastern North Pacific Ocean," _Limnology and Oceanography_, 11(2), 184-190, 1966.

18. Holmes, R. W., "The Secchi Disc in Turbid Coastal Waters," _Limnology and Oceanography_, 15(5), 668-694, 1970.

19. Houck, M., Personal communication between author and M. Houck, Naval Ocean Research and Development Activity, Bay St. Louis, Mississippi, 1979.

20. Ilahude, A. G., "On the Occurence of Upwelling in the Southern Makassar Strait," _Penelitian Laut di Indonesia; Marine Research in Indonesia No. 10_, Indonesian Institute of Science, Jakarta, 3-53.

21. Indonesia, Institute of Marine Research, National Institute of Oceanology, Indonesian Institute of Science, _Oceanographical Cruise Report (1963-1966), Special Issue_, Jakarta, 1971.

22. Indonesia, Institute of Marine Research, National Institute of Oceanology, Indonesian Institute of Sciences, Jakarta, _Oceanographical Cruise Report No. 13, 1974; Oceanographical Cruise Report No. 14, 1974; Oceanographical Cruise Report No. 16_, 1975.

23. International Hydrographic Bureau, _Limits of Oceans and Seas (Special Publication No. 23)_, 3rd ed., 1953.

24. Jerlov, N. G., "Influence of Suspended and Dissolved Matter on the Transparency of Sea Water," _Tellus_, 5, 59-65, 1953a.

25. Jerlov, N. G., "Optical Classification of Ocean Water," _Physical Aspects of Light in the Sea_, University of Hawaii Press, Honolulu, 45-49, 1964.

26. Jerlov, N. G., "Particle Distribution in the Ocean," _Reports of the Swedish Deep-Sea Expedition_, 3, 73-97, 1953b.

27. Jerlov, N. G., Marine Optics, Elsevier Scientific
Publishing Co., Amsterdam, 231 p., 1976.

28. Jerlov, N. G. and Nygard, K., 1961, "Measured Irradiance,"
Optical Measurements in the Eastern North Atlantic,
Medd. Oceanogr. Inst. Goteborg, Ser. B, 8, 22-29, 1961.

29. Joseph, J., "Extinction Measurements to Indicate Dis-
tribution and Transport of Watermasses," Proceeding of
UNESCO Symposium on Physical Oceanography, Tokyo, 59-75,
1955.

30. Korea, Republic of, Fisheries Research and Development
Agency, Annual Report of Oceanographic Observations,
Vol. 16, 1968.

31. Krumboltz, H., Experimental Investigation of System
Attenuation Coefficient for HALS, draft copy, Naval
Air Development Center, Warminster, Pennsylvania, 9 p.,
1979.

32. LaFond, E. C., "Physical Oceanography and Its Relation
to the Marine Organic Production in the South China Sea,"
Ecology of the Gulf of Thailand and the South China Sea,
A Report of the Results of the Naga Expedition, 1959-1961,
SIO Reference No. 63-6, Scripps Institute of Oceanography,
LaJolla, California, 5-38, 1963.

33. Morita, J., "Transparency Observed by the Secchi Disc
in the Western Pacific Ocean," Far Seas Fisheries Research
Laboratory Bulletin, 9, 1-18, 1973.

34. Naval Ocean Research and Development Activity, Hydrographic
Airborne Laser Sounder (HALS) Base Line System, Bay St.
Louis, Mississippi, 1978.

35. Neuymin, G. C. and Sorokina, N. A., "Correlation between
the Vertical Distributions of Optical and Hydrologic
Characteristics in the Ocean," Oceanology, 16(3),
245-250, 1976.

36. Pak, H., Beardsley Jr., G. F. and Park, P. K., "The
Columbia River as a Source of Marine Light Scattering
Particles," Journal of Geophysical Research, 75(24)
4570-4578, 1970.

37. Pak, H. and Zaneveld, J. R. V., "Bottom Nepheloid Layers
and Bottom Mixed Layers Observed on the Continental Shelf
off Oregon," Journal of Geophysical Research, 82(27),
3921-3931, 1977.

38. Poole, H. H. and Atkins, W. R. G., "Photo-electric Measurements of Submarine Illumination Throughout the Year," *Journal of the Marine Biological Association of the United Kingdom*, 16, 297-324, 1929.

39. Postma, H., "Suspended Matter and Secchi Disc Visibility in Coastal Waters," *Netherlands Journal of Sea Research*, 1(3), 359-390, 1961.

40. Rikiishi, K. and Yoshida, K., "On the Kuroshio Counter-current South of Honshu," *Records of Oceanographic Works in Japan*, 12(1), 31-43, 1974.

41. Robinson, M. K., "The Physical Oceanography of the Gulf of Thailand, Naga Expedition," *Naga Report*, Vol. 3, Pt. 1, Scripps Institute of Oceanography, La Jolla, California, 5-110, 1974.

42. Russell, H. D. and Clarke, G. L., *The Transparency of East Indian Waters and Adjacent Areas*, Woods Hole Oceanographic Institution, Woods Hole, Massachusetts, 25 p., 1944.

43. Shannon, J. G., "Correlation of Beam and Diffuse Attenuation Coefficients Measured in Selected Ocean Waters," *Proceedings of the Society of Photo-Optical Instrumentation Engineers, Ocean Optics*, Vol. 64, 3-11, 1975.

44. Shannon, J. G., *An Analysis of the Utility of Airborne Electro-Optical Bathymetry Systems in a Sample Foreign Coastal Region*, draft preliminary report, Naval Air Development Center, Warminster, Pennsylvania, 21 p., 1978a.

45. Shannon, J. G., *Potential Utility of Candidate Airborne E-O Bathymetry Systems in Selected Foreign Coastal Waters*, preliminary report, Naval Air Development Center, Warminster, Pennsylvania, 7 p., 1978b.

46. Shannon, J. G., personal communication between author and J. G. Shannon, Naval Air Development Center, Warminster, Pennsylvania, 1979.

47. Steeman Nielsen, E., "Fertility of the Ocean," In: M. N. Hill, ed., *The Sea*, Vol. 2, Interscience, New York, 129-164, 1963.

48. Stentz, D. A., *A chronological study of the measurement of the optical properties of ocean waters, and an atlas of the diffuse attenuation coefficient, K, of tropical Atlantic Ocean waters*, Naval Postgraduate School, Monterey, 75 p., 1975.

49. Tyler, J. E., "The Secchi Disc," _Limnology and Oceano-graphy_, 13(1), 1-6, 1968.

50. Uda, M., "Oceanography of the Subarctic Pacific Ocean," _Journal of the Fisheries Research Board of Canada_, 20(1), 119-179, 1963.

51. Uda, M., "On the Subtropical Convergence and the Currents in the Northwestern Pacific," _Records of Oceanographic Works in Japan_, 2(1), 141-150, 1955.

52. Uda, M. and Hasunuma, K., "The Eastward Subtropical Countercurrent in the Western North Pacific Ocean," _Journal of the Oceanographical Society of Japan_, 25(4), 201-210, 1969.

53. Verwey, J., "Depth of Coral Reefs and Penetration of Light," _Pacific Science Congress, 4th, Java, Proceedings_, Vol. 2, 1-23, 1929.

54. Voytov, V. I. and Dement'yeva, M. G., "The Relative Transparency of the Indian Ocean Water," _Oceanology_, 10(1), 35-37, 1970.

55. Voytov, V. I., Khalemskiy, E. N., and Shmatko, M. A., "Optical Properties of the Waters of the East China, South China and Java Seas," _Oceanology_, 15(6), 657-658, 1976.

56. Wargelin, R., _Underwater Optical Data_, Cruise Numbers 343407, 342502 and 342606, unpublished data, Naval Oceanographic Office, Bay St. Louis, Mississippi, 1976.

57. Williams, J., _Optical Properties of the Sea_, United States Naval Institute, Annapolis, Maryland, 124 p., 1970.

58. Wyrtki, K., _Physical Oceanography of the Southeast Asian Waters, Naga Report_, Vol. 2, Scripps Institute of Oceanography, LaJolla, California, 195 p., 1961.

59. York, G. L., _Statistical Studies of World-Wide Secchi Data_, M. S. Thesis, U. S. Naval Postgraduate School, Monterey, 150 p., 1974. (AD-781,614)

INITIAL DISTRIBUTION LIST

	no. copies
Defense Technical Information Center (DTIC) Cameron Station Alexandria, VA 22314	2
Library, Code 0142 Naval Postgraduate School Monterey, CA 93940	2
Chairman, Code 68 Department of Oceanography Naval Postgraduate School Monterey, CA 93940	3
Dr. Stevens P. Tucker, Code 68Tx Department of Oceanography Naval Postgraduate School Monterey, CA 93940	5
Director Naval Oceanography Division (OP952) Navy Department Washington, DC 20350	1
Office of Naval Research Code 480 Naval Ocean Research and Development Activity NSTL Station Bay St. Louis, MS 39522	1
Dr. Robert E. Stevenson Scientific Liaison Office, ONR Scripps Institution of Oceanography La Jolla, CA 92037	1
Commanding Officer Fleet Numerical Weather Central Monterey, CA 93940	1
Commanding Officer Naval Environmental Prediction Research Facility Monterey, CA 93940	1
Commander Oceanographic Systems Pacific Box 1390 Pearl Harbor, Hawaii 96860	1

```
Commanding Officer                                            1
Naval Ocean Research and Development Activity
NSTL Station
Bay St. Louis, MS  39522

Commander                                                     1
Naval Oceanography Command
NSTL Station
Bay St. Louis, MS  39522

Commanding Officer                                            1
Naval Oceanographic Office
NSTL Station
Bay St. Louis, MS  39522

Mr Maxim F. van Norden                                        1
Code 8412
U. S. Naval Oceanographic Office
NSTL Station
Bay St. Louis, MS  39522

Mr. John Shannon, Code 3012                                   1
Naval Air Development Center
Warminster, PA  18974

Dr. Arno Witt                                                 1
Code 3010
Naval Air Development Center
Warminster, PA  18974

Mr. H. Krumboltz, Code 3010                                   1
Naval Air Development Center
Warminster, PA  18974

Mr. Steven E. Litts, Code HYAI                                1
DMAHTC
6500 Brookes Lane
Washington, DC  20315

Mr. David B. Enabnit                                          1
National Oceanic and Atmospheric Administration
National Ocean Survey
Rockville, MD  20852

Mr. Mike Cooper, Code 772                                     1
Naval Coastal Systems Lab
Panama City, FL  32407

Mr. Richard M. Wargelin, Code 2000                            1
U. S. Naval Oceanographic Office
NSTL Station
Bay St. Louis, MS  39522
```

Mr. Jim Hammock   1
DMAHTC
6500 Brookes Lane
Washington, DC   20315

Mr. Albert Pressman, Code 335   1
Naval Ocean Research and Development Activity
NSTL Station
Bay St. Louis, MS   39522

Library   1
DMA H/TC
6500 Brookes Lane
Washington, DC   20315

U. S. Naval Oceanographic Office   1
Library, Code 4103
NSTL Station
Bay St. Louis, MS   39522

Mr. Jimmy C. Stribling, Code 8412   1
U. S. Naval Oceanographic Office
NSTL Station
Bay St. Louis, MS   39522

CDR Donald Nortrup, Code 68Nr   1
Department of Oceanography
Naval Postgraduate School
Monterey, CA   93940

Mr. K. Petri, Code 3012   1
Naval Air Development Center
Warminster, PA   18974

Mr. James E. Gillis, Code ST   1
DMA H/TC
6500 Brookes Lane
Washington, DC   20315

Mr. Max Houck, Code 302   1
Naval Ocean Research and Development Activity
NSTL Station
Bay St. Louis, MS   39522

Mr. Duane Bright, Code 302   1
Naval Ocean Research and Development Activity
NSTL Station
Bay St. Louis, MS   39522

CDR Van K. Nield, Code SST   1
Defense Mapping Agency HQ
Bldg 56, U. S. Naval Observatory
Washington, DC   20305

Dr. Boyd Olson, Code 02   1
U. S. Naval Oceanographic Office
NSTL Station
Bay St. Louis, MS   39522

Mr. Robert Higgs, Code 8000   1
U. S. Naval Oceanographic Office
NSTL Station
Bay St. Louis, MS   39522

Mr. David Jenkins, Code 8400   1
U. S. Naval Oceanographic Office
NSTL Station
Bay St. Louis, MS   39522

Mr. Larry Bourquin, Code 8400   1
U. S. Naval Oceanographic Office
NSTL Station
Bay St. Louis, MS   39522

Mr. Dodd Ouellette, Code 8410   1
U. S. Naval Oceanographic Office
NSTL Station
Bay St. Louis, MS   39522

Mr. W. Henry Odum, III   2
Environmental Data Service
National Oceanographic Data Center
Washington, DC   20235

Mr. Andrew Bakun   1
National Marine Fisheries Service
c/o Fleet Numerical Weather Central
Monterey, CA   93940

John Murdock, Code 8412   5
U. S. Naval Oceanographic Office
NSTL Station
Bay St. Louis, MS   39522

Mr. Sargun Tont   1
A-020
Scripps Institute of Oceanography
La Jolla, CA   92093

Dr. Ronald Zaneveld   1
School of Oceanography
Oregon State University
Corvallis, Oregon 97331

Mr. Roswell Austin   1
Visibility Laboratory
University of California, San Diego
Bdlg 348, Scripps Field Annex
San Diego, California   92125